Framing Extreme Precipitation Events in the Context of Cumulative Emissions

Travis Roger Moore

A Thesis
In
The Department
Of
Geography, Planning and Environment

Presented in Partial Fulfillment of the Requirements
for the degree of Doctor of Philosophy (Geography, Urban and Environmental Studies)
at Concordia University

August 2024

CONCORDIA UNIVERSITY

SCHOOL OF GRADUATE STUDIES

This is to certify that the thesis prepared

By: Travis Roger Moore

Entitled: **Framing Extreme Precipitation Events in the Context of Cumulative Emissions**

and submitted in partial fulfillment of the requirements for the degree of

Doctor of Philosophy (Geography, Urban and Environmental Studies)

Complies with the regulations of the University and meets the accepted standards with respect to originality and quality.

Signed by the final Examining Committee:

_____ Chair
Dr. Raymond Paquin

_____ External Examiner
Dr. John R. Gyakum

_____ Arm's Length Examiner
Dr. Alireza Nazemi

_____ Examiner
Dr. Jeannine Marie St-Jacques

_____ Examiner
Dr. Alexandra Lesnikowski

_____ Thesis Supervisor
Dr. Damon Matthews

Approved by

_____
Dr. Damon Matthews, Graduate Program Director

June 7th, 2024

_____
Dr. Effrosyni Diamantoudi, Dean of Faculty

Framing Extreme Precipitation Events in the Context of Cumulative Emissions

Abstract

Travis R. Moore, Ph.D.
Concordia University, 2024

Heavy to extreme precipitation events are often-destructive forms of weather that, despite their infrequency, can lead to significant losses of human life and infrastructural damage. Such events are expected to increase in a warmer world as cumulative carbon emissions continue to rise. However, the extent to which this increase occurs varies considerably across scenarios and spatial scales, especially for the most extreme precipitation. The Transient Response to Cumulative CO_2 Emissions (TCRE) has proven to be a powerful metric that characterizes the linear response of global mean temperature to cumulative carbon emissions, and previous research has shown its potential applicability to other climate indicators, such as regional temperature and precipitation, and heat extremes. By using simulations from nine Coupled Model Intercomparison Project Phase 5 (CMIP5) models, I intend to quantify extreme precipitation indices of one-day maximum (Rx1day) and five-day maximum (Rx5day) events against cumulative CO_2 emissions. I show that the TCRE framework can be applied to represent changes in these precipitation extremes, with validation of this approach at sub-global scales across emissions scenarios. In Chapter 3, I determine whether precipitation extremes respond linearly to cumulative CO_2 emissions, at global to local scales, using simple linear regression modelling. In Chapter 4, I conduct a Generalized Extreme Value (GEV) analysis to model the behavior of the most extreme values of Rx1day and Rx5day and evaluate whether trends in location parameter estimates and specified return levels can be approximated by (regional) TCRE values. For Chapter 5, I extend this analysis to estimate remaining carbon budgets (RCBs) associated with avoiding particular extreme precipitation levels. Overall, my results suggest that extreme precipitation work well within a TCRE framework, and that global and sub-global changes can be well approximated by linear responses to cumulative CO_2 emissions, though with less robustly linear trends at local scales. My results further highlight that location parameter estimates and return levels of Rx1day and Rx5day scale approximately linearly to increasing cumulative carbon emissions. My findings also show that RCBs are generally small to avoid specified present-day 20-year and 100-year return levels. This suggests that such events are becoming commonplace with global warming.

Acknowledgements

First and foremost, I acknowledge my supervisor, Dr. Damon Matthews, for all of his incredible mentorship throughout my Ph.D. studies, and for giving me the opportunity to pursue a Ph.D. altogether. Not only did this program offer me the chance to further develop my research ability, but it also gave me the invaluable opportunity to contribute new knowledge towards understanding extreme weather events in the context of a rapidly warming global and regional climate. Dr. Matthews very often provided me with the tools and encouragement necessary to be successful. He diligently shared thorough feedback through online and in-person follow-ups at every point during our often spirited conversations while always giving more than excellent advice throughout my project and through all other components of the Ph.D. program, especially during the most challenging times. I will always be most grateful for all of his time, exceptional dedication and willingness to help, as well as always offering me such a flexible working environment through it all.

I also would like to extend my thanks to Dr. Yann Chavaillaz, Dr. Silvia Innocenti and Dr. Jonathan Jalbert for their contributions and mentorship towards helping me to further conceptualize and methodologically design my research. They suggested different and interesting angles to approach my research and shape my research objectives, as well as helping manipulate and contextualize the gathered simulated climate data accordingly. I would also like to express my heartfelt gratitude to my committee, including Dr. Martin Leduc and Dr. Jeannine St-Jacques, for their extensive support and mentorship, as well as helping me to formulate research ideas that ultimately synthesized and developed my research objectives. I thank Dr. Chavaillaz for his amazing guidance at Ouranos in closely

working with me to organize and store the simulated precipitation data for later analysis. I additionally thank all of my climate lab mates for their suggestions and feedback along the way, as their ideas and feedback also really helped to develop my project in more interesting/cohesive directions and ultimately consolidate my research goals. I further could not have undertaken this academic journey without the support from Dr. Judith Patterson and Dr. Catherine Moore, providing me with the guidance and encouragement necessary to be successful. I also would like to thank Dr. Daniel Naud for really motivating me to pursue graduate studies from the beginning and having such confidence in me to take my studies further in this very rewarding Ph.D. program.

I extend my gratitude to NSERC for providing me with the funding necessary to undertake my research, as well as Concordia University and our Department for being so resourceful, willing, and offering me the extra support and resources that will forever be cherished.

Finally, I would like to thank my family, especially my parents, brother and grandparents, for all of their extensive support, diligence and encouragement throughout my Ph.D. endeavors, and helping me stay on track with my research and thesis writing collectively.

Dedication

I dedicate this work to my family, including my parents, brother, and grandparents. I also dedicate this project to Dr. Damon Matthews, as he always helped me realize my academic potential, and I cannot thank him enough for this exceptional mentorship at every step of the way.

Contribution of Authors

For this project, I contributed to the data manipulations necessary for data analysis of selected precipitation extreme indices, with Dr. Yann Chavaillaz guiding the extraction procedure of the CMIP5 simulated precipitation data and assisting with the editing of the manuscript contained in Chapter 3. I led the thesis writing, editing and revisions, as well as helped in conceptualizing the research contained in the three Chapters. Dr. Damon Matthews contributed to the thesis editing and revisions (in particular for the Chapter 5 manuscript), as well as contextualizing the work, and framing the central ideas for each of the three principal chapters of this work.

Chapter 3 has been published in the Journal of *Atmosphere-Ocean* as:

Moore, T. R., Matthews, H. D., & Chavaillaz, Y. (2023). Linking Historical and Projected Trends in Extreme Precipitation with Cumulative Carbon Dioxide Emissions. *Atmosphere-Ocean*, 1-18.

Chapters 4 & 5 are being prepared for submission for publication.

All authors reviewed the final manuscript and approved of the contents.

Table of Contents

List of Figures

Chapter 3: Linking historical and projected trends in extreme precipitation with cumulative carbon dioxide emissions

Chapter 4: Using CMIP5 data to model trends in global, regional and local precipitation extremes with a GEV distribution

Chapter 5: Estimating the remaining carbon budget for global, regional and local extreme precipitation thresholds

List of Tables

Chapter 3: Linking historical and projected trends in extreme precipitation with cumulative carbon dioxide emissions

Chapter 4: Using CMIP5 data to model trends in global, regional and local precipitation extremes with a GEV distribution

Chapter 5: Estimating the remaining carbon budget for global, regional and local extreme precipitation thresholds

List of Abbreviations:

1pctCO_2: 1% per year increase in Carbon Dioxide (from pre-industrial period)

C: Celsius

CanESM2: Canadian Earth System Model

CAPE: Convective Available Potential Energy

CESM1: Community Earth System Model

CMIP5: Coupled Model Intercomparison Project Phase 5

CMIP6: Coupled Model Intercomparison Project Phase 6

CO_2: Carbon Dioxide

ENSO: El Nino Southern Oscillation

EVT: Extreme Value Theory

GCM: Global Climate Model

GEV: Generalized Extreme Value

IPCC: Intergovernmental Panel on Climate Change

IPCC AR5: Intergovernmental Panel on Climate Change Fifth (5^{th}) Assessment Report

IPCC AR6: Intergovernmental Panel on Climate Change Sixth (6^{th}) Assessment Report

IPCC SREX: Intergovernmental Panel on Climate Change Managing the Risks of Extreme Events and Disasters to Advance Climate Change Adaptation

IPSL-CM5A-LR: Institut Pierre Simon Laplace low-resolution model

IPSL-CM5A-MR: Institut Pierre Simon Laplace medium-resolution model

IPSL-CM5B-LR: Institut Pierre Simon Laplace low-resolution model

ITCZ: Intertropical Convergence Zone

MIROC-ESM: Japanese Modeling Community Earth System Model

mm/day: millimeters per day

MOHC-HadGEM2: Met Office Hadley Center-Hadley Center Global Environment Model Version 2

MPI-MMPI-ESM-LR: Max Plank Institute Earth System Model low-resolution

MPI-MMPI-ESM-MR: Max Plank Institute Earth System Model medium-resolution

NOAA-GFDL-ESM2G: National Oceanic and Atmospheric Administration Geophysical Fluid Dynamics Generalized Ocean Layer Dynamics

NOAA-GFDL-ESM2M: National Oceanic and Atmospheric Administration Geophysical Fluid Dynamics Modular Ocean Version 4.1

PDF: Probability Density Function

RCB: Remaining Carbon Budget

RCP: Representative Concentration Pathway

RTCRE: Regional Transient Climate Response to Cumulative CO_2 Emissions

Rx1day: One-day maximum precipitation

Rx5day: Five-day maximum precipitation

SE: Standard Error

SSP: Shared Socio-economical Pathways

TCRE: Transient Climate Response to Cumulative CO_2 Emissions

TtC: Teratons of carbon

w/m^2: Watts per meter squared

Chapter 1: General Introduction

Weather and climate extremes are expected to increase in both frequency and intensity as global cumulative emissions, and correspondingly global temperatures, continue to rise. This has prompted more global and regional concerns as such events often yield significant negative impacts to human health and safety, as well as present major environmental stresses. Indeed, according to the World Meteorological Organization, extreme weather events have accounted for more than two million deaths over a 52-year period, from 1970 to 2021, 90% of which occurred in developing nations (World Meteorological Organization, 2022). Mortality due to extreme weather and extreme climate events has, nevertheless, shown a decrease at the global scale despite an increase in extremes (Franzke & Torello, 2020). This suggests an overall better adaptation to such events, including in developing nations (Franzke & Torello, 2020), such as in India (Ray et al., 2021). That said, certain extreme events have been linked to marked increase in the number of fatalities; for example, deaths associated with heat extremes have shown an increase in regions of Europe (e.g. Franzke & Torello, 2020) and globally (e.g. Clarke et al., 2022).

However, while there is strong consensus that these events are likely to increase in frequency and/or intensity in a warmer climate, the extent to which they will do so remains uncertain, including with respect to responses to the various specified global warming targets and related amounts of warming mentioned in international agreements. A large portion of this uncertainty originates with the relatively coarse model resolutions often used to examine many of these extremes and their environmental conditions,

especially since several forms of extreme weather realistically cover much finer scales, such as severe thunderstorms and other related local to mesoscale systems.

Weather and climate extremes are broad terms that make reference to rare events that occur outside of a given region or location's climatology, appearing within the tails of a normal distribution of their frequencies. What constitutes a weather (or climate) extreme is typically presented under a wealth of definitions across the climate impacts literature. The Intergovernmental Panel on Climate Change Sixth Assessment Report (IPCC AR6), for example, defines such events differently based on time scale; weather extremes can be events that take place over some place and time, while a climate extreme can last for extended periods (IPCC, 2021). In consideration of this and related definitions, weather extremes may be described as shorter-term events. These events can, thus, be manifested as a relatively sudden event, such as a tornado outbreak, derecho or a flash-flood event associated with a family of severe thunderstorms in Canada or the United States and elsewhere. Conversely, a climate extreme can be, for instance, in the form of an ongoing dry regime that may contribute to abnormally ubiquitous wildfires in some region or collection of regions, such as the Canadian wildfires of the summer of 2023, or an ongoing wet pattern that may culminate in significant flooding.

A precipitation extreme also may not always necessarily manifest as an extreme precipitation amount over various time scales, but rather can also be a form of precipitation that is not typically observed in a given location or region in question, even if this precipitation comes in lighter amounts and appears only briefly. Weather extremes that occupy longer periods of time, such as over multiple days in succession, may involve ongoing lighter precipitation amounts that may lead to gradual flooding events. Such

flooding situations may be exacerbated by already (near-) saturated ground, rapid snowmelt, and/or rivers having water levels that are above normal coming out of a winter season. Precipitation events that form in this manner often take place in the wake of a prominent atmospheric block (e.g. Rex, 1950; Woollings et al., 2018). Such blocking patterns often cause a particular weather pattern to persist for significant periods of time before the block can break down to allow for the more transient atmospheric flow to be restored. These situations frequently cause a mid-latitude cyclone, for instance, to remain almost stationary over the same regions for several days before it can evacuate normally. Atmospheric blocks also facilitate the extent of flooding that occurs with atmospheric rivers, such as the Pineapple Express, which can constantly direct and energize families of mid-latitude cyclones towards the same areas for as long as weeks, causing substantial flooding events over the West coast of North America (e.g. Newell et al., 1992). For this reason, atmospheric blocks have gained more attention in relation to warmer global temperatures, though projected trends are not well understood because of such patterns being underrepresented by models (e.g. Kennedy et al., 2016; Woollings et al, 2018; Steinfeld et al., 2022).

At the same time, extreme weather and/or climate events are made further complicated because of their ability to trigger other extremes. This is often present as successive and compounding extremes, which are much more significant than a single extreme event because of their ability to exacerbate the impacts tied to the original extreme event (e.g. Bevacqua et al., 2023; Riboldi, 2023). Such events, for example, may begin as an extreme rainfall event whose impacts are enhanced by a mudslide or landslide. Similarly, the flooding that may originate from a severe thunderstorm may be enhanced by

the destructive wind fields associated with either powerful straight-line winds or a (violent) tornado.

The impact of a weather or climate extreme will further vary with the location or region that the event in question is affecting. For example, a flash-flooding event originating with a severe thunderstorm may be handled and managed better in a North America city than it would be in a city located in a third-world nation.

Collectively, weather and climate extremes are commonly referred to as 90th percentile events and are typically analyzed in the climate impacts literature based on the changes in either their frequency or intensity (or both) in response to some prescribed warming threshold(s) (IPCC, 2021). However, despite their rarity, these events can frequently induce catastrophic damages, with effects that can last for years to even decades (Franks & Moore, 2021). Such extremes have the ability to further change the shape of landscapes permanently and can lead to significant losses of human life. Furthermore, in light of continued global warming, there is more concern that current and recent extreme events are no longer necessarily classified as so rare and, as such, may become part of a new normal (e.g. Mallakpour et al., 2018; Stillman, 2019). To that end, because of their sensitivity to even small amounts of warming, weather extremes are likely to become more frequent and intense at warming thresholds much lower than those specified in current global climate warming targets relative to the pre-industrial period.

Among weather and climate extremes, heavy to extreme precipitation events, in particular, have notably received considerable attention across the scientific community and climate impacts literature. Precipitation extremes can be incredibly destructive, as (flash-) flooding often drives substantial socio-economic damage and can lead to numerous

human deaths (Gimeno-Sotelo & Gimeno, 2023). In the United States, flooding accounts for some of the largest numbers of human fatalities among natural disasters; most deaths are attributed to flash-flooding events, with approximately 5,000 deaths worldwide annually, as flash-flooding is responsible for about 85% of all global floods (World Meteorological Organization, 2022). To that end, the flooding events tied to precipitation extremes rank among the deadliest events each year globally and so are of growing importance with the expectation that they will intensify and become more frequent in response to warmer global (and regional) temperature. The most recent flooding event in Libya, for instance, which originated from a series of torrential rainfalls associated with a tropical-like cyclone over the Mediterranean, led to tens of thousands of fatalities alone in what was one of the most disastrous global flooding events (Oduoye et al., 2024).

Extreme precipitation events are specifically expected to decrease in frequency but increase in intensity (IPCC AR6, 2021), much like trends simulated for tropical cyclones under warmer global temperatures (e.g. Knutson et al., 2010; Sugi et al., 2012; Moore et al., 2015). Yet coverage for the response of the most intense precipitation to warmer global and notably regional temperatures in terms of both frequency and intensity remains quite sparse in the literature, despite the significant impacts that such events can have on society (e.g. Myhre et al., 2019). Warmer global temperatures notably have the ability to hold more atmospheric moisture, which guides larger precipitation rates that are especially important in deep convective systems (Donat et al., 2013; Allen, 2018; Neelin et al., 2022). Such events are capable of producing substantial amounts of precipitation in a very limited period of time, which can induce large amounts of water accumulation that subsequently often leads to flash-flooding. In light of the significant impacts linked to extreme precipitation, it

becomes further crucial to better understand how these events may respond to currently specified 'dangerous' climate warming thresholds, and other thresholds that may become of interest.

Much like other extremes, extreme precipitation events are expected to increase in frequency and/or intensity as cumulative emissions continue to rise. A precipitation extreme similarly is presented under a variety of definitions, but the choice of definition impacts how that precipitation event will respond to warming and ultimately impacts expected trends (e.g. Pendergrass, 2018). For example, depending on the precipitation metric in question for tropical cyclones, the extent of scaling in the response of tropical cyclone precipitation to warming can differ, and sometimes greatly (Stansfield & Reed, 2023). As compared with the temperature response to emissions, the weather systems that guide (extreme) precipitation events are realistically much more intricate. Therefore, it is not as clear how such precipitation-bearing events will respond to warmer temperatures directly as global emissions rise, including in response to any internationally-agreed global warming threshold. The term "precipitation" itself is meteorologically meant to be collective in representing all forms of condensed water precipitating to the surface. We may, as such, infer that a precipitation extreme operates in similar ways, in which all forms of condensed water fall at rates that (well) exceed some climatological norm. To that end, extreme precipitation events can often coincide with multiple forms of extremes. For example, large amounts rainfall may occur in a very small timespan during severe thunderstorms or tropical cyclones, while heavy to extreme snowfall associated with the cool sector of a cold-season mid-latitude cyclone (or as intense snowsqualls at other sectors of the cyclone depending on thermodynamic circulations, such as ahead or behind a

cold front) might also constitute an extreme precipitation event. A single dynamical mid-latitude cyclone itself could be responsible for multiple types of precipitation extremes, especially during the colder months. As a result, because extreme precipitation events encompass such a large range of extreme weather, along with other hazards that may accompany them during the same events, they are undoubtedly of scientific interest in climate impacts and other fields.

The climate impacts literature presents such extremes often as one-day and five-day maxima, more formally known as "Rx1day" and "Rx5day", respectively (e.g. Zhang et al., 2013; Valverde & Marengo, 2014; Mondal & Mujumdar, 2015; Mukjubee et al., 2018). Rx1day events may refer to the maximum amount of precipitation that falls over the course of a 24-hour period or less over some space, while an Rx5day event can be interpreted as the maximum cumulative amount of precipitation that is observed during a period of five successive days. Such precipitation indicators are frequently used in the literature to evaluate changes in their character (i.e. their intensity and/or frequency globally to regionally) in relation to warmer temperatures. However, these precipitation indicators are sparsely framed in the context of cumulative emissions directly and are much more poorly understood at sub-global spatial scales. This is further compounded by the scale at which many of these events occur, making it difficult to provide more meaningful evaluations of such systems into the future (e.g. Edwards et al., 2018).

The Transient Climate Response to Carbon Dioxide Emissions (TCRE) describes the proportionality between global mean temperature and carbon dioxide emissions (e.g. Friedlingstein et al., 2014; Tokarska et al., 2019). It is a widely adopted framework for quantifying trends of climate indicators in relation to cumulative carbon emissions and

better understanding impacts at various global warming targets. It has further showed potential for applications for other important climate indicators outside of global mean temperature (e.g. Zickfield et al., 2012; Partanen et al., 2017). The TCRE has been documented extensively in the body of climate impacts literature as a means for framing the linear response of global mean temperature to cumulative CO_2 emissions. It has more widely gained recognition in light of its ability to directly relate temperature, and potentially even other climate indicators, to emissions. This makes the TCRE a useful metric for estimating the extent to which a certain climate indicator may respond per unit increase in carbon emissions. Therefore, estimates derived from the TCRE can be of value in the climate policy and adaptation sectors for being able to more practically determine critical carbon emissions concentrations that are linked to notably dangerous warming thresholds increasing the likelihood of certain weather/climate extremes. Previous studies have tested the TCRE in global contexts as a means for evaluating the response of global temperature to emissions, finding that temperature responds approximately linearly to carbon emissions (e.g. Matthews et al., 2009; Gillett et al., 2013). More recent research has extended the TCRE framework to regional temperature patterns, similarly showing a regional linear response to carbon emissions (e.g. Leduc et al., 2016). In light of the linear relationship that characterizes the regional TCRE (RTCRE) in the context of temperature, it is further shown to be a promising tool for estimating trends for indicators of precipitation (e.g. Partanen et al., 2017). The TCRE has also shown to have useful applications in other sectors, such as in infrastructure and energy management (Priore et al., 2023).

As an extension of the TCRE, carbon budgets are used in climate policy-making for setting emission reduction targets. Remaining carbon budgets may be defined as the total

allowable carbon dioxide emissions that can be emitted into the future in order to reach a specified global warming target (Matthews et al., 2020). The remaining carbon budget is, thus, a useful quantity in that it has the ability to flexibly communicate climate impacts in relation to cumulative emissions concentrations. To that end, carbon budgets specifically inform the extent to which global emissions need to be reduced in order to avert a certain climate impact, such as thresholds of global temperature that may be linked to dangerous heat wave events, or a catastrophic precipitation event. Furthermore, the ability to link emissions directly to temperature and other climate impacts can provide a meaningful estimate of the amount of carbon emissions needed to reach some stipulated emissions threshold associated with a given climate impact. Such carbon budgets are often calculated by using the present-day or near-present-day emissions value relative to an emissions level of interest into the future across a range of scenarios (e.g. Rogeli et al., 2016). Previous studies, for example, have applied the TCRE to estimate the remaining carbon budget to reach certain global warming thresholds of interest, such as the 1.5 C threshold mentioned as part of the range of warming targets in the Paris Climate Agreement. These remaining carbon budgets, as they are known, represent the amount of remaining (CO_2) emissions needed to reach a certain climate impacts threshold. However, the concept of the remaining carbon budget considers CO_2 emissions only, and so non-CO_2 forcing contributions together with carbon emissions are likely to reduce the extent of emissions budgets necessary for achieving certain warming thresholds in question (Mengis & Matthews, 2020).

Because the TCRE has shown promise in the evaluation of precipitation relative to CO_2 emissions (e.g. Partanen et al., 2017; Myhre et al., 2019), it has great potential for estimating carbon budgets for climate indicators beyond merely global temperature. Such

estimates could similarly be of value for regional to even local-scale climate impacts as a means for framing impacts with emissions.

Extreme Value Theory (EVT) has also frequently been used to statistically model extreme values across a wide range of fields. EVT is formulated around a statistical methodological framework that makes inferences about the extremes of a probability distribution (Coles, 2001). It is especially applied across several scientific fields and has useful applications in forecasting and management, but its framework has been extended to many other fields outside of the natural sciences (Jacob et al. 2019). In hydrology, it is commonly used to forecast precipitation extremes for flood risk management and other applications by modeling extreme values of precipitation (e.g. Goldstein et al., 2003; Mondal & Mujumdar, 2017). Such analyses have proven useful in estimating the probability that an extreme event of specified magnitude would occur over some given time period. Such return levels, thus, can be of use to policy makers and scientists alike in determining the average period of time that would be expected for a specific magnitude of extreme to return.

Numerous studies have shown previously the success of EVT in its ability to effectively model precipitation extremes (Feng et al., 2007; Triphonia et al., 2016; Johnson & Smithers, 2019; Innocenti et al., 2019; Lhamo et al., 2023). Much like flooding events and other extremes, extreme weather events have also been frequently placed in the context of EVT. As a branch to EVT, the Generalized Extreme Value (GEV) theory specifically uses a set of continuous probability distributions to model extremes by applying a block maxima approach. This approach employs a series of blocks, with each containing a sample of extreme values that can be used to statistically model the behavior of extremes through

time by using derived parameter estimates of location, scale and shape. The continuous probability distributions that comprise the GEV include Gumbel, Frechet, and Weibull, representing Type 1, Type II and Type III distributions, respectively (Coles, 2001). Each probability distribution focuses on the rate of decay, or the heaviness of the tails of a probability density function (PDF). The Frechet distribution, for example, describes higher probabilities of extreme events through heavier-tailed behavior, as compared with the lower probabilities linked with the lighter-tailed tendency that follows the Gumbel and Weibull distributions (Carney, 2016). These probability distributions are, thus, used to assess the heaviness of the tails of the extreme probability distributions based on changes in shape parameter estimates calculated from block maxima. Location parameter estimates further provide useful information as to how the mean of the distribution of extremes is shifting, and estimates of scale provide insight of how much more or less compressed the distribution becomes over time.

In the present work, I propose a variety of approaches for examining trends in indicators of precipitation extremes, specifically for Rx1day and Rx5day. As an extension of the TCRE framework, and in an attempt to address the gaps in the literature for the most intense extreme precipitation, I first endeavor to determine whether precipitation extremes at the global, regional and local scale can be approximated by the TCRE using simulations from a consistent set of nine global climate models (GCMs) from the Coupled Model Intercomparison Project Phase 5 (CMIP5). I specifically investigate trends in one-day maxima (Rx1day) and five-day maxima (Rx5day) as representative indicators of extreme precipitation. In doing so, I estimate the extent to which precipitation extremes change per unit of carbon emissions among a set of emissions scenarios, as well as with

respect to historical simulations. In the next stage of this work, I apply a GEV analysis to determine trends in precipitation extremes using estimates of location, scale and shape. I further use the GEV analysis to determine historical and future trends for certain return levels at specified return periods. In the final stage of this research, I then extend the GEV analysis by using the block maxima approach to derive remaining carbon budgets. Using this method, it was possible to estimate these budgets by calculating the difference in cumulative CO_2 emissions between the time 20-year return levels in the future become or exceed 10-year levels, and similarly for when 100-year return levels of extreme precipitation become 20-year levels in future. Using these estimates can help to better understand the extent of emissions concentrations that are required to avoid specified thresholds of precipitation extremes at various spatial scales. This is especially true for precipitation extremes that can cause particularly significant damage through flooding and other related hazards, especially in nations/regions that are already prone to such events altogether. Therefore, framing selected indicators of precipitation extremes in the context of cumulative CO_2 emissions can provide potentially useful information for emission levels that are linked to particularly dangerous precipitation thresholds. As such, the three overlapping principal objectives surrounding the TCRE in relation to precipitation extremes in this dissertation are as follows:

1) I assess the extent to which indicators of extreme precipitation (Rx1day and Rx5day) can be approximated by the TCRE framework at various spatial scales across different emissions thresholds and historical simulations. I then evaluate regional and local responses to determine whether selected precipitation indicators follow a linear response to cumulative CO_2 emissions at these spatial scales.

2) Using the GEV analysis, I endeavor to examine the response of location parameter estimates and specified return levels to determine whether the most extreme Rx1day and Rx5day maxima can be approximated by a linear response to cumulative CO_2 emissions, from the global to local scales, as a means for addressing the gaps in the literature concerning trends in the most intense precipitation extremes.

3) Expanding on this GEV analysis, I attempt to use the TCRE framework to derive remaining carbon budgets associated with changes in Rx1day and Rx5day return levels at various spatial scales.

Chapter 2: Literature Review

An overview of trends in weather extremes

Extreme weather events are shown to increase either in frequency or intensity, or a combination of these two, as global to regional temperatures rise. Such trends in weather extremes range from an increased severity in thunderstorms (e.g. Trapp et al., 2007; Trapp et al., 2009; Brooks, 2013; Moore et al., 2015) to extreme heat waves and drought (e.g. Chavaillaz et al., 2019; Ullah et al., 2022). It is these extreme events that are globally responsible for widespread economic and infrastructural damages, changing ecosystems and human society in such profound ways that impacts can resonate for a lifetime. This is especially true with respect to human health, where psychological and physical stresses can endure for years at a time in notably vulnerable groups, such as children and the elderly (e.g. Franks & Moore, 2021; Butsch et al, 2023). Among most significantly influenced sectors is agriculture, taking about 26% of the impact from weather extremes (Monteleone et al., 2023).

As global temperatures increase in tandem with growing populations, more people are also expected to be touched by extreme events more substantially. For example, impacts from more intense and enduring daytime and nighttime heat waves are likely to increase as exposure to these extremes rises globally (Chavaillaz et al., 2019), particularly impactful in the (densely) populated zones of South Asia (Ullah et al., 2023), Africa (Igun et al., 2022; Birch et al., 2022) and North America (e.g. Thompson et al., 2022). At the same time, more frequent and intense heat waves are expected to increase the likelihood for flash droughts at a global scale; since the 1950s, a 74% jump in these dry events has been

observed (Yuan et al., 2023). Increased drought intensity under warmer temperatures is also likely to increase soil erosion rates (e.g. Kronnas et al., 2022; Tripathy et al., 2023). Especially at mid-latitudes, the impact of increased heat is typically felt more with warmer minimum temperatures, which decreases the diurnal temperature range.

Atmospheric blocking patterns further play a crucial role in the intensity and duration of heat waves and drought; such weather patterns can bring very hot temperatures and dry conditions that can last for more than a week, and, in some cases, on the order of months before the block breaks down. Extended drought and heat wave events have additionally been linked previously to more intense and longer-lasting wildfires (e.g. Lyons et al., 2023) and worsening health costs associated with wildfire smoke (Clarke et al., 2023), such as during the widespread Canadian and European wildfires that emerged during the summer of 2023. Combined with dry lightning/thunderstorms, such fires have been associated with the persistently dry atmospheric conditions plaguing the regions, which is attributable to warmer global and regional temperatures.

The impact of ENSO on extremes

The extent to which weather extremes occur is also heavily dependent on important global climate modulators of climate variability, such as the El Nino Southern Oscillation (ENSO). ENSO is the principal mode of natural variability, which can profoundly dictate how frequent and intense certain modes of weather extremes can become (Lieber et al., 2022). For example, ENSO-warm phases (El Nino) often create conditions suitable for flooding in South America because of warmer than normal sea-surface temperatures frequently present at the Eastern portion of the tropical Pacific. This becomes conducive to

enhanced convection there, which contributed to the Peru flooding event that had materialized during the super El Nino of 1997-1998 (e.g. Bas, 2023). ENSO-cool phases (La Nina) have also been linked to more frequent extreme heat events at mid-latitudes (Luo & Lau, 2020).

That said, warmer global temperatures have been previously shown to potentially affect the character of ENSO in terms of its variability and period (e.g. Moore et al., 2015; Cai et al., 2023), as well as other oscillations that are integral for guiding the formation of certain weather events that are, in turn, responsible for specific extremes. However, climate change can often work in the same direction as natural variabilities, enhancing the impacts associated with various weather extremes, such as flooding, drought, extreme heat, and wildfire (Zhai et al., 2016). This is especially true during moderate to strong El Nino events, when the warmest annual global temperatures are often expected, and there is growing concern that the extreme convective precipitation tied to potentially stronger El Nino events in a warmer climate may increase (e.g. Zhai et al., 2016; Pathirana et al., 2023; Cai et al., 2023). Correspondingly, these changes can culminate in, for example, more frequently strong and longer-lasting tropical cyclones, especially in those basins that favor a combination of warmer sea-surface temperatures, and where wind shear can be suppressed (Knutson et al., 2010).

Some challenges facing the study of weather extremes

In light of the high degree of uncertainty surrounding weather and climate extremes, modelling such events consequently comes with a plethora of challenges. Notably, there are several forms of extreme weather that occur at rather fine spatial scales.

This often creates barriers to examining extremes when using larger-scale models, such as GCMs, to properly resolve the small-scale features that are important to the formation of such systems (Brooks, 2016). Notably, the extreme precipitation rates that regularly originate with strong to severe thunderstorms are difficult to meaningfully evaluate in terms of future trends because such events occur at scales on the order of just a few kilometers or less, especially if the thunderstorms producing them are in the form of single-cells, or pulse thunderstorms. The dynamic and thermodynamic elements that are important contributors to the development of organized thunderstorms are, thus, underrepresented in coarser model resolutions. This makes it challenging to determine how these factors will respond to warming and, ultimately, the trend that extreme precipitation will follow over time.

For this reason, there exists a disparity in coverage for extremes in the literature, where the extent of research varies depending on the extreme in question. For example, there is a wealth of studies aimed at tropical cyclones and extreme heat but comparatively little focus on events such as severe thunderstorms and tornadoes, and other hazards associated with thunderstorms collectively, including with very little attention given to such meso- to microscale events in the reports provided by the IPCC (Brooks, 2013). Much of this void in research dedicated to finer-scale extremes comes from the challenges to, as mentioned, adequately simulate these weather events encompassing only a few kilometers, as well as the availability of data for such events altogether (Edwards, 2018). To that end, for sub-synoptic scale events, such as at the mesoscale, significant inhomogenieties in the observational record exist, owing largely to changes in the manner that such events are documented and detected. For example, increasing trends shown for tornadoes in the

historical record are likely mostly artificially-driven, since they are an artifact of enhanced detection in the wake of more sophisticated tracking systems that increase the chance of such events being covered and detected through time and space (Brooks, 2013; Allen, 2018; Edwards, 2018). As such, this makes these events more challenging to properly diagnose in GCMs. At the same time, changes in the methods design, or the location of the observation stations for studying the same events over time in some region or location, can further introduce spurious trends in the historical records (Allen, 2018).

Extreme precipitation trends

Extreme precipitation events are among the most impactful forms of weather extreme. In light of their often destructive nature, these events are of particular importance to the scientific community and across other fields. Such extremes have significant environmental impacts that can be very harmful to human society. These events are, as such, comprehensively documented in the literature in the context of warmer global and regional temperatures since notably the 1980s in an effort to makes sense of future trends (Neelin et al., 2022). However, although the response of global mean precipitation is of value, precipitation extremes specifically carry notably much more importance because of their potentially much larger responsive magnitude at the regional scale, making such regional signals increasingly crucial to study (Sun & Ao, 2013), such as in the tropics (e.g. Neelin et al., 2022). Globally, extreme precipitation has been shown to increase sharply since the Industrial Revolution at particularly low and high latitudes, and at the highest rates of increase into the future at low latitudes (e.g. Sun et al., 2023). At the regional scale, similar observed and future trends are documented. For example, Potter et al. (2023)

showed that extreme precipitation in a high-emissions scenario in the glacierized regions on the Andean River Basin increased by 14% by the end of the 21st century, when temperatures rise by 3.6 C to 4.1 C. Similarly, in central Asia over the last 60 years, a model ensemble from the Coupled Intercomparison Project Phase 6 (CMIP6) showed an over 100% increase and 20% increase in the intensity and frequency, respectively, of precipitation extremes due to anthropogenic forcing (Fallah et al., 2023). Similar results were also shown in Reddy & Saravanan (2023) for India, with a predicted increase of 52% and 46% in Rx1day and Rx5day, respectively, in a CMIP6 ensemble. Precipitation extremes have similarly increased in the mid-Atlantic to Northeast United States over the 1979-2019 period, owing to enhancement of atmospheric rivers in winter and spring, and in light of increased event frequency in summer and fall (Henny et al., 2023). Myhre et al. (2019) also showed that the most intense precipitation extremes globally increase in frequency historically, though with weak trends in terms of the intensification of such events. South Asia is also shown to have significant increases in heavy precipitation, with China showing an increase in such events by about 6.5% per degree of warming in a CMIP5 multi-model ensemble (Zhang & Zhou, 2020).

Trends in precipitation extremes with tropical cyclones and severe thunderstorms

Extreme precipitation events also occur in conjunction with different forms of weather and climate extremes, including tropical cyclones, strong to severe thunderstorms, and those heavy precipitation events that originate with mid-latitude cyclones, in general. Notably, tropical cyclones are a major source of precipitation extremes. These events are shown to increase in intensity (e.g. higher mean rainfall rates, storm surge and sustained

wind speeds) over their lifetime because warmer global temperatures are expected to favor environments suitable for enhanced tropical cyclone intensification (Knutson et al., 2010). This includes warmer sea-surface temperatures affecting tropical cyclone longevity and intensity (Knutson et al., 2010; Sobel et al., 2016; Bhatia et al., 2018), though there is general consensus in the decreasing number of such events to climate warming (e.g. Moore et al., 2015; Walsh et al., 2019; van Westen et al., 2023). Other studies have shown a trend towards a slowing in hurricane movement, such as Hurricane Harvey of 2017 or Hurricane Dorian in 2019, suggesting that affected locations would be more exposed to the extreme rainfall rates characteristic of these tropical systems for prolonged periods (e.g. Hall & Kossin, 2019). The slower movement of such systems further suggests more time to strengthen over warmer source regions prior to making landfall (Li & Chakraborty, 2020), such as in the case of Hurricane Dorian.

The link between warmer global temperatures and tropical cyclone intensification has further been extensively examined, with exhaustive discussions placed on changes in tropical cyclone hazards, such as more extreme rainfall rates (Bhatia et al., 2018; Wu et al., 2022; Utsumi & Kim, 2022) and increased storm surge (Xi et al., 2023), with impacts expected to be exacerbated with sea level rise. Regionally, the tropical cyclone precipitation extremes have similarly been shown to increase. For example, the most extreme precipitation events with tropical cyclones increased over the last 300 years over the United States East coast (Maxwell et al., 2021). Tropical cyclone Rx1day precipitation amounts are also enhanced across cyclones globally when temperatures are allowed to increase by 4 Celsius relative to the pre-industrial period, including an increase in 90th to 99th percentile Rx1day values in a zone stretching from Hawaii to Japan (Kitoh et al., 2019).

Largely because of the lack of representation of finer-scale deep convective systems, such as severe thunderstorms, the literature dedicated to such events is currently very sparse (Brooks, 2013), though it is a rapidly growing area of research due to severe thunderstorms being an important source of precipitation extremes and other hazards (Allen, 2018). Despite limited observational records, researchers have turned more towards understanding the environments of severe thunderstorms, and how those specifically would change in response to a warmer climate. For example, trends of severe thunderstorms, as well as other forms of deep convection have been quantified through environmental indicators like convective available potential energy (CAPE). Increasing trends in the amount of CAPE have been documented in a warmer climate, mostly because of an increase in atmospheric moisture under warmer temperatures (Trapp et al., 2009; Brooks, 2013). This suggests that strong to severe thunderstorms would more likely yield enhanced precipitation rates as temperatures warm, increasing the risk for flash-flooding, as well as even more damaging hail events that could potentially induce costlier damage associated with such events (Allen, 2018) and compounding extremes (e.g. Bevacqua et al., 2023). Conversely, other studies show that, despite enhanced instability in a warmer climate, thunderstorm environments, in general, may become less favorable in light of increased convective inhibition, dry air entrainment and lower relative humidity, leading to less precipitation extremes attributed to thunderstorms (Taszarek et al., 2021). However, these modelled decreasing thunderstorm trends are shown to be regionally-dependent (e.g. Trapp et al., 2009; Brooks et al., 2016).

Precipitation extremes and atmospheric moisture

A warmer global climate is expected to increase the severity of precipitation extremes because of principally the extent to which warmer global (and regional) temperatures enhance atmospheric water vapor (Allan et al., 2022; Neelin et al., 2022; Zhou et al., 2023). This temperature-moisture relationship is shown to follow an exponential trend, with global atmospheric water vapor rising by about 7% for every degree Kelvin of global warming under constant atmospheric pressure, as described by the Clausius-Clapeyron relation (Donat et al., 2013). Such increases in moistening suggest that any precipitation event can potentially yield approximately 7% more total precipitation for every degree Kelvin/Celsius of global warming. Correspondingly, this would enhance the likelihood for intensified flooding events due to the more substantial precipitation rates that would occur with humidification, such as in South and East Asia during the wet monsoonal period (e.g. Lee et al., 2018), or over the course of tropical cyclones (Stansfield & Reed, 2023). In tandem with this increase, studies have similarly shown that global precipitation extremes scale approximately linearly with temperature, increasing appreciably for every degree Celsius of warming (Aleshina et al., 2021), though other studies have argued that such a relationship may be too rudimentary for the realistically complex nature of the events that give rise to precipitation extremes (e.g. Pendergrass et al., 2019). While global mean precipitation can be described as proportionally increasing with temperature, extreme precipitation specifically may respond in non-linear ways, especially in the tropics (Pendergrass et al., 2019). However, the extent of non-linearity in extreme precipitation varies with the climate model used and is more apparent in the

tropics, though the most distinct non-linear response in Rx1day precipitation was shown in the CESM1 model among CMIP5 models (Pendergrass et al., 2019).

Although the extent of research is restricted for the most intense precipitation extremes, some studies have shown that such events may increase by as much as 95% per degree Kelvin of global warming, which well exceeds the 7% per degree Kelvin increase described in the Clausius-Clapeyron relation (Liu et al., 2009; Utsumi et al., 2011). Such super Clausius-Clapeyron relations were similarly shown in India for dewpoint temperature historically over the 1979-2015 period (Mukherjee et al., 2018), as well as with respect to extreme precipitation in the contiguous United States over 1950-2009 (Mishra et al., 2012). Super Clausius-Clapeyron relations have also been documented for stratiform precipitation extremes, which scaled strongly linear with surface air temperature in Russia over the 1966-2017 period, though globally, linear scaling similar to the Clausius-Clapeyron relationship was found for precipitation extremes (Aleshina et al., 2021). The role that humidity in the atmosphere plays is instrumental for the successful formation of multiple forms of weather extremes; this includes severe thunderstorms, tropical cyclones, wet monsoonal rainfall, and the mid-latitude cyclones that give birth to other types of extremes, such as snowstorms and ice storms, making humidification central in the study of future trends of such events collectively.

The TCRE framework

The TCRE has been widely adopted for examining the response of temperature to cumulative carbon emissions and is regarded as a highly effective framework in climate science and policy in terms of explaining trends in climate impacts (Frolicher & Paynter,

2015). The TCRE is a quantity that describes principally the linear increase of global mean temperature to cumulative CO_2 emissions (Matthews et al., 2009; Gillett et al., 2013; Jones & Friedlingstein, 2020). It may also be described as the rate of change in globally averaged surface temperature per unit of CO_2 emissions (de Mora et al., 2023). The collective response of (global) temperature is the combination of the TCRE and non-CO_2 greenhouse gas emissions, which is represented in future climate scenarios, such as the Representative Concentration Pathways (RCPs). As a result, the TCRE represents the response to CO_2 emissions only.

The TCRE has significant potential to effectively communicate climate impacts expected at a variety of warming targets because of its ability to relate the response of these impacts to cumulative CO_2 emissions directly, which can be useful in sectors such as climate adaptation and mitigation. In light of its effectiveness to show the linear response of temperature in relation to CO_2 emissions, the applications of the TCRE have further proved useful in estimating the response of other climate indicators. For example, the TCRE, as mentioned previously, has been applied to assess the future response of winter sea ice to cumulative carbon emissions (e.g., Zickfield et al., 2012). The TCRE has further been shown to be useful for estimating patterns of temperature change at the regional scale with emissions, as well as seasonally (Leduc et al., 2016; Partanen et al., 2017). For instance, Partanen et al. (2017) showed regional TCRE estimates of precipitation at 5.5 Celsius and 2.0 Celsius warming in the Arctic during Northern Hemisphere winter and summer, respectively. Other studies have previously used the TCRE to examine the response of temperature extremes and regional precipitation changes to cumulative emissions. Partanen et al. (2017) used the TCRE to quantify precipitation trends across

several regions; in Northeastern Africa, for example, they found that precipitation increased by 40% per teraton of carbon (TtC) emitted. Chavaillaz et al. (2019) showed regional TCRE estimates of extreme heat exposure, with heat exposure over land increasing linearly with cumulative carbon emissions, which includes an 18-19 K-day increase per TtC above the deadly heat exposure threshold.

GEV applications to precipitation extremes

The applications of GEV analysis in the climate change impacts literature are quite extensive. GEV is further widely used across a plethora of fields to evaluate extremes and predict changes in their behavior over time. As an extension to EVT, some studies have previously employed GEV analyses to examine the extent to which extreme rainfall may change over time at the regional scale. For example, Gentilucci et al. (2023) used a GEV framework to identify pattern changes in precipitation extremes over time in Eastern Italy. Other studies have fitted a GEV to identify trends in specific return levels of precipitation thresholds in South America and Africa (e.g., Fullhart et al., 2023), as well as using a GEV to model winter precipitation extremes in relation to ENSO (Mahajan et al., 2023) and their impacts on atmospheric rivers (e.g. Singh et al., 2023). GEV analyses also showed that the 5- to 500-year return periods corresponding to 1- to 5-day maxima increase by 10% to as much as 35% with anthropogenic warming (e.g. Mukherjee et al., 2018). In a historical analysis, Van den Besselaar et al. (2016) further found that European 20-year Rx1day and Rx5day maxima become more frequent towards the end of the 1951-2010 period relative to the first 20 years of that period. Outside of precipitation extremes, heat waves or extreme temperatures have received considerable attention in EVT. The GEV framework,

for instance, has been used to examine changes in heat wave probability in certain regions, such as in the Yangtze Basin (Yuan, 2023) or Western North America (e.g., Bjarke et al., 2023). The impacts of such heat extremes are likely to be most amplified in population-dense centers, such as in China, India and Pakistan (e.g., Ullah et al., 2023), as well as in other major populated areas globally.

Framing extremes with the remaining carbon budget

The global carbon budget has become a central concept in climate science that has helped developed better understanding of the global carbon cycle, as well as being instrumental in shaping climate policies and offering a dimension for predicting future climate impacts (Le Quére et al., 2018).

Carbon budgets have become more widely recognized since the IPCC Fifth Assessment Report (AR5) and are more heavily integrated in the climate policy-making framework (Lahn, 2020). A useful variant of the broader concept of carbon budgeting, called the remaining carbon budget, is based on the assessment of the allowable additional carbon emissions that can be emitted into the future while limiting global warming below specified temperature targets (Matthews et al., 2020; Matthews et al., 2021).

A remaining carbon budget may be calculated based on the TCRE of a given climate indicator, in addition to the response of these indicators to greenhouse gas emissions other than CO_2 (Tokarska et al., 2020). These budgets, thus, can serve as a useful tool for determining the extent of cumulative carbon emissions that can be emitted to avoid critical thresholds (of warming) relative to the pre-industrial period (or other baseline periods of

interest) which are subsequently needed to avoid specified climate impacts and meet climate targets (e.g. van der Ploeg, 2018; Rogeli et al., 2019).

Similarly, the remaining carbon budget can have useful applications with respect to specified climate indicators of interest, such as precipitation (e.g. Rodrigues et al., 2021). Bauer et al. (2023), for example, examined climate impacts, including heat exposure and marine ecosystem degradation, when overshooting those carbon emissions associated with the 1.5 C temperature threshold relative to the pre-industrial period. Baker et al. (2018) found that the increase in atmospheric CO_2 emissions directly impacts climate extremes in the Northern Hemisphere, such as heat stress, tropical precipitation and temperature extremes, even with a low climate response. This suggests that weather extremes collectively can be sensitive to even small amounts of additional carbon emissions and, thus, relatively small remaining carbon budgets to reach certain thresholds of extremes. To another end, studies have used carbon budgets to determine when the transition to widespread renewable energy use needs to be made in order to avoid specified warming targets (e.g. Howard et al., 2018).

However, caution should be exercised when using the (remaining) carbon budgeting concept, since the degree of uncertainty is large, much of which comes from biogeochemical Earth system uncertainty (Jones & Friedlingstein, 2020), as well as internal variability (Tokarska et al., 2020), and the uncertainties that stem from the choice of methodological framework and assumptions used to calculate them (e.g. Matthews et al., 2020). How much remaining carbon budgets increase or decrease further heavily depends upon the choices humans make with respect to reducing the extent of non-CO_2 forcings (Matthews et al., 2021).

Chapter 3: Linking historical and projected trends in extreme precipitation with cumulative carbon dioxide emissions

This chapter was published as:

Moore, T. R., Matthews, H. D., & Chavaillaz, Y. (2023). Linking Historical and Projected Trends in Extreme Precipitation with Cumulative Carbon Dioxide Emissions. *Atmosphere-Ocean*, 1-18. https://doi.org/10.1080/07055900.2023.2259328

Abstract

Extreme weather events are expected to increase in frequency and intensity in response to higher global temperatures, augmenting societal exposure to these events. While the magnitude of projected changes in extremes varies considerably among future emission scenarios, a large part of this uncertainty is driven by the choice of scenario, rather than by the climate response to a particular emission scenario. A growing body of research has identified robust linear relationships between climate changes and cumulative carbon emissions; for global average temperature change, this relationship is known as the transient climate response to cumulative carbon emissions (TCRE). Extensions of the TCRE framework to other variables, such as regional and seasonal temperature and precipitation changes, have also shown to be effective, raising the possibility that changes in weather extremes could be linked to cumulative carbon dioxide (CO_2) emissions. Here, we estimate changes in historical and projected trends in one-day (Rx1day) and five-day maximum precipitation (Rx5day) events as a function of cumulative carbon emissions across a range of future emission scenarios and global climate models. Our results show that median Rx1day and Rx5day generally increases linearly with increasing cumulative emissions, consistent with studies that have previously employed the TCRE framework to estimate changes in precipitation extremes, as well as other climate indicators. Overall, we show that a linear response to cumulative CO_2 emissions is a good approximation for both historical and future trends in precipitation extremes.

Keywords: Extreme weather; climate change; global warming; extreme precipitation; climate crisis; greenhouse gases; flood; severe thunderstorms

Introduction

Although rare phenomena relative to a given climatology, weather extremes frequently yield significant short- and long-term impacts in the regions that they affect. Impacts from such events are often manifested economically, environmentally, culturally, and even psychologically; many of which that can last for years to even decades (Bergquist et al., 2019; Franks & Moore, 2021). However, such events are expected to become less exceptional as global/regional temperature continues to warm (IPCC, 2021; Estrada et al., 2021).

Extreme precipitation is a form of weather extreme that has received considerable attention in climate science in recent decades (Khandakar, 2013), since they are among some of the most impact-relevant consequences of climate change (Pfahl et al., 2017; EPA, 2017). There exists a variety of definitions that express what constitutes extreme precipitation across the body of climate impacts literature, causing a range of differences in the response of these extremes to warming (Pendergrass, 2018). Furthermore, what is considered as extreme varies geographically in relation to a given location's or region's climatology. For example, a location that normally does not receive snowfall may consider a light snowfall as an extreme event. Extreme precipitation may further be divided into separate categories of events. For instance, an event may exhibit abnormally high precipitation rates that lead to significant amounts of surface water accumulation over a short period of time. For these reasons, the Intergovernmental Panel on Climate Change Sixth Assessment Report (IPCC AR6) defines a weather extreme as some event that is rare relative to a specified time of the year and location/region in question (Seneviratne et al., 2021).

Precipitation extremes frequently create conditions suitable for flash-flooding, as well as in situations of previously saturated ground, high water levels and unseasonably wet conditions that may be in place prior to these events. In other cases, precipitation may occur at lighter rates but persist over an extended period of time, such as over a succession of days because of atmospheric blocking. This may similarly induce conditions suitable for significant water accumulation and, thus, may be classified as an extreme event.

Assessing the response of these events to a changing climate is, therefore, critical due to the significant impacts that can result from heavy to extreme precipitation, ranging from coastal and inland flooding and landslides (Ban et al., 2017) to enhanced soil water stress in terrestrial ecosystems (Knapp et al., 2008) and waterborne diseases (Curriero et al., 2001). Tropical cyclones are also commonly a source of extreme precipitation that may lead to extensive coastal and inland flooding. Globally, these tropical systems could intensify in a warmer climate, in part by producing more significant rainfall rates (e.g. Knutson et al. 2010; Moore et al., 2015).

Several studies have previously documented trends in precipitation extremes in recent decades, as well as in the context of future warming. The northeastern United States, for example, observed an increase in extreme precipitation over the last 15 years, mostly associated with frontal boundaries of mid-latitude cyclones, as opposed to precipitation related to tropical cyclones (Collow et al., 2017). Similarly, extreme daily precipitation events and rainy days were shown to increase over a 70+ year period in Sao Paulo (Zilli et al., 2017), as well as in Indonesia, from 1983 to 2012 (Tangang and Aldrian, 2017). Bush et al. (2019) also mentioned that Canada's precipitation extremes are expected to increase into the future, though the observations do show more inconsistencies throughout the country with respect to the changes in short-duration extreme precipitation events. The IPCC Managing the Risks of Extreme Events and

Disasters to Advance Climate Change Adaptation (SREX) further stated high confidence in a likely increase in heavy precipitation events across North America since 1950 (Seneviratne et al., 2012; Kirchmeier-Young & Zhang, 2020). The return periods of extreme precipitation were additionally shown to be reduced over the 20th century, with a global increase in extreme precipitation of about 6% per degree in a Coupled Model Intercomparison Project Phase 5 (CMIP5) model ensemble (Kharin et al., 2013), consistent with the Clausius-Clapeyron relationship (e.g. Pall et al., 2007). Pfahl et al. (2017) showed that, by itself, thermodynamics in a warmer climate would cause a uniform fractional increase in heavy to extreme precipitation events, though more regional variations were found in dynamically-constrained scenarios. The increase in the most extreme precipitation events among several Australian cities also scaled more significantly than near-surface water vapor in a warmer future climate (Bao et al., 2017). Using indices pertaining to extreme weather in CMIP5 multi-model datasets, the most intense precipitation extremes were documented to substantially increase in Australia by the end of the century relative to present-day (Alexander and Arblaster, 2017). However, for validating the skill of CMIP5 models simulating extreme precipitation at regional scales, natural variability and observed seasonality are paramount. For example, Janssen et al. (2016) showed that climate change model experiments from CMIP5 models tended to overestimate and underestimate observed spring and summer extreme precipitation across the United States, causing a magnification in errors with projections.

The transient climate response to cumulative carbon dioxide (CO_2) emissions (TCRE) has recently received more recognition as a useful tool to assess the response of global mean surface temperature to global cumulative CO_2 emissions. The TCRE may be defined as the ratio of global mean surface air temperature to cumulative CO_2 emissions, taking into account

physical climate processes, and land and ocean carbon sinks (Matthews et al., 2009; Gillett et al., 2013; Simmons and Matthews, 2016; Leduc et al., 2016). It was previously shown that the TCRE could have a useful methodological framework because of its ability to directly relate global warming to emissions. It can, therefore, be a means to more flexibly communicate climate changes for mitigation policy purposes and be used as a metric for comparative analyses of carbon-climate models (Gillett et al., 2013). The TCRE has been extensively mentioned in the IPCC Fifth Assessment Report (AR5) and AR6 as distinctly outlining the proportionality between temperature and cumulative CO_2 emissions across several climate models (Friedlingstein et al., 2014; Rogeli et al., 2018; Canadell et al., 2021). For this reason, it has been a useful metric to estimate carbon budgets and identify critical levels of cumulative emissions that correspond to dangerous global warming thresholds relative to pre-industrial levels (Matthews et al., 2020; Matthews et al., 2021).

The response of higher global temperatures has been extensively shown to be virtually independent of emission pathways and approximately linear to cumulative CO_2 emissions across a range of emission scenarios in carbon climate model simulations (Gillett et al., 2013). This robust proportionality between surface air temperature change and cumulative CO_2 emissions was confirmed by other studies (e.g. Krasting et al., 2014) and was shown to be similarly robust at regional scales, both over land and ocean (Leduc et al., 2016). Applications of the TCRE framework have also been used in the assessment of extreme heat (e.g. Chavaillaz et al., 2019).

The TCRE further has the potential to assess trends in precipitation. Previous studies have examined the extent to which precipitation extremes scale with global warming (e.g. Seneviratne et al., 2016; Wartenburger et al., 2017; Partanen et al; 2017; Kharin et al., 2018; Tebaldi & Knutti, 2018). In their study, for instance, Partanen et al. (2017) demonstrated that

precipitation scaled similarly with global cumulative carbon emissions, including a 30-40% increase per teraton of carbon (TtC) in northeastern Africa in a regional TCRE analysis across a suite of CMIP5 models. Donat et al. (2016) also found that average extreme precipitation scaled approximately linearly with model-specific global temperature change in dry regions.

In this study, we present an analysis of extreme precipitation that is framed in the context of cumulative emissions in order to determine whether global extreme precipitation may be scaled linearly with increasing cumulative emissions. Part of the motivation of this work comes from the conceptual framework between cumulative emissions and precipitation extremes that can be inferred from this existing literature. However, the primary goal of our study is to estimate extreme precipitation with cumulative (carbon) emissions from a consistent set of models. This work could, therefore, be a useful contribution for understanding to what extent the TCRE could be applied to indicators of precipitation extremes at a variety of spatial scales.

Methodology

In this section, we describe in detail the methods used in this study. We begin with a description of the extreme precipitation data considered, followed by some discussion pertaining to the global climate models (GCMs) considered here, as well as model interpolation procedures. We then discuss the statistical tests selected to analyse the data.

Data and scenarios

Daily precipitation data relevant to this study was available in nine GCMs that were a part of a CMIP5 ensemble. While we acknowledge that Coupled Model Intercomparison Project Phase 6 (CMIP6) Earth System Models represent an improvement in the representation of the carbon cycle, as well as for simulations of precipitation extremes where notably significant

variations in topography exist (Seneviratne et al., 2021), the selection of GCMs here was based on Gillett et al. (2013) and Chavaillaz et al. (2019). Therefore, this involved selecting models whose output included both daily precipitation and the carbon cycle variables required to diagnose cumulative CO_2 emissions. We also used CMIP5 data due to its availability at the time this project started, and to be consistent with the related work of Chavaillaz et al. (2019). However, the medium-resolution version of the MPI model (MPI-MMPI-ESM-MR) was the only model that had precipitation data available for the 1pctCO_2 scenario, and so we excluded this model from our analysis to ensure the use of the same set of model simulations across scenarios. As such, the nine GCMs for which data were extracted are as follows: CanESM2, IPSL-CM5A-LR, IPSL-CM5A-MR, IPSL-CM5B-LR, MPI-MMPI-ESM-LR, MOHC-HadGEM2, MIROC-ESM, NOAA-GFDL-ESM2G, and NOAA-GFDL-ESM2M.

Cumulative emissions are calculated from the changes in oceanic, land and atmospheric pools and do represent fossil fuel emissions only. These three principal pools represent carbon stocks that are contained in the ocean, land and atmosphere. These carbon stocks flow between the ocean, land and atmosphere as fluxes through complex biophysical and geochemical processes as part of the global carbon cycle (e.g. Rackley, 2017). There were three scenarios considered for this study: "1pctCO_2", "rcp45", and "rcp85". This represents one percent CO_2, Representative Concentration Pathways 4.5 (RCP 4.5) and Representative Concentration Pathways 8.5 (RCP 8.5), respectively. The 1pctCO_2 scenario (140 years) denotes a scenario where the atmospheric CO_2 concentration increases by one percent per year until CO_2 quadruples relative to the pre-industrial period. The two RCP scenarios (90 years, from 2006 to 2095) are defined based on greenhouse gas concentrations and represent two different future climates by the year 2100. The greenhouse gas trajectory depends upon the extent to which greenhouse gases

are released into the atmosphere over time. RCP 4.5 is a scenario that is defined by stabilizing and then declining emissions, such that radiative forcing is limited to 4.5 watts per meter squared (W/m^2) by the year 2100. This pathway is characterized by emissions increasing until approximately the year 2040 prior to declining thereafter. In the case of the RCP 8.5 scenario, emissions will continue to increase throughout the 21st century, leading to a radiative forcing of 8.5 W/m^2 by the year 2100. In light of these scenario differences, 1pctCO_2 is an emission scenario that represents the climate system's response to atmospheric CO_2 only, while the RCP scenarios reflect a more collective response to both CO_2 and other greenhouse gases and aerosols, as well as those emissions originating from land use changes. As a result, the TCRE represents the climate response in 1pctCO_2, whereas in the RCP scenarios, the response is a combination of the TCRE and other contributions. Finally, the historical period used in this study spans 145 years (1861-2005), following the beginning of the pre-industrial period.

Climate indicators and model interpolation

We isolated the largest value among daily maximum values for each year, effectively extracting the 'most extreme' annual maxima globally for each model and scenario. We also obtained five-day maximum values using the original daily data available. These newly created indicators are hereafter known as "Rx1day" and "Rx5day" and are used herein to define what constitutes precipitation extremes, which includes all types of precipitation.

We regridded Rx1day and Rx5day data to a common grid that corresponds to that of the CanESM2 model, which was the coarsest grid amongst the available nine (9) CMIP5 models. Once converted, all Rx1day and Rx5day values were interpolated onto a resolution defined by grid cells that were each the size of 2.8 degrees longitude by 2.8 degrees latitude. To account for

gridding inconsistencies in surface area extent between the equator and the poles, we calculated weights for Rx1day and Rx5day across each raster layer by using the cosine of latitude. We then derived the maximum values across each grid cell for each year and then averaged across those to derive annual estimates of global, regional and local precipitation, as needed. As such, we computed annual means for Rx1day and Rx5day across each grid cell on the Earth's surface for each year, similar to the procedure employed by Seneviratne et al. (2016) for heavy precipitation. This was repeated for each of the GCMs considered for this study. We follow the same procedure for each emissions scenario, as well as for the historical period. We then calculated the difference between the 30-year mean at the beginning of the historical and the 30-year mean centered around 1 TtC of cumulative emissions (Figure 1). The spread of trends across models represents our range of uncertainty, and we present the model range of percent changes at 1 TtC (Tables 1-3).

Statistical tests

All statistical analyses were performed using R software. For this study, we used simple linear regression modelling. Linear regression was used herein to assess the effect of cumulative emissions on extreme precipitation by deriving rates of change of precipitation extreme indicators per TtC of cumulative emissions and associated standard errors that are based on model medians. We, therefore, infer trends that are centered on the regression line corresponding to the model medians in our study. Since the response of extreme precipitation could be assumed to follow linearity, it was, thus, relevant to also use Pearson correlation analysis. Following Chavaillaz et al. (2019), we assumed that the response of extreme precipitation was linear if the correlation coefficients and *p*-values were sufficiently strong. Though we acknowledge that a Pearson correlation coefficient of less than one (1) could be attributed to noise, or a functional

non-linear relationship, we consider in this study that high correlation coefficients reaching/exceeding 0.75 are inferred as a linear relationship, and if *p*-values were at or below 0.01 with respect to the linear regression model.

National and local selection

In the next stage, we selected specific regions to specific locations of interest to assess similarities and/or differences in the response of extreme precipitation at those larger scales relative to global trends. First, we isolated land and ocean only to spatially average extreme precipitation values over either land or water. While somewhat arbitrary, our selection of nations (and specific locations) was on the basis of appreciably large percent change increases in extreme precipitation at one TtC among scenarios, relative to the beginning of the historical period (Figure 1). Our choice was also partly based on locations with larger population density, recent significant to catastrophic precipitation events, lower elevation relative to sea level, and/or their proximity to large bodies of water that could all contribute to exacerbating impacts associated with intensified precipitation extremes in the future. This selection is, therefore, meant to be illustrative of changes in precipitation extremes that can be expected at certain regions and locations as a function of cumulative emissions. This could also be potentially useful for policymakers who are interested in planning for adaptation needs in relation to future precipitation extremes, given some expectation of future global emissions trends. Further, there is scientific interest to explore to what extent the linearity of the relationship that we find at the global scale could extend to specific regions, and at the grid cell. As such, the following 12 nations/regions were chosen for this study: Canada, United States, Japan, Brazil, India, South Africa, Australia, Sweden, Russia, China, Indonesia, and the North-central tropical Pacific.

As mentioned, we then extended the analysis to more localized areas to determine trends at those spatial scales. These locations typically occupied spaces at the grid cell, or a small grouping of cells. This meant that local-scale selections could be a combination of small countries occupying only a few grid cells, or a single cell. These were aggregated by spatially averaging across only those grid cells. The selected 10 locations were as follows: New York City, Philippines, Guyana, Montreal, Florida, Paris, Madagascar, Hong Kong, St. Louis, and Melbourne. For situations where we select cities for our analysis of local-scale trends, we note here that our focus is on the grid cell that surrounds those cities, as opposed to the cities themselves. Further, while we acknowledge that other locations and/or small countries could face increased vulnerability to precipitation extremes, we use this selection as a representation of potential impacts elsewhere at more localized scales. While we did not consider specific thresholds for population density, elevations relative to sea level, and the sizes of water bodies, we selected representative areas that could potentially experience increased negative impacts linked to precipitation extremes. For example, the New York City region is very densely populated, is only slightly above sea level and is located in close proximity to the Atlantic Ocean. Guyana is a nation that is conversely not so densely populated, but most of its population resides near the Atlantic Ocean, and the capital of Georgetown lies modestly below sea level. The Montreal region is generally well above sea level, but it is a densely populated area that is surrounded by two rivers, with Rivieres-Des-Prairies flooding many areas twice in a very small period of time, both in 2017 and shortly again in 2019, as a result of partly significant amounts of precipitation. Therefore, though we did not consider flooding risk directly in our analysis, we included these selected locations and regions as representative areas with particular vulnerability to extreme precipitation that may be compounded by their low elevation relative to sea-level.

All statistical results for global, regional and local trends are summarized in Tables 1-3, with extreme precipitation trends shown graphically as line plots in the results section.

Results

Global TCRE patterns of extreme precipitation

Figure 1 shows global patterns of percent changes in Rx1day and Rx5day, highlighting a general global increase in precipitation at around 1 TtC relative to the 30-year mean at the beginning of the historical period. Under the RCP scenarios, we found up to a 90-100% increase in Rx1day at 1 TtC in the central equatorial Pacific, and up to 60% with respect to 1pctCO_2 in this region. Thus, the central equatorial Pacific represents the greatest rates of increase for Rx1day, but we also found other significant increases in North-central Africa, South Asia, portions of Indonesia, as well as central Antarctica and North of the Arctic Circle among the RCP scenarios. In the case of Rx5day, overall much lower rates of increase are shown, with most areas displaying up to a 10% increase across scenarios. However, we found similarities in the global to regional patterns that are highlighted for Rx1day. For example, the largest rates of increase consistently occur in the central equatorial Pacific across scenarios, as well as in North-central Africa, where up to a 50-60% increase at 1 TtC is shown. Elsewhere, we consistently found decreases of up to 30-40% at 1 TtC, with the largest rates shown in the Northern (sub-) tropical Atlantic, as well as portions of the Middle East and extreme Northern Africa for both Rx1day and Rx5day. Similar decreases are uniformly shown across the Southern Hemisphere sub-tropical high pressure belt in oceanic regions for both precipitation indices. Notably, the greatest decreases were in the Southern portion of the (sub-) tropical Eastern Pacific and

Atlantic. We also found decreases in the oceanic region West of Australia though with generally larger decreases in Rx5day (up to 20%) than for Rx1day (up to 10%).

The broad area in the central equatorial Pacific displaying the sharpest increases for both Rx1day and Rx5day among scenarios may be the result of increased moisture availability and evaporation across most regions under the higher global temperatures expected at 1 TtC of cumulative emissions, likely contributing to intensified (deep) convection. For this reason, the robust increasing signal over the East-central equatorial Pacific may further be related to higher sea-surface temperatures at higher background emissions, possibly in response to more El Nino events that comprise the El Nino Southern Oscillation (ENSO) (e.g. Moore et al., 2015). A change in the size and strength of the Intertropical Convergence Zone (ITCZ) may also contribute to the enhancement in extreme precipitation consistently found across scenarios in this region (e.g. Byrne & Schneider, 2016). Conversely, the consistent decrease in our precipitation indices in oceanic sub-tropical regions may be attributed to intensified and expansive sub-tropical high pressure over oceanic regions as global temperatures warm at higher emissions (e.g. Schmidt & Grise, 2017).

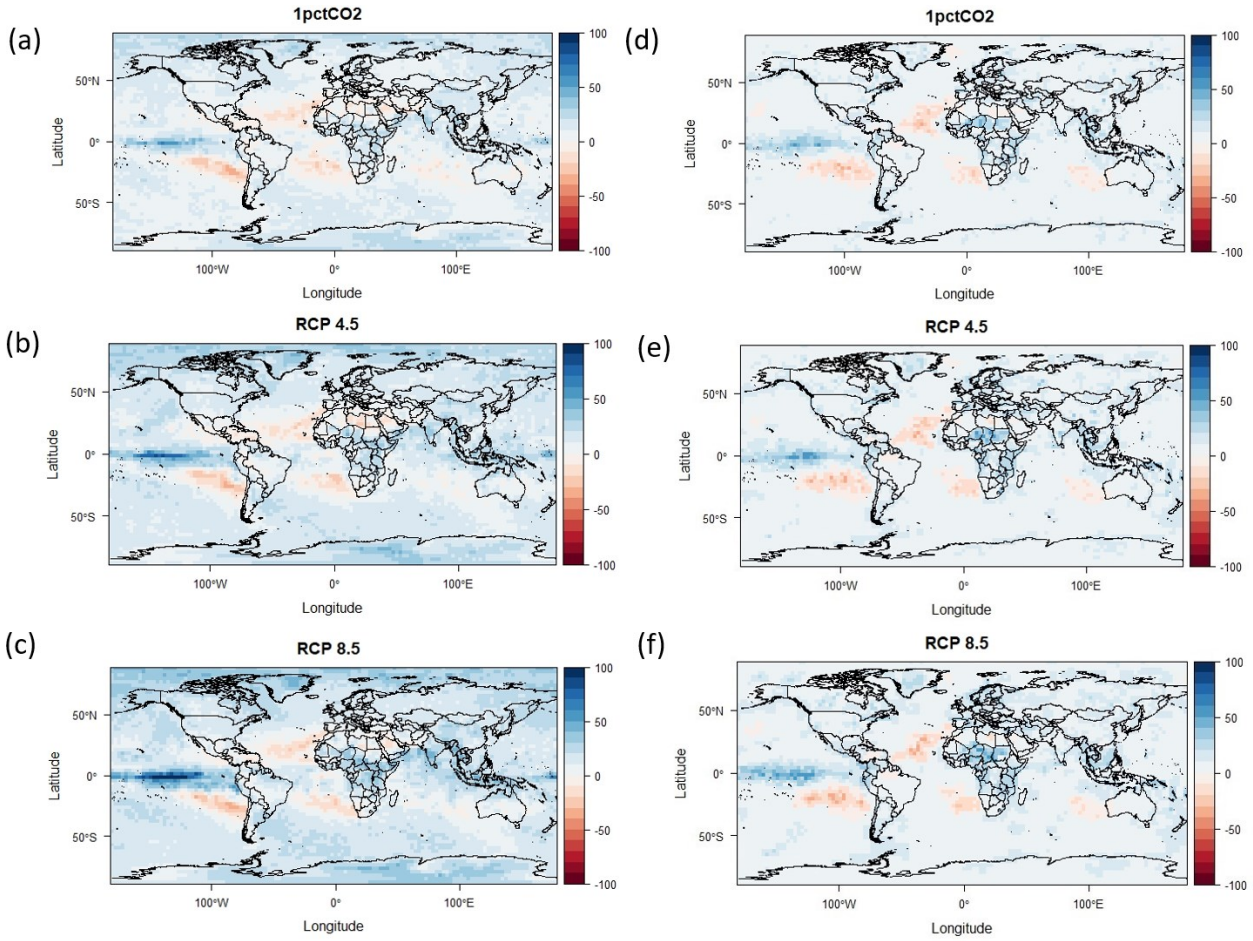

Figure 1. Percent change in global Rx1day (a-c) and Rx5day (d-f) under the 1pctCO_2, RCP 4.5 and RCP 8.5 scenarios based on the difference between the 30-year model mean precipitation at around 1 TtC of cumulative emissions relative to the historical first 30-year model mean precipitation.

Statistical results for median global extreme precipitation are summarized in Table 1. Global extreme precipitation increases linearly (Figure 2) in response to cumulative carbon emissions for all emissions scenarios for Rx1day and Rx5day across most of the global climate model simulations considered in this study. Global median extreme precipitation trends exhibit robust linearity for Rx1day and Rx5day for all of the scenarios (Figure 2, Table 1) and are highly statistically significant, as well as for the historical period ($p < 0.01$, Table 1). Indeed, we found correlation coefficients greater than 0.75 across all emissions scenarios for both our extreme

precipitation indicators (Table 1). Linearity is especially strong for the 1pctCO_2 and RCP 8.5 scenarios ($r >= 0.90$). The more enhanced linearity that we found under the 1pctCO_2 and RCP 8.5 scenarios is a reflection of the larger extents of warming and higher signal-to-noise ratio. Indeed, global median Rx1day, under the 1pctCO_2 and RCP 8.5 scenarios, increases by an average of 7.11% and 14.78% per TtC, respectively. Similarly, global median Rx5day increases by 4.18% per TtC for 1pctCO_2, and an 8.36% per TtC increase under the RCP 8.5 scenario. With respect to the historical period, the results show a significant linear increase for median Rx1day ($r = 0.80$, Table 1), where precipitation increases by an average rate of about 12% per TtC. This is larger than the increase shown by 1pctCO_2 but less than RCP 8.5, and similar to RCP 4.5. Further, this reflects a mean increase that is approximately 5% less per TtC in the RCP 4.5 scenario relative to the historical period, and a ~3% increase per TtC in median Rx1day in the RCP 8.5 scenario. This is similarly shown for global Rx5day, where the mean increase per TtC in the historical period is larger than in the 1pctCO_2 and RCP 4.5 scenarios. For both median Rx1day and Rx5day, the mean increase per TtC was highest for the RCP 8.5 scenario, with an increase of 14.78% and 8.36%, respectively.

Regional TCRE patterns in extreme precipitation: Land and oceanic regions

The results show that both median Rx1day and Rx5day increase linearly per TtC across all emissions scenarios for land and ocean (Figure 2, Table 1). For all scenarios, this increase is significant within the 1% significance level, and linearity is shown to be large (Figure 2, $r > 0.75$), with the exception of ocean median Rx5day under RCP 4.5. In particular, the increase was substantial for land for the RCP 4.5 and RCP 8.5 scenarios for median Rx1day, where precipitation increased by 12.08% and 13.58% per TtC, respectively (Table 1). For ocean, the increase was notably high for median Rx1day under RCP 4.5 (12.79%) and RCP 8.5 (15.16%).

For the RCP 8.5 scenario, we found a strong linear increase ($r > 0.79$) for Rx1day, where precipitation increased by 12.69% per TtC ($p < 0.01$, Table 1).

Table 1. Trends for global, land and ocean median Rx1day and Rx5day for the 1pctCO_2, RCP 4.5 and RCP 8.5 emissions scenarios, and for the historical period. Findings are given as mean percent changes per TtC based on linear regression analyses, and Pearson correlation coefficients are provided. The model range at 1 TtC is also reported. *, ** and *** indicates results that are statistically significant at or within the 10%, 5% and 1% significance levels, respectively.

Emissions scenario	Change	% change per TtC	Standard error	Pearson's correlation coefficient r	Model range at 1 TtC
Global extreme precipitation					
Rx1day					
1pctCO_2	Increase***	7.11	0.11	0.98	0.33 to 12.50
RCP 4.5	Increase***	12.62	0.58	0.92	5.92 to 23.44
RCP 8.5	Increase***	14.78	0.27	0.99	4.60 to 27.59
Historical	Increase***	12.02	0.75	0.80	-1.20 to 13.12
Rx5day					
1pctCO_2	Increase***	4.18	0.16	0.92	-1.17 to 9.97
RCP 4.5	Increase***	7.17	0.68	0.75	4.77 to 16.35
RCP 8.5	Increase***	8.36	0.35	0.93	3.57 to 29.89
Historical	Increase***	7.45	1.01	0.53	0.62 to 14.71
Land extreme precipitation					
Rx1day					
1pctCO_2	Increase***	6.75	0.12	0.98	-1.49 to 16.09
RCP 4.5	Increase***	12.08	0.51	0.94	4.69 to 20.99
RCP 8.5	Increase***	13.58	0.26	0.99	8.00 to 26.23
Historical	Increase***	9.92	0.88	0.69	-0.37 to 11.59
Rx5day					
1pctCO_2	Increase***	4.47	0.14	0.94	-0.65 to 15.17
RCP 4.5	Increase***	8.58	0.58	0.85	6.99 to 12.58
RCP 8.5	Increase***	8.08	0.32	0.94	1.88 to 37.52
Historical	Increase***	7.99	0.96	0.57	1.48 to 14.43
Ocean extreme precipitation					
Rx1day					
1pctCO_2	Increase***	7.23	0.13	0.98	0.78 to 12.78
RCP 4.5	Increase***	12.79	0.67	0.90	5.76 to 24.27
RCP 8.5	Increase***	15.16	0.32	0.98	3.35 to 28.05
Historical	Increase***	12.69	0.84	0.79	-1.41 to 13.63
Rx5day					
1pctCO_2	Increase***	4.07	0.19	0.88	-1.63 to 10.76
RCP 4.5	Increase***	6.61	0.84	0.64	3.43 to 18.31
RCP 8.5	Increase***	8.47	0.42	0.91	3.80 to 33.11

Historical	Increase***	7.24	1.17	0.46	-0.89 to 17.82

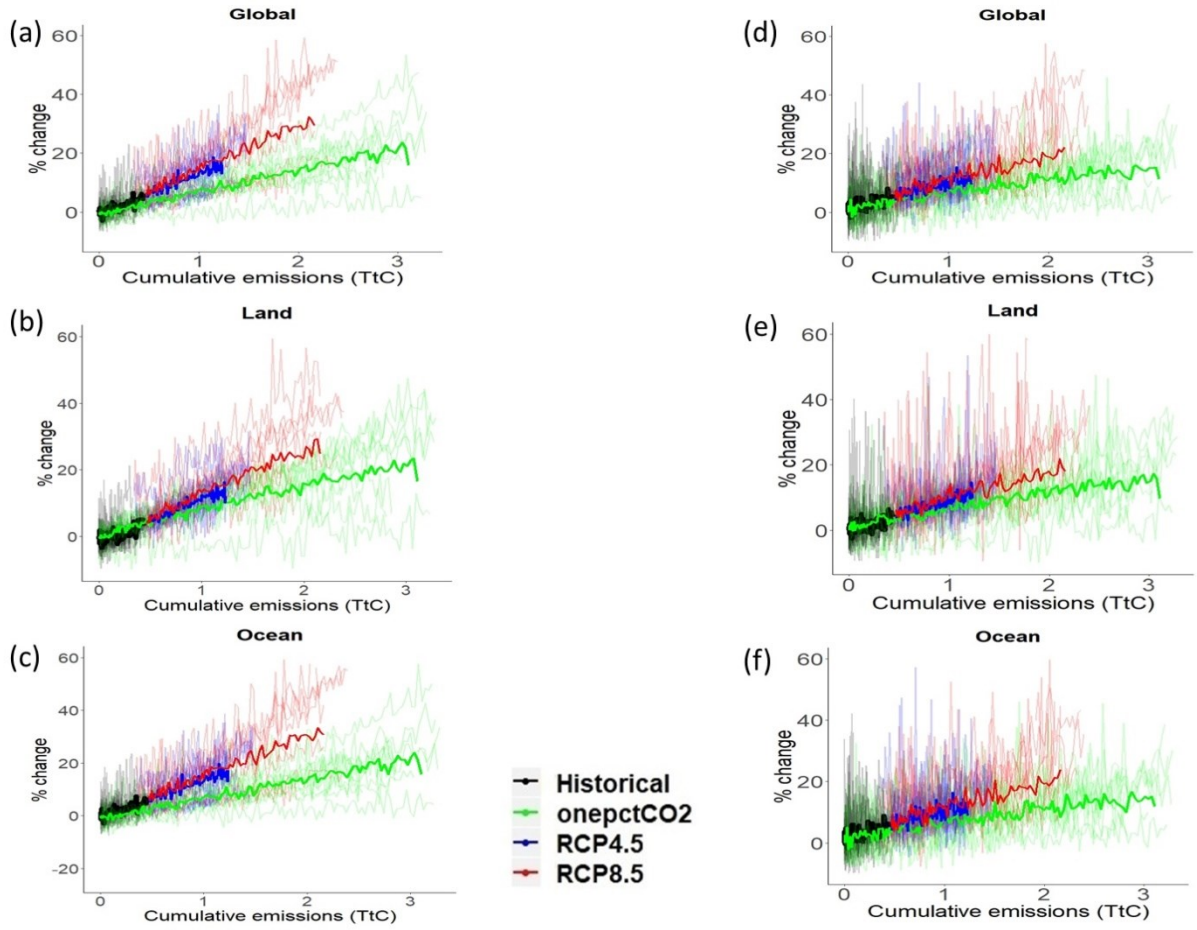

Figure 2. Global, land and ocean median trends for the historical period (black), and the 1pctCO_2 (green), RCP4.5 (blue) and RCP8.5 (red) scenarios for Rx1day (a-c) and Rx5day (d-f). Annual percent changes for the RCP scenarios, and the historical period are given. Percent changes for 1pctCO_2 are relative to Year 1 of that scenario. Trends for other individual model simulations are shown in the background for each scenario and represent the range of uncertainty.

Regional TCRE patterns of extreme precipitation: National/regional trends

To determine if robust linear trends exist at the regional scale, we examine trends for our selected 12 nations/regions.

Our results generally highlight statistically significant increases in median Rx1day and Rx5day across the selected nations/regions studied for all emissions scenarios, and for the historical period ($p < 0.01$, Table 2). The largest increases in precipitation mostly occur in the case of the RCP 4.5 and RCP 8.5 scenarios. For instance, Canadian Rx1day increased by an average rate of approximately 14%-15% per TtC for the RCP 4.5 and RCP 8.5 scenarios, which represents a 4-5% per TtC increase above what is shown in the historical period. We also found similar increases for median Rx5day for the RCP scenarios (Table 2).

The rate of increase was notably large for Rx1day. Among the nations/regions studied, Indonesia exhibited the largest value for Rx1day, with an increase of about 15%, 29% and 41% per TtC for the 1pctCO_2, RCP 4.5 and RCP 8.5 scenarios, respectively, all of which were highly statistically significant ($p < 0.01$). Historically, Rx1day in Indonesia increased by about 26% per TtC ($p < 0.01$). This signifies a rise of 3% and 15% per TtC under the RCP 4.5 to RCP 8.5 scenarios, respectively, reflecting a substantial increase under higher global cumulative emissions for this nation. India also showed large increases for its Rx1day under the RCP scenarios, with a rise of 24-27% per TtC. Japan similarly showcased substantial increases across the RCP scenarios for Rx1day, with rises of approximately 18% per TtC ($p < 0.01$). This represents a 10% increase per TtC relative to Japan's historical period. Brazil, Sweden, Russia, China, and the North-central tropical Pacific further had large increases in Rx1day (11-18% per TtC across these regions), with all being significant within the 1% significance level. Sweden notably had the largest increase in Rx5day among the regions studied, rising by 14-16% per TtC in RCP 4.5 and RCP 8.5 ($p < 0.01$). China additionally showed an average increase of 12% per TtC for Rx5day under the RCP 4.5 scenario, as did Russia, at 11-12% per TtC for the RCP scenarios ($p < 0.01$).

Among extreme precipitation indicators, linear trends were largely found across most regions/nations investigated in the case of Rx1day (Figure 3, Table 2). However, we found that linear tendencies were notably stronger for certain countries and scenarios. With the exception of Australia and South Africa, as well as in the case of Sweden's 1pctCO_2 trend, coefficients of > 0.75 for 1pctCO_2 and RCP 8.5 for median Rx1day were shown (Figure 3, Table 2). Among these, Canada, the United States, China, and Russia showed the most pronounced linear trends (r >= 0.90), with Russia exhibiting especially robust linearity for Rx1day for the RCP 8.5 scenario (r = 0.98), all of which were strongly statistically significant. We similarly found coefficients of > 0.75 for median Rx5day for Canada (RCP 8.5), the United States (1pctCO_2). and Russia (all scenarios), with Russia showcasing the highest coefficients.

Table 2. National trends for median Rx1day and Rx5day for the 1pctCO_2, RCP 4.5 and RCP 8.5 emissions scenarios, and for the historical period. Findings are given as mean percent changes per TtC based on linear regression analyses, and Pearson correlation coefficients are provided. The model range at 1 TtC is also reported. *, ** and *** indicates results that are statistically significant at or within the 10%, 5% and 1% significance levels, respectively.

Emissions scenario	Change	% change per TtC	Standard error	Pearson's correlation coefficient r	Model range at 1 TtC
Canada extreme precipitation					
Rx1day					
1pctCO_2	Increase***	7.94	0.20	0.96	2.70 to 22.07
RCP 4.5	Increase***	13.99	0.94	0.85	-4.64 to 13.97
RCP 8.5	Increase***	15.14	0.40	0.97	0.62 to 38.43
Historical	Increase***	10.55	1.23	0.59	-14.03 to 18.61
Rx5day					
1pctCO_2	Increase***	4.96	0.44	0.69	-11.56 to 16.44
RCP 4.5	Increase***	13.21	2.28	0.53	-6.43 to 29.78
RCP 8.5	Increase***	11.15	0.85	0.81	-55.12 to 35.61
Historical	Increase**	7.55	3.22	0.19	-25.23 to 41.32
United States extreme precipitation					
Rx1day					
1pctCO_2	Increase***	6.36	0.23	0.93	-9.78 to 15.24
RCP 4.5	Increase***	11.19	1.16	0.72	-0.40 to 27.36
RCP 8.5	Increase***	11.09	0.57	0.90	-0.04 to 24.36

Historical	Increase***	10.12	1.43	0.43	-13.22 to 10.87
Rx5day					
1pctCO_2	Increase***	4.40	0.33	0.76	-39.79 to 30.39
RCP 4.5	Increase***	8.71	1.89	0.44	-9.27 to 45.70
RCP 8.5	Increase***	8.68	0.87	0.73	-0.36 to 67.13
Historical	Increase***	8.50	2.60	0.24	-17.03 to 80.24
Japan extreme precipitation					
Rx1day					
1pctCO_2	Increase***	9.40	0.6	0.80	-5.28 to 86.22
RCP 4.5	Increase***	17.53	2.66	0.58	-4.68 to 33.86
RCP 8.5	Increase***	17.82	1.49	0.79	-9.21 to 76.84
Historical	Increase***	7.87	3.74	0.17	-20.62 to 21.99
Rx5day					
1pctCO_2	Increase**	5.27	0.67	0.56	-18.86 to 42.55
RCP 4.5	Increase***	8.50	3.21	0.27	-15.27 to 55.86
RCP 8.5	Increase***	10.49	1.56	0.58	-18.91 to 95.86
Historical	Increase***	14.60	4.43	0.27	-18.78 to 63.73
Brazil extreme precipitation					
Rx1day					
1pctCO_2	Increase***	7.08	0.42	0.82	-12.87 to 8.10
RCP 4.5	Increase***	11.69	2.03	0.52	-15.85 to 24.06
RCP 8.5	Increase***	14.30	0.89	0.86	-28.24 to 62.21
Historical	Increase***	6.06	2.25	0.22	-21.75 to 43.83
Rx5day					
1pctCO_2	Increase***	4.15	0.55	0.55	-8.24 to 43.24
RCP 4.5	Increase**	5.09	2.14	0.25	-25.38 to 22.61
RCP 8.5	Increase***	6.06	1.13	0.50	-30.57 to 39.60
Historical	Increase**	6.31	3.17	0.17	-13.54 to 53.69
Australia extreme precipitation					
Rx1day					
1pctCO_2	Increase***	3.27	0.57	0.44	-17.86 to 77.13
RCP 4.5	Increase***	10.45	2.86	0.36	-27.79 to 65.47
RCP 8.5	Increase***	4.99	1.30	0.38	-8.78 to 76.89
Historical	Increase***	9.38	3.44	0.22	-10.45 to 43.80
Rx5day					
1pctCO_2	Increase***	1.86	0.50	0.31	-9.86 to 41.31
RCP 4.5	Increase*	4.26	2.43	0.18	-19.93 to 39.72
RCP 8.5	Increase**	2.38	1.13	0.22	-43.19 to 36.22
Historical	No change	3.55	3.10	0.10	-8.44 to 25.47
India extreme precipitation					
Rx1day					
1pctCO_2	Increase***	16.03	0.89	0.84	-19.30 to 80.24
RCP 4.5	Increase***	23.72	3.04	0.64	-12.46 to 102.62
RCP 8.5	Increase***	26.79	1.58	0.84	-2.85 to 95.55
Historical	Increase***	12.96	3.92	0.27	-19.01 to 31.95

Rx5day					
1pctCO_2	Increase***	6.15	0.55	0.69	-9.97 to 80.66
RCP 4.5	Increase***	10.40	2.39	0.44	-19.39 to 62.73
RCP 8.5	Increase***	8.08	1.20	0.58	-42.47 to 53.04
Historical	No change	6.33	4.17	0.13	-20.88 to 44.26
South Africa extreme precipitation					
Rx1day					
1pctCO_2	Increase***	3.14	0.60	0.41	-14.84 to 31.30
RCP 4.5	Increase***	6.86	2.71	0.26	-19.82 to 49.20
RCP 8.5	Increase**	3.25	1.39	0.24	0.84 to 72.08
Historical	No change	4.69	3.83	0.10	-22.06 to 31.67
Rx5day					
1pctCO_2	Increase***	2.28	0.52	0.35	-24.28 to 30.09
RCP 4.5	No change	4.66	2.85	0.17	-26.79 to 31.89
RCP 8.5	Increase*	2.50	1.30	0.40	-42.28 to 42.33
Historical	No change	5.86	3.77	0.13	-29.72 to 50.82
Sweden extreme precipitation					
Rx1day					
1pctCO_2	Increase***	5.68	0.50	0.70	-18.89 to 75.85
RCP 4.5	Increase***	13.55	2.72	0.47	0.48 to 101.21
RCP 8.5	Increase***	16.79	1.14	0.81	-6.39 to 36.75
Historical	Increase***	11.41	3.55	0.24	-12.07 to 41.32
Rx5day					
1pctCO_2	Increase***	9.50	0.93	0.66	-28.57 to 62.39
RCP 4.5	Increase***	13.65	3.16	0.42	-55.65 to 47.86
RCP 8.5	Increase***	15.96	1.33	0.75	-14.27 to 67.43
Historical	Increase**	11.06	4.98	0.20/0.02	-23.06 to 32.14
Russia extreme precipitation					
Rx1day					
1pctCO_2	Increase***	7.88	0.18	0.97	-2.32 to 18.44
RCP 4.5	Increase***	15.29	0.69	0.92	7.31 to 35.93
RCP 8.5	Increase***	15.20	0.33	0.98	5.74 to 32.86
Historical	Increase***	6.62	1.14	0.24/0.01	0.70 to 16.81
Rx5day					
1pctCO_2	Increase***	6.40	0.20	0.94	-1.31 to 11.75
RCP 4.5	Increase***	11.13	0.93	0.79	-0.75 to 15.51
RCP 8.5	Increase***	11.60	0.47	0.94	5.33 to 21.97
Historical	Increase***	6.93	1.28	0.30	-2.34 to 14.78
China extreme precipitation					
Rx1day					
1pctCO_2	Increase***	8.72	0.27	0.94	1.49 to 16.90
RCP 4.5	Increase***	16.19	1.28	0.80	8.57 to 39.34
RCP 8.5	Increase***	18.19	0.60	0.92	7.04 to 36.33
Historical	Increase***	9.57	1.65	0.44	-12.18 to 22.87
Rx5day					

1pctCO_2	Increase***	4.66	0.38	0.73	0.25 to 33.90
RCP 4.5	Increase***	12.65	1.81	0.60	-4.91 to 20.69
RCP 8.5	Increase***	8.02	0.92	0.70	-27.79 to 34.87
Historical	Increase***	13.63	3.35	0.32	-9.67 to 21.84
Indonesia extreme precipitation					
Rx1day					
1pctCO_2	Increase***	14.73	0.68	0.88	-10.07 to 26.31
RCP 4.5	Increase***	28.63	3.60	0.65	-0.40 to 46.31
RCP 8.5	Increase***	41.03	2.24	0.85	-11.26 to 46.87
Historical	Increase***	25.97	4.42	0.44	-2.67 to 37.93
Median five-day maximum precipitation					
1pctCO_2	No change	0.26	0.58	0.04	-10.17 to 19.73
RCP 4.5	No change	0.61	2.65	0.03	-42.02 to 23.67
RCP 8.5	No change	1.84	1.39	0.11	-39.74 to 31.36
Historical	No change	-4.46	3.89	-0.10	-22.38 to 28.76
East to central tropical Pacific extreme precipitation					
Rx1day					
1pctCO_2	Increase***	7.50	0.44	0.83	-1.82 to 25.51
RCP 4.5	Increase***	17.63	2.04	0.68	-15.34 to 40.72
RCP 8.5	Increase***	16.91	1.22	0.83	-18.60 to 64.61
Historical	Increase***	10.87	2.81	0.29	-21.54 to 10.57
Rx5day					
1pctCO_2	Increase***	5.19	1.89	0.23	-26.09 to 58.87
RCP 4.5	No change	12.92	9.52	0.14	-40.27 to 252.79
RCP 8.5	Increase***	13.91	4.61	0.31	-12.53 to 291.47
Historical	No change	13.69	12.81	0.09	-62.53 to 60.35

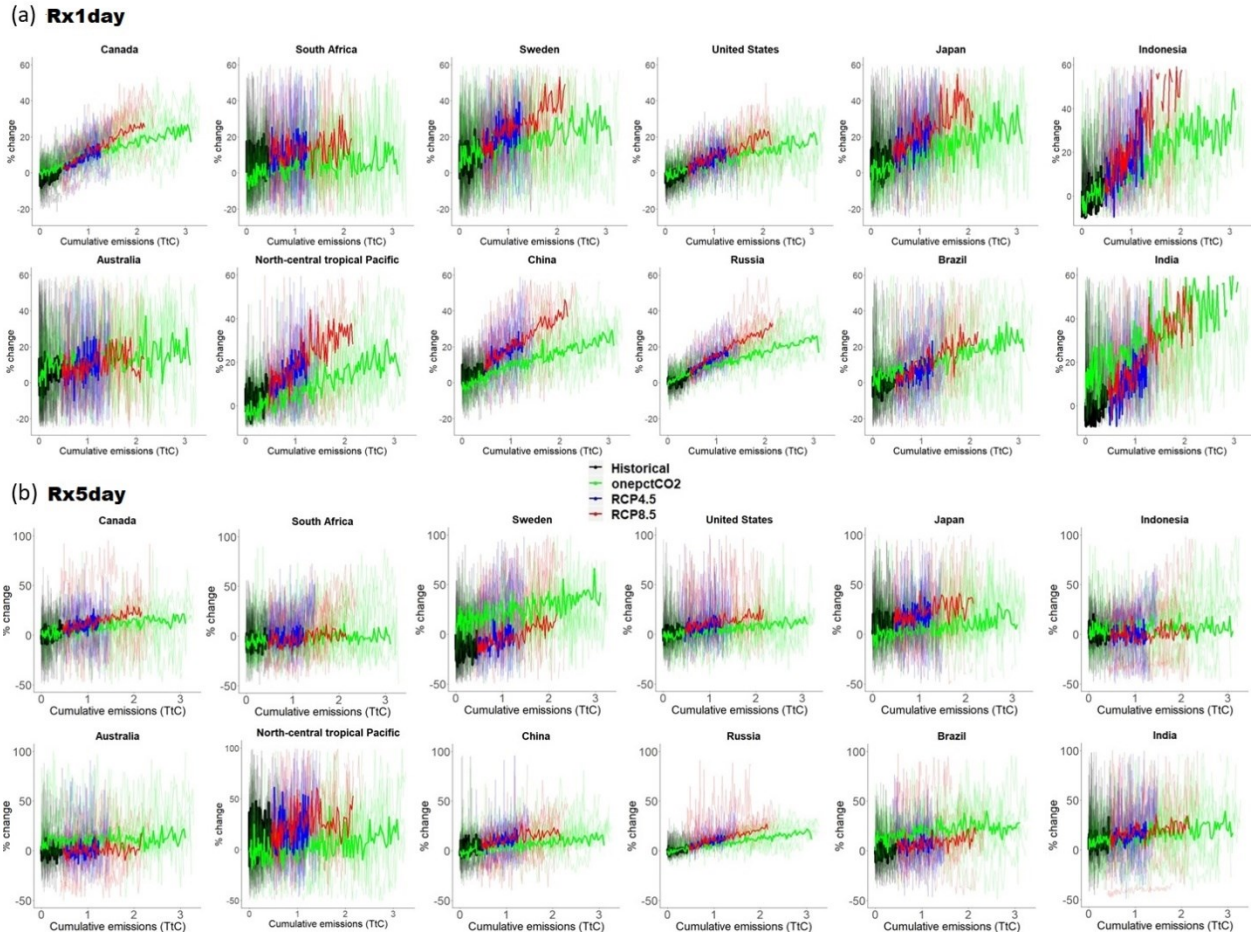

Figure 3. Median trends for selected countries/regions for the historical period (black), and the 1pctCO_2 (green), RCP4.5 (blue) and RCP8.5 (red) scenarios for Rx1day (a) and Rx5day (b). Annual percent changes for the RCP scenarios, and the historical period, are given. Percent changes for 1pctCO_2 are relative to Year 1 of that scenario. Trends for other individual model simulations are shown in the background for each scenario and represent the range of uncertainty.

TCRE patterns of extreme precipitation: Local scale

In this section, we examine precipitation trends at a more localized scale. These were considered as areas that represented the spatial domain of a single grid cell, or a small grouping of cells. Results are summarized in Table 3.

Unlike at the global to regional/national scale, we did not find particularly high correlation coefficients for all locations considered here (Figure 4, Table 3). It is worth mentioning that some of these selected locations did exhibit relatively high coefficients, though these would not be sufficient to attribute linearity according to our stated criteria. That said, the correlation coefficients were reasonably high, and in combination with low p-values, we feel confident that there remains a functional linear relationship in these localized median trends. For example, in the case of the 1pctCO_2 and RCP 8.5 scenarios for Rx1day, the New York City region showed appreciably high coefficients under these scenarios ($r = 0.56$ and $r = 0.64$ for the 1pctCO_2 and RCP 8.5 scenarios, respectively). The Montreal region also showed a reasonably large coefficient for its Rx1day ($r = 0.63$), as did the Philippines for both the 1pctCO_2 and RCP 4.5 scenarios ($r = 0.60$ and $r = 0.72$, respectively). However, to be consistent, we acknowledge again that these trends do not meet our strict criteria for linearity.

Though we found lower coefficients, these locations generally showed highly statistically significant increases in Rx1day and Rx5day, which was similar to trends shown globally and regionally/nationally (Table 3). For instance, for the New York City region, with the exception of Rx5day over the historical period, an increase per TtC was found across all scenarios, as well as for Rx1day for the historical period ($p < 0.01$ to 0.02). In particular, we found a 45% increase per TtC in Rx1day for the Philippines ($p < 0.01$) over its historical period, and a 22% increase per TtC under the RCP 8.5 scenario. Guyana also had a 19% increase per TtC in median Rx1day for the RCP 8.5 scenario ($p < 0.01$), and Florida showed about a 24% increase over its historical period ($p < 0.01$). Historical Rx5day was additionally increasing significantly for the St. Louis (19% per TtC) and Paris (27% per TtC) regions, both of which were statistically significant within the 1% significance level.

Table 3. Localized trends for median Rx1day and Rx5day for the 1pctCO_2, RCP 4.5 and RCP 8.5 emissions scenarios, and for the historical period. Findings are given as mean percent changes per TtC based on linear regression analyses, and Pearson correlation coefficients are provided. The model range at 1 TtC is also reported. *, ** and *** indicates results that are statistically significant at or within the 10%, 5% and 1% significance levels, respectively.

Emissions scenario	Change	% change per TtC	Standard error	Pearson's correlation coefficient r	Model range at 1 TtC
New York City region extreme precipitation					
Rx1day					
1pctCO_2	Increase***	6.76	0.87	0.56	-32.02 to 20.32
RCP 4.5	Increase***	17.48	5.01	0.35	-16.29 to 83.80
RCP 8.5	Increase***	20.93	2.66	0.64	-24.94 to 58.51
Historical	Increase***	22.86	7.38	0.25	-49.84 to 128.34
Rx5day					
1pctCO_2	Increase***	6.85	1.17	0.45	-54.60 to 114.19
RCP 4.5	Increase**	14.47	6.27	0.24	-42.32 to 125.20
RCP 8.5	Increase***	9.03	3.18	0.29	-64.16 to 404.88
Historical	No change	11.13	8.29	0.11	-49.77 to 80.69
Philippines extreme precipitation					
Rx1day					
1pctCO_2	Increase***	17.98	2.05	0.60	-27.96 to 372.48
RCP 4.5	Increase*	14.35	7.38	0.72	-53.97 to 86.57
RCP 8.5	Increase***	21.88	3.18	0.59	-11.70 to 100.14
Historical	Increase***	45.73	9.36	0.38	-49.59 to 28.87
Rx5day					
1pctCO_2	No change	1.94	1.25	0.13	-53.67 to 306.13
RCP 4.5	No change	3.30	5.88	0.06	-75.70 to 64.50
RCP 8.5	No change	2.18	3.57	0.07	-45.50 to 68.09
Historical	No change	6.01	8.03	0.06	-44.65 to 75.45
Guyana extreme precipitation					
Rx1day					
1pctCO_2	Increase***	7.61	1.05	0.53	-62.56 to 325.86
RCP 4.5	No change	9.18	5.73	0.17	-22.83 to 121.22
RCP 8.5	Increase***	18.79	2.66	0.60	-15.67 to 118.48
Historical	No change	9.08	6.16	0.12	-18.93 to 52.40
Rx5day					
1pctCO_2	Increase***	5.28	1.00	0.41	-11.89 to 81.43
RCP 4.5	No change	2.33	3.81	0.07	-35.30 to 55.27
RCP 8.5	Increase***	8.26	1.76	0.45	-39.25 to 52.53
Historical	No change	2.70	5.65	0.04	-44.15 to 42.31
Montreal region extreme precipitation					

Rx1day					
1pctCO_2	Increase***	8.33	0.89	0.63	-10.59 to 38.12
RCP 4.5	Increase***	15.59	3.73	0.41	-18.90 to 38.53
RCP 8.5	Increase***	8.15	2.03	0.39	-14.09 to 65.25
Historical	No change	-4.39	5.30	-0.07	-26.40 to 48.37
Rx5day					
1pctCO_2	Increase***	4.54	1.05	0.35	-56.01 to 38.71
RCP 4.5	No change	11.33	7.20	0.17	-25.43 to 52.25
RCP 8.5	Increase***	11.21	3.01	0.37	-9.84 to 65.04
Historical	Increase**	22.20	9.74	0.19	-24.77 to 161.80
Florida extreme precipitation					
Rx1day					
1pctCO_2	Increase***	4.05	0.88	0.37	-27.57 to 52.25
RCP 4.5	No change	5.18	5.68	0.10	-33.40 to 52.94
RCP 8.5	Increase***	9.11	2.65	0.34	-37.28 to 156.86
Historical	Increase***	23.62	7.74	0.25	-33.02 to 65.93
Rx5day					
1pctCO_2	Increase***	4.20	1.05	0.32	-48.78 to 179.34
RCP 4.5	Increase**	7.83	3.91	0.21	-23.30 to 134.95
RCP 8.5	Increase***	6.15	2.11	0.30	-18.04 to 163.06
Historical	No change	5.44	7.15	0.06	-76.65 to 143.41
Paris region extreme precipitation					
Rx1day					
1pctCO_2	Increase***	4.45	0.84	0.42	-35.35 to 101.55
RCP 4.5	Increase***	11.23	4.33	0.27	-25.76 to 38.14
RCP 8.5	Increase***	12.41	1.76	0.60	-12.58 to 122.11
Historical	No change	5.62	5.85	0.08	-38.80 to 58.00
Rx5day					
1pctCO_2	Increase***	9.24	1.35	0.51	-22.21 to 125.44
RCP 4.5	No change	7.78	6.16	0.13	-55.23 to 169.01
RCP 8.5	Increase***	13.65	2.98	0.44	-8.55 to 144.98
Historical	Increase***	27.13	10.32	0.22	-79.24 to 128.14
Madagascar extreme precipitation					
Rx1day					
1pctCO_2	Increase***	7.23	1.30	0.42	-35.30 to 128.62
RCP 4.5	Increase**	16.31	7.25	0.23	-39.48 to 153.16
RCP 8.5	Increase***	16.53	3.33	0.47	-43.19 to 92.45
Historical	Increase*	16.15	9.09	0.15	-57.52 to 56.67
Rx5day					
1pctCO_2	No change	1.44	1.01	0.12	-33.51 to 63.06
RCP 4.5	No change	0.81	4.48	0.02	-41.83 to 61.62
RCP 8.5	No change	2.86	1.86	0.16	-17.11 to 107.81
Historical	No change	-1.04	6.83	-0.01	-23.35 to 22.78
Hong Kong region extreme precipitation					
Rx1day					

1pctCO_2	Increase***	6.60	2.06	0.27	-25.66 to 86.30
RCP 4.5	No change	17.40	11.03	0.17	-39.34 to 93.24
RCP 8.5	Increase**	11.25	5.41	0.22	-37.24 to 47.47
Historical	No change	3.21	15.82	0.02	-50.11 to 79.89
Rx5day					
1pctCO_2	Increase***	3.83	1.46	0.22	-34.57 to 212.08
RCP 4.5	No change	5.01	6.42	0.08	-52.01 to 212.54
RCP 8.5	No change	-0.44	3.07	-0.02	-65.30 to 138.72
Historical	No change	8.36	10.21	0.07	-36.09 to 66.04
St. Louis region extreme precipitation					
Rx1day					
1pctCO_2	Increase***	6.17	0.85	0.53	-29.89 to 57.13
RCP 4.5	Increase***	13.06	4.89	0.27	-25.82 to 40.52
RCP 8.5	Increase***	12.80	2.38	0.50	-5.38 to 75.51
Historical	Increase**	13.46	6.50	0.17	-59.50 to 51.37
Rx5day					
1pctCO_2	Increase***	7.02	1.06	0.51	-32.11 to 237.88
RCP 4.5	Increase**	12.67	5.43	0.24	-39.29 to 82.82
RCP 8.5	Increase***	10.18	2.80	0.36	-37.14 to 233.16
Historical	Increase***	18.55	6.84	0.22	-65.80 to 87.89
Melbourne region extreme precipitation					
Rx1day					
1pctCO_2	Increase***	4.73	1.30	0.30	-77.46 to 162.15
RCP 4.5	No change	3.97	6.42	0.07	-41.85 to 129.79
RCP 8.5	Increase***	8.56	2.51	0.34	-19.69 to 35.12
Historical	No change	6.77	8.69	0.07	-49.08 to 95.28
Rx5day					
1pctCO_2	No change	1.15	1.02	0.10	-10.39 to 92.34
RCP 4.5	No change	4.86	6.22	0.08	-43.07 to 277.11
RCP 8.5	No change	3.12	2.70	0.12	-25.75 to 166.70
Historical	No change	3.97	8.94	0.04	-48.66 to 95.28

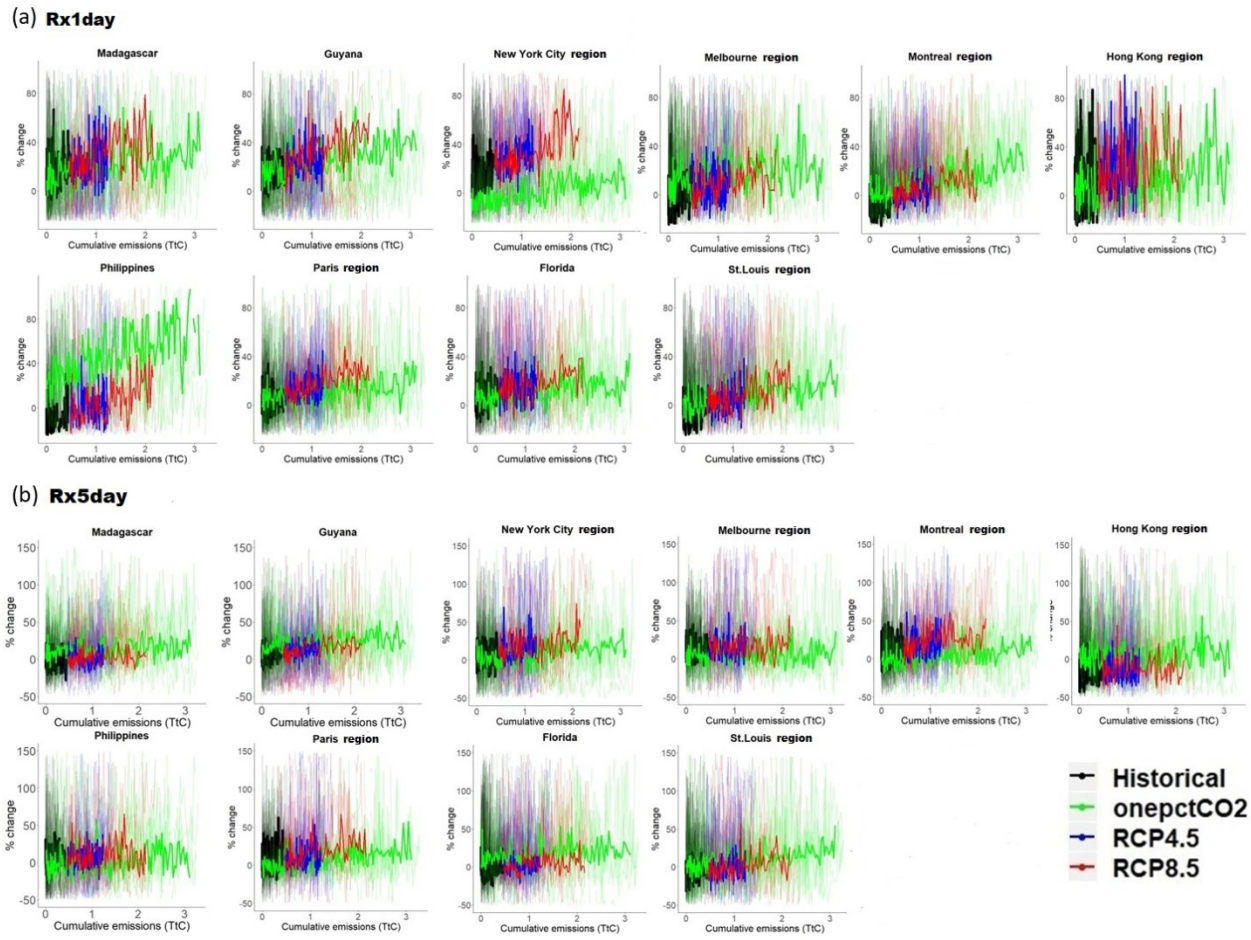

Figure 4. Median trends for selected localized areas for the historical period (black), and the 1pctCO_2 (green), RCP4.5 (blue) and RCP8.5 (red) scenarios for Rx1day (a) and Rx5day (b). Annual percent changes for the RCP scenarios, and the historical period, are given. Percent changes for 1pctCO_2 are relative to Year 1 of that scenario. Trends for other individual model simulations are shown in the background for each scenario and represent the range of uncertainty.

Discussion

Our results show that the TCRE framework, representing a near-linear response of climate variables to cumulative CO_2 emissions, may be applied to extreme precipitation, extending analyses previously conducted in other studies, such as Leduc et al. (2016), Partanen et al. (2017) and Chavaillaz et al. (2019). These findings are also consistent with previous works

that have investigated the extent that precipitation extremes scale with global warming (e.g. Seneviratne et al., 2016; Wartenburger et al., 2017; Tebaldi & Knutti, 2018). Indeed, using a suite of nine CMIP5 models for the purposes of this work, we found strong positive linear scaling for indicators of extreme precipitation against global cumulative emissions, as well as statistically significant increases per TtC. These trends are shown to generally apply in both a TCRE-only context (1pctCO_2), as well as with respect to a combination of CO_2 and other greenhouse gas forcings (i.e. TCRE + non-CO_2 forcings in RCP 4.5 and RCP 8.5). However, the extent to which this linearity occurs is dependent on the spatial scale and/or the emission scenario in question. The greatest linearity ($r >= 0.75$) was uniformly found at the global scale, where both median Rx1day and Rx5day increase significantly for all scenarios, as well as for the historical period in terms of Rx1day. Land-only and ocean-only analyses similarly revealed a strongly linear signal for both the median Rx1day and Rx5day. In the case of land, precipitation exhibited similar linear trends across all scenarios but was weaker historically. This held true for oceanic areas, as well, where the response was strongly linear across all scenarios.

The strong positive linear trends of extreme precipitation found here were further consistent with the Clausius-Clapeyron relationship. With increased greenhouse gas forcing, global temperatures correspondingly rise, allowing the moisture holding capacity to increase. The Clausius-Clapeyron relation describes the exponential increase in water vapor pressure with warmer temperatures, where water vapor increases by approximately 7% per degree Kelvin under constant relative humidity. Indeed, we show that extreme precipitation scales strongly linearly with higher cumulative emissions globally to locally at rates similar to or exceeding that of the Clausius-Clapeyron relationship (i.e. a super Clausis-Clapeyron relationship). This was especially true for trends in Rx1day under the RCP runs, where the rates of increase per TtC

were frequently at or exceeding 11% per TtC. Similar rates of change also occur under 1pctCO_2 at the upper end of our spread of model trends (Figure 2); for instance, at 1 TtC, we find a similar increase (> 10%) globally under 1pctCO_2. Similar results were also shown in Pall et al., (2007), for example, where they found that increases in extreme precipitation under CO_2 forcing agreed with the Clausius-Clapeyron relation, especially at mid- to high-latitudes. Our findings also consistently show that the rate of increase is greater in the RCP 8.5 scenario than it is for 1pctCO_2 (often approximately a doubling in RCP 8.5 relative to 1pctCO_2), which we would expect as a result of the RCP scenarios accounting for non-CO_2 forcings and land-use change emissions. This is consistent with other studies (e.g. Pendergrass & Hartmann (2014) and Seneviratne et al., (2021)). In Pendergrass & Hartmann (2014), for instance, they found that 99.99-percentile rain rate responses are sometimes shown to be 75% to more than 100% larger in RCP 8.5 than in 1pctCO2 for selected CMIP5 models, with relatively small uncertainties (e.g. in the IPSL-CM5A-LR, MIROC5 or NorESM1-M models). However, we also stress that rates of increase for individual models would differ across model simulations, ranging from larger to much smaller disparities between 1pctCO_2 and RCP 8.5 relative to what we show for the median trends.

These patterns would further suggest intensifications of annual Rx1day and Rx5day events due to more moisture availability in a warmer atmosphere. For instance, particularly strong deep convective systems have a tendency of forming in environments that are and/or become moisture-abundant. With enhancement, this moisture would create thermodynamic environments suitable for strong to severe thunderstorms and other mesoscale convective complexes in light of an increase in the amount of convective available potential energy. More moisture availability would also favorably augment the amount of atmospheric precipitable

water. Consequently, more water could be condensed out of the air during a given heavy precipitation event at higher background temperatures that would, therefore, increase the frequency and severity of these events through enhanced precipitation rates. Our results show strongly linear intensification rates in median Rx1day and Rx5day (increases of 4-15% per TtC globally), suggesting more substantial precipitation rates under higher global emission concentrations.

These tendencies were further implied in Figure 1, showing general increases at lower latitudes for the most extreme Rx1day and Rx5day at mean 1 TtC of cumulative emissions among scenarios, relative to the beginning of the historical period. This was especially true in tropical oceanic regions. The increase in precipitation among scenarios may be the result of increased atmospheric moisture availability and evaporation in low-latitude oceanic regions under higher global temperatures expected at 1 TtC of cumulative emissions. This would likely contribute to intensified convection in more favorable thermodynamic environments, which, for example, may intensify rainfall rates in tropical cyclones over their oceanic source regions (e.g. Knutson et al. 2010). In particular, the overall increase across scenarios in the most extreme Rx1day and Rx5day over a narrow latitudinal band in the North-central tropical Pacific (approximately 9-16 degrees North of the equator) is large (Figure 1). For this region, we found that precipitation extremes increase generally by as much as 90-100% at 1 TtC in the RCP scenarios for Rx1day relative to the beginning of the historical period. The results show that the most intense Rx1day and Rx5day events increase significantly across all emissions scenarios (Table 2), and this increase is strongly linear for Rx1day for the 1pctCO_2 and RCP 8.5 scenarios. As mentioned previously, this could suggest tropical convective enhancement due to potentially stronger and more frequent ENSO-warm phases (El Nino events) at higher cumulative

emissions, favoring intensification in the most extreme precipitation under the higher (sea-surface) temperatures. A shift towards stronger El Nino events with greenhouse forcing would be consistent with enhanced ENSO variability (e.g. Moore et al., 2015). Using fossilized coral oxygen isotope records in the central Pacific, ENSO variance was also shown to be approximately 25% stronger over the past five decades relative to 3000-5000 years ago (Grothe et al., 2019). As mentioned previously, the increase shown for extreme precipitation indicators in this region may also be attributed to changes in the size and strength of the ITCZ.

When regionally constraining our analysis, we found a wider range of correlation coefficients. In general, larger nations, such as Canada, the United States, Russia and China, had a stronger linear signal for both Rx1day and Rx5day. However, the robustness of this linearity was most pronounced for Rx1day under the 1pctCO_2 and RCP 8.5 scenarios across most of the nations considered. This was also true for India, Brazil, and as described previously, the North-central tropical Pacific. In the case of India, this may imply intensification in the warm season South Asian monsoon through more intense rainfall rates from deep convection/thunderstorms in a warmer climate (e.g. Moore et al., 2015; Lui et al., 2019). One exception to this pattern was Australia, where consistently weaker linear trends were found across scenarios, and historically. This could be that much of the central portion of Australia climatologically spends few days annually with measurable precipitation in light of the influence of sub-tropical high pressure in this region. It is principally these high pressure systems that restrict precipitation development due to the sinking air motions (i.e. subsidence) that are endemic to much of Australia. Therefore, much of the nation's precipitation is mostly limited to coastal areas, notably the East and North coasts. Nevertheless, we found highly statistically significant increases per TtC in Australian

Rx1day and Rx5day for all scenarios. This finding is consistent with Bao et al. (2017), who showed an increase in the most extreme precipitation in Australia.

Although linearity was generally weaker at the local scale, this study similarly showed statistically significant increases in Rx1day intensification at specific locations across North America, including the Montreal, St. Louis and New York City regions, as well as the state of Florida. These findings generally agree with Li et al. (2019), showing increases in local extreme precipitation across North America with climate warming, as well as in Canada historically (e.g. Bush et al., 2019), although Kunkel (2003) found no changes in the most extreme precipitation historically in Canada. The increases per TtC found in the United States was further in agreement with the significant increases in daily extreme precipitation events in southeastern Virginia over the 21st century, as documented in Sridhar et al. (2019).

Comparatively smaller nations exhibited similar results for Rx1day under the 1pctCO_2 and RCP 8.5 scenarios, notably Japan, Sweden and Indonesia. Conversely, at the local scale, while linear trends may well exist based on our results, we consistently found no robust trends. Intuitively, this would make sense, as there are likely to be larger-scale influences that affect extreme precipitation locally, thereby increasing the extent of noise. Locally to regionally, for instance, natural variability can more significantly affect the frequency and/or severity of extreme precipitation events over annual to multi-decadal time scales. Such natural variabilities can reduce the signal-to-noise ratio and, thus, can mask linearity at these localized scales, as compared to the stronger linear signal shown globally. Also, the scale at which these precipitation events occur is rather small, making them difficult to capture meaningfully in coarser model resolutions. For example, extreme precipitation events are often the result of deep convective systems, such as (severe) training thunderstorms (e.g. Maddox et al., 1977), that can

yield considerable amounts of rainfall over a very short time. Due to the mesoscale processes involved in the formation of such events, it becomes increasingly difficult to sufficiently resolve these dynamics at coarser resolutions and, therefore, outside of convection-permitting models. The lower correlation coefficients found at the local scale may further be related to shifts in the overall storm tracks as a result of changes in atmospheric circulations, or it may be related to changes in the frequency of high and low pressure systems that preferentially impact some of these locations.

As such, while the TCRE is shown here to be a good approximation for extreme precipitation at all spatial scales, it is more distinct at larger scales as opposed to smaller ones. However, strong linear relationships also appear in regionally-constrained analyses, mostly for the largest nations/regions (i.e. Canada, Russia, the United States, China, and the North-central tropical Pacific). This may be due to the potentially more prevalent influence of the Clausius-Clapeyron relation at mid- to high-latitudes (in which many of the selected nations are located), as described by Pall et al. (2007). The stronger linearity shown for these regions could also be partly an artifact of spatially aggregating over a larger number of grid cells over larger areas, increasing data sampling size. The differences in linearity from one location or region to another could also be at least partly explained by differences in the atmospheric circulation response to higher cumulative emissions (and, thus, warmer temperatures). For example, a strengthening of the monsoon circulation in India (e.g. Li et al., 2019) under warmer global/regional temperatures could foster conditions suitable for substantial increases in Rx1day and Rx5day rates. Indeed, as reported here, precipitation rates in India are shown to be much larger than all other nations/regions considered, especially for Rx1day (which are statistically significant across scenarios).

While we would have expected both Rx1day and Rx5day to increase at all spatial scales considered herein, it is interesting to note that our results point to larger rates of increase in Rx1day than in Rx5day. This is especially true globally, and for land and ocean. However, the extent to which this occurs is somewhat more varied at the national/regional to local scale than what we report globally or for land/ocean. For example, in Japan and China, historically, Rx5day exhibits a larger increase than for Rx1day events. This pattern is also shown for Sweden, and locally we see this appear in the Montreal and St. Louis regions, for Florida, and especially in the case of the Paris region. These regional to local patterns could suggest (substantial) changes in the properties of convective systems, as well as the broader, synoptic circulation features that are important for their development and evolution, depending upon the extent of regional warming (e.g. Seneviratne et al., 2021). The larger increases in the intensity of Rx5day regionally to locally shown here may be the result of an atmospheric configuration that favors more (consecutive) days spent with precipitation as cumulative emissions rise. In turn, this could more likely allow for precipitation to be observed over multi-day time periods that would effectively enhance five-day precipitation events. It could also be that increases in Rx1day events significantly contribute to increases in the magnitude of Rx5day events, which could partially be why increases in Rx5day events are generally expected. These regional to local variations are consistent with other studies. Valverde & Marengo (2014), for instance, showed some regionally-different trends between Rx1day and Rx5day in Brazilian basins, where Rx5day events exhibited a decrease in the upper Tocantins, while Rx1day events increased. Similarly, Kirchmeier-Young & Zhang (2020) found a larger scaling factor for Rx1day than for Rx5day over much of North America historically.

We also generally found that the rate of increase in 1pctCO_2 was largely much lesser than that of RCP 8.5. In particular as mentioned, we would expect such a consistently larger response of precipitation extremes to the RCP 8.5 emissions scenario as compared to that of 1pctCO_2 due to the RCP scenarios including not only CO_2 forcing, but also non-CO_2 forcings, in addition to the emission contributions from land-use changes. To that end, Seneviratne et al. (2021) show that the increase is about 40% larger in RCP 8.5 than it is in 1pctCO_2. At the same time, this larger disparity becomes somewhat less distinct nationally/regionally to locally, though the reported changes across median trends still reflect fairly high differences between the two scenarios.

Summary & Conclusion

Using a suite of nine CMIP5 climate model simulations, this study presented TCRE-based estimates of extreme precipitation changes by examining trends in the most intense Rx1day and Rx5day events as a function of global cumulative emissions. The results show that the TCRE framework can be a good approximation for precipitation extremes and, therefore, expands on the research that had previously applied the TCRE to evaluate trends in global to regional temperature and precipitation in the context of global cumulative emissions (e.g. Leduc et al., 2016, Partanen et al., 2017, Chavaillaz et al., 2019). As such, the TCRE framework is shown here to similarly be a useful quantity in the assessment of extreme precipitation, especially at larger spatial scales, and further casts insight in the extent to which extreme precipitation may respond to higher cumulative emission concentrations. Indeed, the results presented in this study typically showed that extreme precipitation is likely to intensify significantly per TtC globally to locally in response to higher emissions, including where linearity is generally not robust and/or could not be inferred. While we recognize that there are

many regions and specific locations not covered in this work that face equally, if not more vulnerability to precipitation extremes, the results shown here for the selected locations/regions may be extrapolated to other (grid-point) locations/regions. These patterns suggest significant impacts within a warmer climate that may be linked to more frequent and intense flooding, for example, such as those extreme precipitation events that contributed to the California flooding of January 2023, the British Columbia flooding of November-December 2021, the Australian flood of March 2021, the United States flooding associated with tropical cyclone Harvey in 2017, as well as the Southern Quebec floods of spring 2017 and spring 2019, to name just a few. This study highlighted that the most significant linear increase occurred with median Rx1day under the 1pctCO_2 and RCP 8.5 scenarios, not only globally, but for nations located principally at the mid- to high-latitudes. This was further shown at singular grid cells that contain major metropolitan areas, where impacts could be particularly significant in response to more substantial water accumulation and runoff in situations of intense one-day precipitation events (e.g. the Indonesian flash-flood of April 2021 or the Montreal flash-flood of July 1987). In light of efforts to maintain global warming below the 1.5 C to 2.0 C levels of the Paris Agreement, this study provides some perspective as to what extent extreme precipitation could increase at global cumulative emission levels associated with such magnitudes of warming or even less. The findings presented here and other works that previously reported similar results could, therefore, be of value for localized policy makers where notably growing concerns of more extreme precipitation become increasingly favorable in a warmer global to local climate. To that end, although local policy makers do not have control over global emissions, these results can provide a framework for better adapting to a world that would likely feature more intense and frequent extreme precipitation events. However, using cumulative emissions to explain past and future

trends offers only a broad scope for examining precipitation extremes. For this reason, this study also indirectly stresses that further research could potentially derive TCRE-based estimates of the synoptic to mesoscale systems and their environments that often generate the precipitation extremities investigated here, or for the forms of natural variability that may affect their frequency and/or intensity (e.g. ENSO). A closer inspection of important feedbacks not accounted for in this analysis, such as the water vapor feedback, could also be useful. Such approaches could offer an additional dimension for further understanding future trends in the dynamics of precipitation extremes as cumulative emissions rise.

Chapter 4: Using CMIP5 data to model trends in global, regional and local precipitation extremes with a GEV distribution

This Chapter is in preparation for submission for publication

Abstract

Precipitation extremes are rare events that often have significant negative societal, environmental and economic impacts. For this reason, such events are of increasing importance to society in terms of how they may change in frequency and/or intensity in light of continued warmer global and regional temperatures as emissions rise. The Transient Climate Response to Cumulative Emissions (TCRE) has been a significant contribution for better understanding the response of global to regional temperature to cumulative CO_2 emissions, showing linear scaling of temperature and other climate indicators with CO_2 emissions. At the same time, the Generalized Extreme Value (GEV) distribution has previously been widely adopted in the analysis of extreme events across a variety of fields, particularly in the assessment of trends for climate extremes, including for modeling extreme precipitation. Using Coupled Model Intercomparison Project Phase 5 (CMIP5) model data, I apply a GEV distribution to quantify trends in historical and projected annual Rx1day and Rx5day at various spatial scales. Results indicate that annual maxima shift towards larger values and exhibit higher variability. Furthermore, location parameter estimates for Rx1day and Rx5day events scale approximately linearly with higher cumulative CO_2 emissions at all spatial scales considered, consistent with the TCRE framework. Correspondingly, this contributes to largely linear increases in 20-year and 100-year return levels with increasing cumulative CO_2 emissions. My findings also show that the probability of the highest annual maxima quantiles is generally lower due to decreasing shape parameter estimates as cumulative emissions rise, although this response is shown to be spatially-dependent. These results imply an increase in the frequency and intensity of annual maxima over time, which may contribute significantly to a higher frequency of flooding events and other hazards globally to locally.

Introduction

Extreme precipitation events frequently induce significant negative impacts to human society, including substantial property damages and loss of life. The degree to which these events may change in response to warmer global temperatures, by extension of rising greenhouse gas concentrations, is of primary interest in the climate change sector (Pfahl et al., 2017). However, quantification of these events is often challenging because of their rarity. The lack of meaningful representation of such events in coarser model resolutions (e.g. Raupach et al., 2021) is further compounded by other inhomogeneity issues in the observational records, such as the incomplete reporting of these events, sparse observation networks, inadequate monitoring systems, and relatively short historical periods (Taszarek et al., 2021; Taszarek et al., 2019; Tippett et al., 2016; Stott et al., 2016; Edwards et al., 2018). Other data inhomogeneities are also often related to the joining of observations from closely neighboring observation stations to create a longer time series (Vincent & Mekis, 2006; Edwards et al., 2018).

Although there exist several definitions, precipitation extremes may be broadly defined as precipitation quantities per unit time that exceed the climatology of a specified region or location (EPA, 2017). According to the Intergovernmental Panel on Climate Change Managing the Risks of Extreme Events and Disasters to Advance Climate Change Adaptation (IPCC SREX), changes in heavy to extreme precipitation events are based on late-20th century 90th percentile or greater values, such as 95th-99th percentile events (e.g. Herring et al., 2014). Flash-flooding commonly occurs in situations of unusually high rainfall rates occurring over short time durations, such as over a single day or over sub-daily temporal scales. Most conducive to generating such rainfall is (deep) convective events, typically manifested as strong to severe thunderstorms, where, in some cases, rainfall may exceed average monthly amounts in just a

matter of hours or less. One such case was during the Montreal flooding event of July 14th, 1987, where almost precisely 100 millimeters (mm) (approximately 4 inches) of rainfall occurred in association with a severe multi-cell thunderstorm family that lasted for about two hours. Another situation where little to no convective available potential energy (CAPE) was involved, was a low pressure system that yielded the all-time largest 24-hour rainfall (120 mm) for the Montreal area, on November 8th-November 9th, 1996 (149.2 mm total between the two days at the McTavish station, and 134 mm at YUL). Such flooding may be exacerbated by anomalously high water levels, higher than normal soil moisture and previously wetter than normal conditions. There may further be situations where flooding materializes out of conditions that feature consecutive days spent with precipitation, even if this precipitation occurs in lighter amounts.

Extreme value theory (EVT) is a sector of statistics designed to make inferences about the probability of extreme events or outliers. It has been widely adopted in the area of risk assessment statistics and applied for a broad range of purposes across many fields of study, particularly in climatology and hydrology. A branch of EVT, called the Generalized Extreme Value (GEV) distribution, is comprised of a family of continuous probability distributions that can be used to model extremes. The individual probability distributions that make up the GEV are the Gumbel, Frechet and Weibull distributions, representing Type I, Type II and Type III distributions, respectively. Each type is used to describe the overall rate of decay exhibited by the upper tail of these distributions (Batista et al., 2019) and is determined by a range of values given by shape parameter estimates. Typically, the extremes of a normal distribution lie in the tail regions of those distributions. Within these tails exists a separate distribution (i.e. a sub-distribution that appears right-skewed) that is often of interest to researchers and policy-makers,

as it is here that the most extreme values are found. The GEV distribution could be used to derive parameter estimates of location, scale and shape and model how these may each be changing through time.

A large body of climate impacts and hydrology literature has previously employed EVT-related analyses to explore return periods of anomalously significant rainfall or rare flooding events by fitting a GEV. For example, several studies have considered fitting a GEV regionally to explore precipitation extremes, such as Northeastern North America (Innocenti et al., 2019), the Brazilian Amazon (Santos et al., 2015; Assis et al., 2018; Batista et al., 2019), the United States (Fix et al., 2016), the Mediterranean (Blanchet et al., 2016), or the United Kingdom (Brown, 2018). Other studies have used the GEV to assess trends in a variety of climate indices, such as testing the effect of the El Nino Southern Oscillation (ENSO) and North Atlantic Oscillation on seasonal precipitation extremes in North America (Whan & Zwiers, 2017), or the United Kingdom (Brown, 2018). Return periods may be defined as a given event of some magnitude (i.e. return level) being reached or exceeded once every specified interval of time, on average. It is this information that can be useful in policy-making and risk management to better understand how given events may change in time with prescribed levels of global warming under specified cumulative emissions concentrations. As such, return levels are often of interest in climate adaptation, policy-making, urban, road and highway drainage planning, as well as hydrological structure risk assessment, such as for levees and dams.

The TCRE is a useful framework as a means for highlighting the linear relationship between global mean temperature and emissions (e.g. Tokarska et al., 2019), demonstrating that temperature responds approximately proportionally to global cumulative CO_2 emissions. It specifically represents a constant value that describes the increase in global temperature in

response to cumulative CO_2 emissions (Matthews et al., 2009; Gillett et al., 2013; Matthews et al., 2023) and, as such, has the ability to link impacts directly to carbon emissions. The TCRE has further shown more promise for applications at sub-global scales (e.g. Leduc et al., 2016), as well as with respect to other climate indicators, such as precipitation (Partanen et al., 2017), extreme precipitation (Moore et al., 2023) or even sea ice (Zickfield et al., 2012). Therefore, the TCRE can also more broadly be thought of as the physical climate response to cumulative CO_2 emissions (Herrington & Zickfield, 2014), which includes the response of climate indicators other than the most used climate index (i.e. global mean temperature) (MacDougall & Friedlingstein, 2015).

As such, this framework can be of value in climate mitigation as a means of communicating climate impacts flexibly as cumulative carbon emissions rise. For example, the TCRE enables policy makers to better determine expected impacts linked to specified warming targets that may be associated with certain weather extremes (Tachiri et al., 2019). It should be noted, however, that extreme weather events at global to local scales have very different stakeholders. Further, global scale trends tend to be more believable, while sub-global scales, where trends are often noisier, are of more interest to stakeholders.

The TCRE also holds potential for framing precipitation extremes by modelling them using EVT. This could, therefore, be a useful tool to evaluate the response of the most extreme precipitation events to increasing global cumulative emissions and, at the same time, address the gaps in the literature concerning such events.

In the current study, using a suite of CMIP5 model data, I endeavor to quantify trends in one-day and five-day maxima (previously referred to as Rx1day and Rx5day, respectively) and

20-year and 100-year return levels of precipitation extremes with increasing concentrations of cumulative greenhouse gas emissions by using a GEV distribution to model extremes. I specifically use a GEV analysis to examine observed and projected trends in the most extreme Rx1day and Rx5day events at different spatial scales, including globally, regionally and locally, as a function of cumulative emissions, and determining whether location parameter and return level estimates can be approximated by the TCRE framework at each of these scales. I discuss first the type of data used, and the formulation of the GEV to model this data accordingly. I focus on analyzing trends in various distribution parameters derived from the GEV and assess return level patterns of specified return periods under different cumulative emission scenarios established by the IPCC.

Methodology

In this section, I describe in detail the methods used for this study. I begin with a description of the extreme precipitation data considered. I then discuss the procedure of fitting a GEV, and the statistical test used to analyse the data.

Data and Scenarios

Daily precipitation data was extracted from nine (9) global climate models (GCMs) as part of a CMIP5 ensemble. The GCMs for which annual maximum one-day and five-day maximum precipitation data were available are the following:

Table 1. Selected 9 CMIP5 models and model descriptions.

Model name	Description
CanESM2	Canadian Center for Climate Modeling and Analysis (2.8 x 2.8)
IPSL-CM5A-LR	Institut Pierre Simon Laplace, France (3.75 x 1.8)
IPSL-CM5A-MR	Institut Pierre Simon Laplace, France (2.5 x 1.25
IPSL-CM5B-LR	Institut Pierre Simon Laplace, France (2.75 x 1.8)
MPI-MMPI-ESM-LR	Max-Planck-Institute for Meteorology (low-resolution)
MOHC-HadGEM2	Met Office Hadley Center, UK (1.88 x 1.25)
MIROC-ESM	Japan Agency for Marine-Earth Science and Technology, Atmosphere and Ocean Research Institute (The University of Tokyo), and National Institute for Environmental Studies (2.8 x 2.8)
NOAA-GFDL-ESM2G	National Oceanographic and Atmospheric Administration Geophysical Fluid Dynamics Laboratory, USA (2.5 x 2.0)
NOAA-GFDL-ESM2M	National Oceanographic and Atmospheric Administration Geophysical Fluid Dynamics Laboratory, USA (2.5 x 2.0)

As discussed in Chapter 3 of this dissertation, I used here three greenhouse gas emissions scenarios, which are titled "1pctCO_2", "rcp45", and "rcp85", referring to one percent CO_2, Representative Concentration Pathways 4.5 (RCP 4.5) and Representative Concentration Pathways 8.5 (RCP 8.5), respectively. The cumulative emissions data used here are derived from changes in oceanic, atmospheric and land pools, as described in Chapter 3. Furthermore, cumulative emissions represent fossil fuel emissions only. The 1pctCO_2 scenario (140 years) denotes a situation where the atmospheric CO_2 concentration increases by one percent per year until CO_2 quadruples relative to the pre-industrial period. The two RCP scenarios (90 years) are defined based on greenhouse gas concentrations and represent two different future climates by the year 2100. The RCP scenarios span a period covering 2006 to 2095. The historical period

spans 145 years following the beginning of the pre-industrial period to approximately present-day (2005).

Variable creation and model interpolation

Extreme precipitation data was converted into units of millimeters per day (mm/day). Daily precipitation derived referred to the maximum amount of precipitation achieved for a given day for a given grid cell, model and scenario. I isolated the largest value among these daily maximum values for each year, which effectively extracts the 'most extreme' annual maxima globally for each model and scenario. I also obtained five-day maximum values using the original daily data available. These newly created variables were known as "Rx1day" and "Rx5day" and are used herein to define what constitutes precipitation extremes, which includes all types of precipitation. As previously described in Chapter 3, I then converted individual model resolutions to a common grid system that carried the coarsest resolution (based on CanESM2, consisting of grid cells with sizes of about 2.8 x 2.8 degrees).

Region and location selection

I analyze land areas by applying a mask that isolated those grid point centers located only over land. This procedure was repeated for ocean grid cells only. Therefore, it was possible to consider annual maxima over either land or ocean, or for any specific nation of interest. I limited this study to a selection of five nations where precipitation extremes may be particularly impactful in light of significant population density, the extent of urbanized areas, sea level rise, as well as proximity to large water bodies: United States, Australia, India, Brazil, and South Africa.

Because impacts of extreme precipitation are likely to be most significant in densely populated zones, I then extended the analysis to localized areas to determine trends at those spatial scales, and whether these trends can be approximated by the TCRE in terms of location parameter estimates and specified return levels derived from the GEV. These locations typically occupied spaces that were at the grid cell, or a small grouping of adjacent cells. Small groupings of cells could comprise small nations or be comparable to the size of states in the United States. The selected five locations are as follows: Hong Kong, Philippines, St. Louis, Florida, and Montreal.

Fitting a GEV

For this study, I used a GEV analysis to assess trends in the most extreme Rx1day and Rx5day values at different spatial scales. In order to fit a GEV to annual maximum extreme precipitation, it was necessary to first create "blocks" containing annual maxima precipitation data. Fitting a GEV in this manner is referred to as the "block maxima approach". Each individual block would contain an equal number of non-overlapping years, with each year consisting of an annual maximum value. Consistent with Innocenti et al. (2019), I chose a seven-year timespan for the blocks (hereafter referred to as "sub-period") for this study. Since the RCP scenarios and historical period have a maximum number of years that do not work out evenly with the selected seven-year allocation for each block, I applied a truncation procedure by removing the last five years for the historical period and last six years for the RCP scenarios to ensure that each block carried an even number of years. While this procedure creates a 5-year gap between the historical period and the beginning of the RCP periods, the present-day was adjusted to the first block of the RCP period (now ending in 2012, as opposed to 2005). This allows for the present-day to be more reasonably close to the actual present-day. For each

block/sub-period, the cumulative emissions corresponding to the central year was used (e.g. emissions at Year 4 in the first block/sub-period, which spans Year 1 to Year 7).

I then applied a data pooling procedure to gather annual maxima for the sub-periods. I first pooled the highest annual Rx1day and Rx5day values for each sub-period. To accomplish this, I selected the largest value for each year for all available years. Thus, the grid cell containing the highest value was selected for each specific year for all available years, effectively creating vectors consisting of seven annual maxima values for each block/sub-period. Figures 1 & 2 show this procedure:

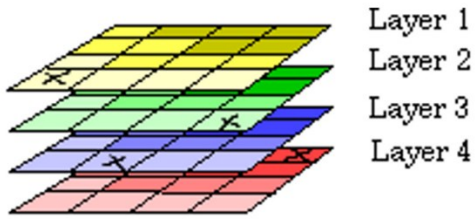

Figure 1. Representation of the block maxima approach for a given model for selecting the largest maxima for Rx1day and Rx5day. Each layer represents an individual year. Black "X" marks show the grid cell containing the largest values across all grid cells for each layer/year.

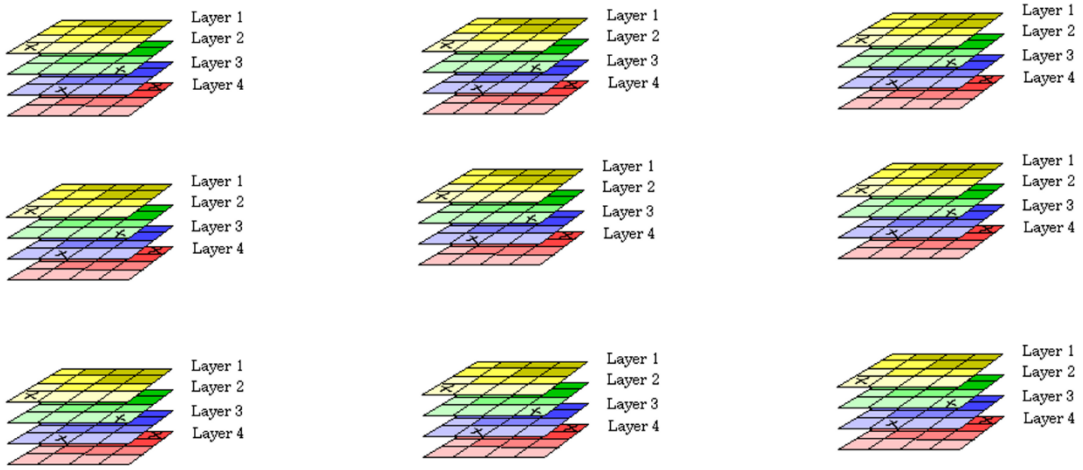

Figure 2. As with Figure 1, but with a representation of the procedure applied for all 9 models.

This was applied for the historical period and each cumulative emissions scenario. However, GEV parameter estimates tend to exhibit higher degrees of uncertainty under smaller sample sizes (e.g. Koutsoyiannis, 2004a). Therefore, in order to maximize sampling size for each sub-period, I selected the highest values across each model for each year. For instance, for the first year, under the RCP 4.5 scenario, the highest values for each of the nine GCMs would be selected for that year. This would then be applied for the next six years in that block/sub-period, creating a sample size of 63 observations (i.e. 63 annual maxima) per sub-period. For each sub-period, Quantile-Quantile diagnostic plots were then used to assess how well fitted the data were for validating the use of the GEV. The Maximum Likelihood Method was then used when fitting a GEV. This method is used to estimate the parameters of probability density functions from a GEV distribution and is considered as one of the best methods in doing so (Raynal-Villasenor, 2012), notably for shorter lengths of data (Hossain et al., 2021).

The GEV distribution is based on the three individual extreme value continuous probability distributions mentioned previously. As such, the three principal probability distributions are termed Gumbel (light-tailed), Frechet (heavy-tailed) and Weibull (bounded-tail), representing Type 1, Type II and Type III, respectively. The Weibull distribution is a variety of light-tailed distribution (Girard). In light of its heavier-tailed distribution, the Frechet distribution is representative of higher probabilities of given extreme events, while lower probabilities are found with faster rates of decay typical of the Gumbel and Weibull distributions (Ferreira, 2011; Carney, 2016). These probabilities may be illustrated as shown in Figure 3:

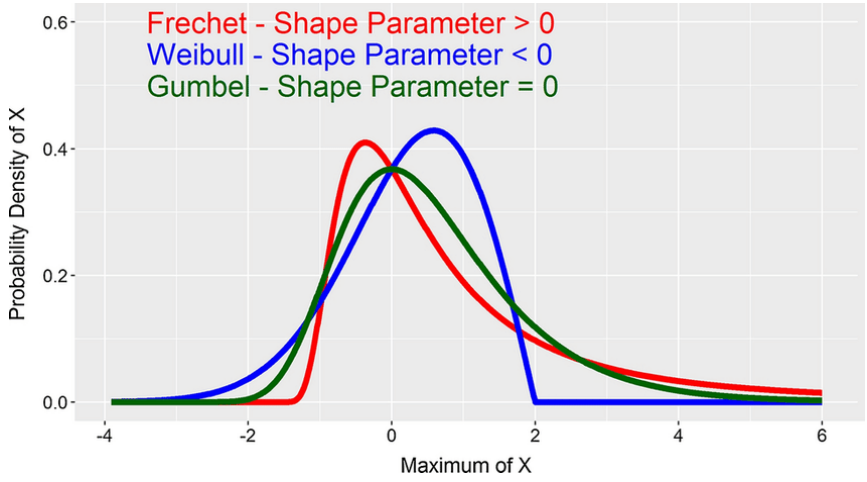

Figure 3. Probability density functions corresponding to Frechet (red), Weibull (blue) and Gumbel (green) distributions. Adapted from "The application of extreme value theory to pharmacometrics", by P. L. Bonate (2021). *Journal of Pharmacokinetics and Pharmacodynamics*, *48*(1), 83-97.

Each of these families represents a different asymptotic distribution of extreme values (Coles, 2001). The GEV distribution combines these families of probability distributions in the following form:

$$F_t(x) = \exp\left\{-\left[1+\xi_t\left(\frac{x-\mu_t}{\sigma_t}\right)\right]^{-1/\xi_t}\right\}, \quad (1)$$

Where, "μ", "σ" and "ξ" represents the location, scale and shape parameters, respectively. Both μ and σ must be greater than negative infinity and less than infinity, while sigma must be greater than 0 and less than infinity. Using this equation, it was possible to compute estimates of location, scale and shape for each sub-period. This is done by fitting a GEV to each block/sub-period to solve for these parameters. Since location estimates are of particular interest, I focus on plotting these as a function of cumulative emissions, as well as with the calculated standard errors derived from these estimates. I further use probability density functions of GEV distributions fitted with location, scale and shape parameter estimates centered at around 0 teratons of carbon (TtC), and then using those parameter estimates at every 0.5 TtC thereafter (Figures 5, 8 & 11). Similar to Innocenti et al. (2019), location estimates derived for the historical period were merged with those estimates of the two RCP scenarios (referred to herein as "Historical + RCP 4.5" and "Historical + RCP 8.5"), creating a time series consisting of 32 sub-periods, while for the 1pctCO_2 scenario, 20 sub-periods were created.

Using the same procedure, I further show trends in 20-year and 100-year return levels as a function of cumulative emissions, including the historical period and RCP scenarios, as well as for the 1pctCO_2 scenario.

Statistical test

All statistical tests were performed using R, a programming software utilized for statistical computing. For the purposes of this study, I used trend analyses to evaluate the statistical significance of trends in location, scale and shape parameter estimates. Trends were assessed using the Mann-Kendall statistical test. The Mann-Kendall test is specifically designed to assess and detect trends in time series data and has been widely used in trend detection for hydrometeorological time series datasets (e.g. Wang et al., 2020). This statistical test was, therefore, useful for analyzing patterns for the three distribution parameters comprising the GEV distribution. However, due to serial correlation (autocorrelation), a pre-whitened version of the Mann-Kendall test was often used to improve trend accuracy. Serial correlation refers to similarities that occur between values of the same variables over successive intervals of time, implying that the data is correlated with itself (Koutsoyiannis, 2004a). Pre-whitening is, therefore, applied to reduce frequent trend detections (Bayazit & Onoz, 2007). As such, for each of the distribution parameters, I used an autocorrelation detection function as a diagnostic tool. Specifically, I used the Autocorrelation Function (ACF), which is a function designed to calculate estimates of autocorrelation that may exist in a time series. The threshold used in this study to determine whether sufficient autocorrelation exists was 0.40. Therefore, if the data showed an autocorrelation value of 0.40 or greater, a pre-whitened version of the Mann-Kendall test would be applied to correct for autocorrelation. The Mann-Kendall test additionally provides an estimate of the Sen's slope, or a pre-whitened Sen's slope in situations of sufficiently large autocorrelation. The Sen's slope is designed to display and focus on the median slope of all slopes among data points in a time series. It is also recommended by the World Meteorological Organization that Sen's slope be used as a part of the trend detection of hydrometeorological

data, partly because it is not affected by the number of outliers and any errors in the data, as compared with linear regression (Aditya et al., 2021). Sen's slope is represented mathematically as follows:

$$Q_i = (x_j - x_i) / j - i,\ i = 1, 2, 3 \ldots n \quad (2)$$

Where n refers to the number of paired values, "x_j" and "x_i" represent data values at time "j" and "i" when j > i (Aditya et al., 2021).

The statistical significance of these trends was then estimated with calculated p-values. Results are summarized in Tables 2-4 for parameters of both Rx1day and Rx5day for each of the emissions scenarios.

Results

Global trends

Globally, the results generally show highly statistically significant trends ($p < 0.01$) in location, scale and shape estimates for both Rx1day and Rx5day as cumulative emissions increase (Table 2, Figure 4). For location parameter estimates, the responses scaled approximately linearly with cumulative emissions (Figure 4), notably for Rx1day ($p < 0.01$). The global PDFs of GEV distributions for both Rx1day and Rx5day also correspondingly show a shift towards higher extreme precipitation values in response to significant increases in both location and scale values with higher cumulative CO_2 emissions (Figure 5). This pattern is further representative of the rightward shift and stretched and reduced peaks in the GEV distributions at higher emissions (Figure 5). The shape parameter also largely decreased significantly ($p < 0.01$) at higher emissions, corresponding to a median rate of change of -0.0057 (Table 2). This suggests a shift towards a lighter-tailed distribution at higher emissions for

Rx1day and Rx5day as shape values decrease. Consistent with the robust increases in location and scale parameter estimates shown for both global Rx1day and Rx5day, the results further display a significant increase in 20-year and 100-year return levels with larger cumulative emissions (Figure 6). This is particularly notable for global Rx1day, where both 20-year and 100-year return levels also trend approximately linearly. Similar trends are also shown for Rx5day precipitation, especially for 20-year return levels.

Land and ocean trends

I found significant increasing (linear) trends across scenarios for land and ocean annual maxima (Table 2, Figures 4 & 5). With the exception of the Historical + RCP 8.5 case, my results largely show robustly increasing linear trends in location parameter estimates for both Rx1day and Rx5day as cumulative emissions rise ($p <= 0.02$). Among these increasing trends, I found that the median slope was noteworthy for the 1pctCO_2 scenario, where a rate of change of 7.19 mm/day was shown. Conversely, for the Historical + RCP 8.5 ocean trends, I found a significant decreasing trend ($p = 0.07$). The results further showed significant increasing linear trends ($p <= 0.01$) in scale parameter estimates for annual maxima for land and ocean (Table 2). The significant increasing trends in both location and scale parameter estimates are reflective of the rightward and more stretched tendencies in the GEV distributions towards larger extreme precipitation values, from the beginning of the historical period towards the end of the RCP and 1pctCO_2 scenarios (Figure 5). Correspondingly, much like at the global scale, higher probabilities are shown for the largest pre-industrial extreme precipitation events as CO_2 emissions rise; for example, a 400 mm/day event at 0 TtC is shown to increase in probability at higher emissions for both land and ocean (Figure 5). The shape parameter estimate trends for land and ocean generally exhibit significant linear decreases ($p <= 0.10$) for Rx1day and Rx5day,

with a median rate of decrease ranging typically from -0.01 to -0.03 (Table 2). Also similar to global trends, shape parameter estimates for land/ocean Rx1day and Rx5day mostly shift from a heavier-tailed to a lighter-tailed distribution as shape parameter values reach negative values – Table 2. This decreasing trend is especially notable for Rx1day Historical + RCP 4.5 and Historical + RCP 8.5 cases, and for the Rx5day under 1pctCO_2 (p <= 0.02). Correspondingly, I found a robust increase in the intensity of return levels with higher cumulative emissions. Figure 6 displays the generally increasing linear trends in both 20-year and 100-year return levels at larger emission levels. For example, for land Rx1day, owing to the robust increases in location and scale parameter estimates, an approximately 300 mm/day 100-year return level at the beginning of the historical period increases to about 450 mm/day at two TtC of cumulative emissions under the RCP 8.5 scenario.

Table 2. Trends for global, land and ocean Rx1day and Rx5day precipitation for the location, scale and shape parameters under Historical + RCP 4.5 and Historical + RCP 8.5, and for 1pctCO_2. Results are given as the Sen's slope for trends in parameters, as well as the distribution tendency based on the shape parameters over the time series. *, ** and *** indicate trends that are statistically significant at or within the 10%, 5% and 1% significance levels, respectively.

Global				
Rx1day trends (Historical + RCP 4.5)				
	Trend	Sen's slope	Distribution	p-value
Location	Increasing***	0.8560	Lighter-tail	<0.01
Scale	Increasing***	0.6924		<0.01
Shape	Decreasing***	-0.0057		<0.01
Rx1day trends (Historical + RCP 8.5)				
	Trend	Sen's slope	Distribution	p-value
Location	No trend	-0.1066	Lighter-tail	0.61
Scale	Increasing**	0.3163		0.05
Shape	Decreasing***	-0.0030		<0.01
Rx1day trends (1pctCO_2)				
	Trend	Sen's slope	Distribution	p-value
Location	Increasing***	5.0241	Lighter-tail	<0.01
Scale	Increasing***	1.7933		<0.01
Shape	Decreasing***	-0.020		<0.01
Rx5day trends (Historical + RCP 4.5)				

	Trend	Sen's slope	Distribution	p-value
Location	Increasing***	0.7532	Lighter-tail	<0.01
Scale	Increasing***	0.9670		<0.01
Shape	No trend	-0.0015		0.30
Rx5day trends (Historical + RCP 8.5)				
	Trend	Sen's slope	Distribution	p-value
Location	Increasing**	0.6033	Lighter-tail	0.03
Scale	Increasing***	1.4364		<0.01
Shape	Decreasing*	-0.0045		0.09
Rx5day trends (1pctCO_2)				
	Trend	Sen's slope	Distribution	p-value
Location	Increasing***	0.9591	Lighter-tail	<0.01
Scale	Increasing***	2.0900		<0.01
Shape	Decreasing***	-0.0091		<0.01
Land				
Rx1day trends (Historical + RCP 4.5)				
	Trend	Sen's slope	Distribution	p-value
Location	Increasing***	1.3131	Lighter-tail	<0.01
Scale	Increasing***	0.8078		<0.01
Shape	Decreasing***	-0.0100		<0.01
Rx1day trends (Historical + RCP 8.5)				
	Trend	Sen's slope	Distribution	p-value
Location	Decreasing*	-0.1702	Lighter-tail	0.07
Scale	No trend	0.0963		0.29
Shape	Decreasing***	-0.0113		<0.01
Rx1day trends (1pctCO_2)				
	Trend	Sen's slope	Distribution	p-value
Location	Increasing***	4.2292	No trend	<0.01
Scale	Increasing***	1.5771		<0.01
Shape	No trend	-0.0036		0.60
Rx5day trends (Historical + RCP 4.5)				
	Trend	Sen's slope	Distribution	p-value
Location	Increasing***	0.4022	No trend	<0.01
Scale	Increasing***	0.9050		<0.01
Shape	No trend	-0.0032		0.12
Rx5day trends (Historical + RCP 8.5)				
	Trend	Sen's slope	Distribution	p-value
Location	Increasing**	0.5504	Lighter-tail	0.02
Scale	Increasing***	0.1251		<0.01
Shape	Decreasing*	-0.0043		0.07
Rx5day trends (1pctCO_2)				
	Trend	Sen's slope	Distribution	p-value
Location	Increasing***	7.1915	Lighter-tail	<0.01
Scale	Increasing***	2.9754		<0.01
Shape	Decreasing*	-0.0067		0.10

Ocean				
Rx1day trends (Historical + RCP 4.5)				
	Trend	Sen's slope	Distribution	p-value
Location	Increasing***	0.8299	Lighter-tail	<0.01
Scale	Increasing***	0.7401		<0.01
Shape	Decreasing***	-0.0050		<0.01
Rx1day trends (Historical + RCP 8.5)				
	Trend	Sen's slope	Distribution	p-value
Location	No trend	-0.0076	Lighter-tail	0.99
Scale	Increasing***	0.3799		0.01
Shape	Decreasing**	-0.0042		0.02
Rx1day trends (1pctCO$_2$)				
	Trend	Sen's slope	Distribution	p-value
Location	Increasing***	2.9137	Lighter-tail	<0.01
Scale	Increasing***	1.8671		<0.01
Shape	Decreasing***	-0.0263		<0.01
Rx5day trends (Historical + RCP 4.5)				
	Trend	Sen's slope	Distribution	p-value
Location	Increasing***	0.4281	No trend	<0.01
Scale	Increasing***	0.8450		<0.01
Shape	No trend	-0.0004		0.73
Rx5day trends (Historical + RCP 8.5)				
	Trend	Sen's slope	Distribution	p-value
Location	Increasing*	0.5554	No trend	0.06
Scale	Increasing***	1.4716		<0.01
Shape	No trend	-0.0038		0.11
Rx5day trends (1pctCO$_2$)				
	Trend	Sen's slope	Distribution	p-value
Location	Increasing***	4.0396	Lighter-tail	<0.01
Scale	Increasing***	2.7663		<0.01
Shape	Decreasing***	-0.0097		<0.01

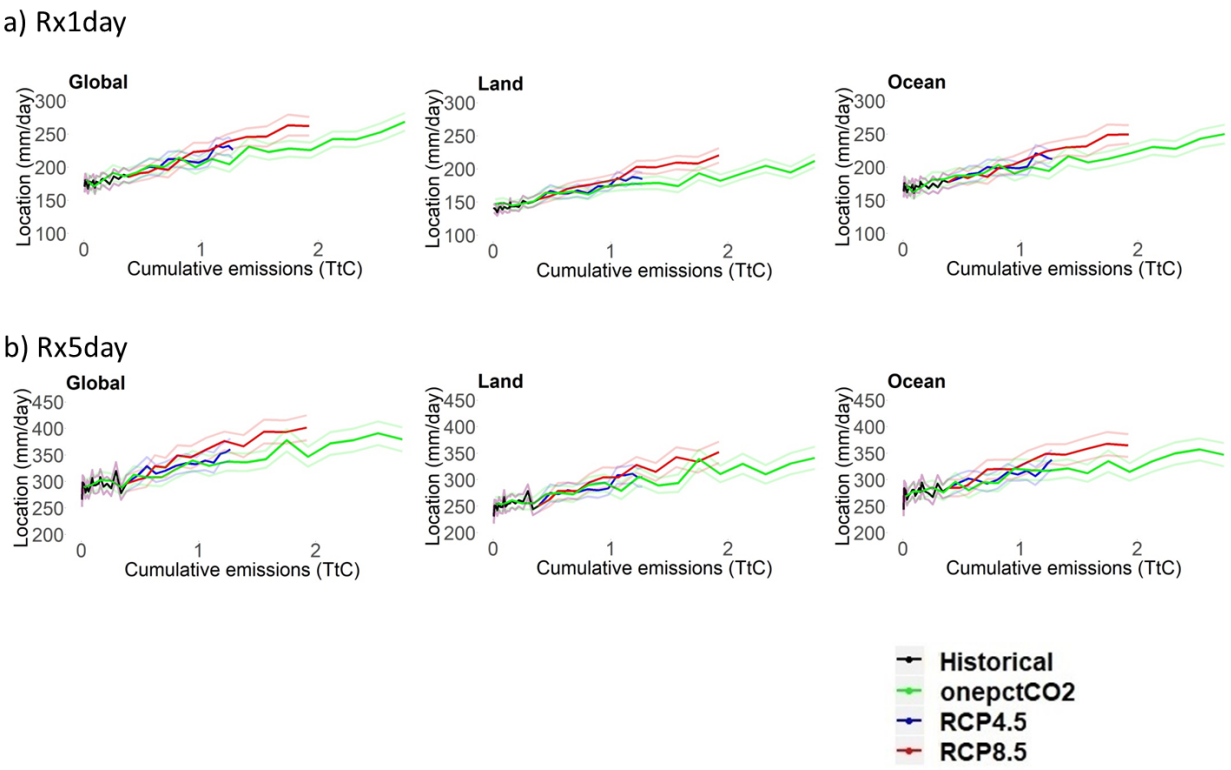

Figure 4. Global, land and water trends for location parameter estimates for (a) annual Rx1day and (b) Rx5day maximum precipitation as a function of cumulative emissions. The black curve represents the historical period, while the green, blue and red curves represent the 1pctCO_2, RCP 4.5 and RCP 8.5 scenarios, respectively. Transparent curves highlight the range of uncertainty that is reported based on the standard error.

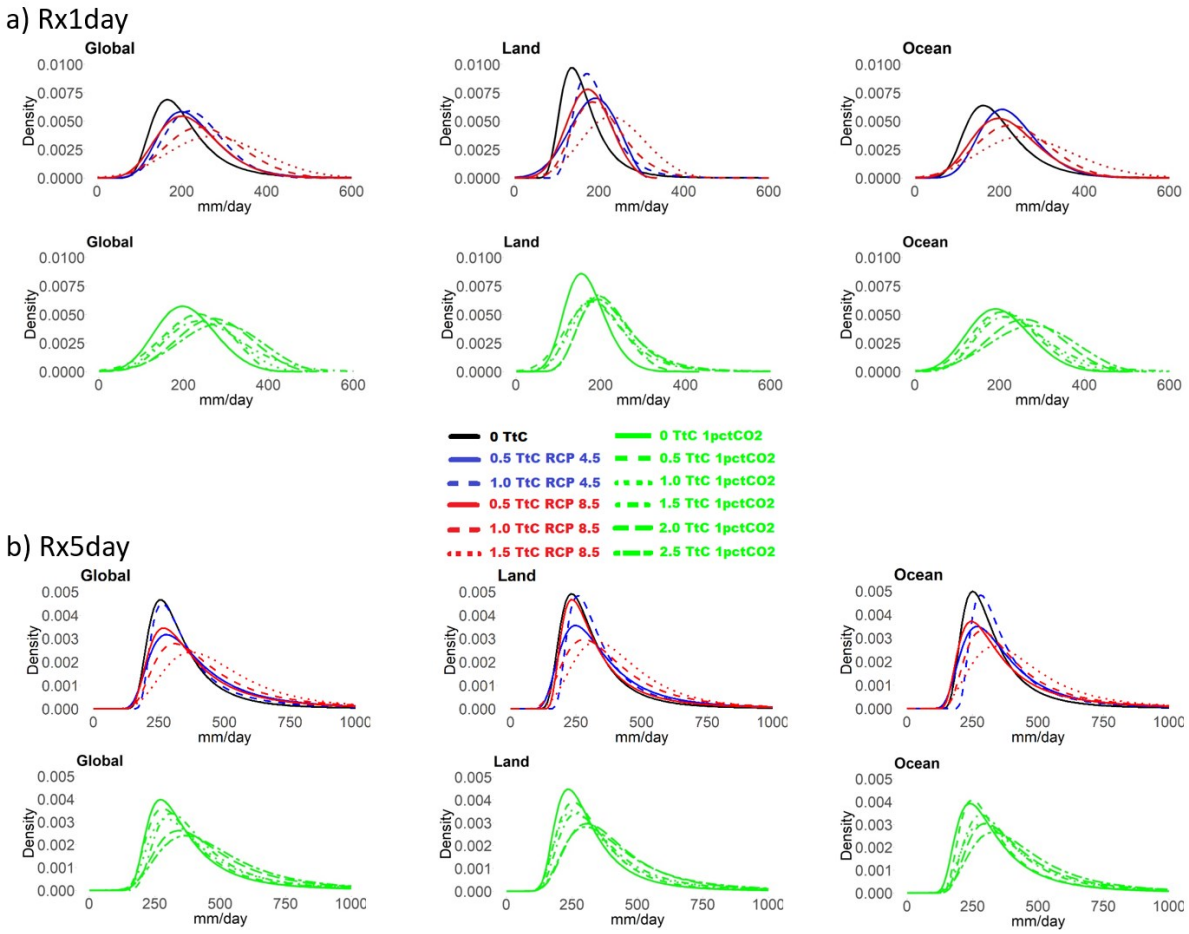

Figure 5. Global, land and ocean probability density functions of GEV distributions displaying trends in extreme precipitation indicators. Curves represent estimates at 0 TtC, and then estimates centered on increments of 0.5 TtC thereafter. Estimates are shown for global, land and ocean for (a) Rx1day and (b) Rx5day for the historical period (black), RCP 4.5 (blue), RCP 8.5 (red), and 1pctCO_2 (green).

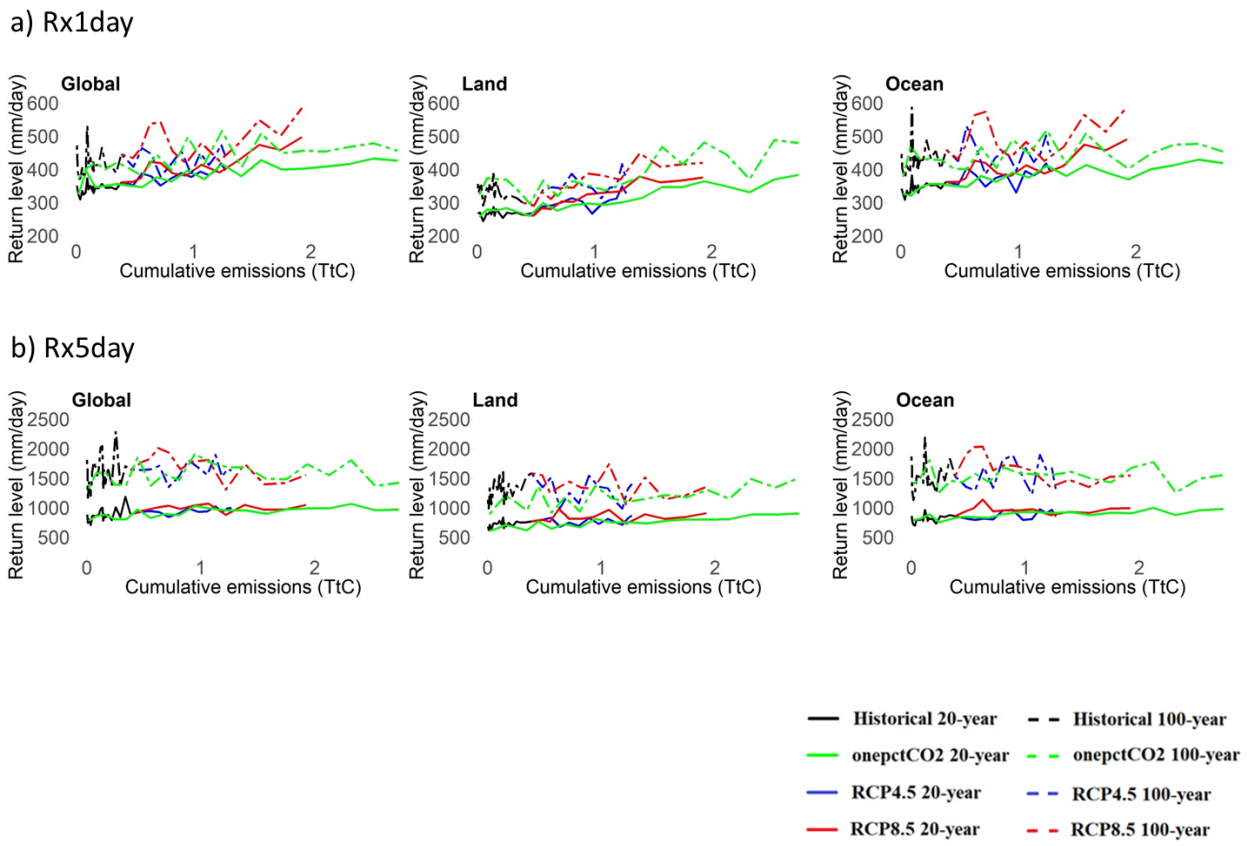

Figure 6. 20-year and 100-year return level trends for global, land and ocean for (a) Rx1day and (b) Rx5day.

National trends

In this section, I analyze trends in Rx1day and Rx5day for the five selected nations. Results are summarized in Table 3 and Figures 7-9.

For all nations studied, my results largely show statistically significant increasing trends in Rx1day and Rx5day for both location and scale estimates as cumulative emissions increase ($p <= 0.10$). Much like global, water and land trends, national location parameter estimates respond mostly linearly (Figure 6). I also found significant rates of change for some countries. For example, as shown in Table 3, the United States yields a Sen's slope that is about 0.08 to 1.28 mm/day ($p < 0.01$) and 0.06 to 0.48 mm/day ($p <=0.05$) for location and scale, respectively.

Table 3 shows particularly significant location estimate increases for annual maxima for Australia and India, with a median rate of increase of 0.17 to 1.39 mm/day and 0.49 to 1.53 mm/day ($p < 0.01$), respectively. Figure 8 correspondingly reflects this tendency, much like what was previously shown for global, land and ocean trends, with all nations showing significant shifts towards higher location parameter estimates in especially 1pctCO_2 and RCP 8.5 for both extreme precipitation indicators, as well as with flattening peaks and more stretched distributions at higher emissions in response to increased scale parameter estimates. Nationally, higher probabilities for the most extreme precipitation events at 0 TtC are generally shown to increase at higher cumulative CO_2 emissions (Figure 8).

Brazil notably exhibited statistically significant trends for all parameters for Rx1day and Rx5day ($p <= 0.10$). Results also show that the Sen's slope estimate for the scale parameter is particularly high for India (1.56 mm/day, $p < 0.01$, Table 2), under the 1pctCO_2 scenario for Rx1day, while for Brazil, the location estimate increases by 1.71 mm/day for 1pctCO_2 ($p < 0.01$, Table 3).

By contrast, shape estimates more frequently showed no significant trend with increasing cumulative emissions (Table 3), as compared to the more significant declining trend captured globally, and for land/ocean. However, some notable significant trends should be acknowledged. Brazil, for instance, consistently showed significant but opposing trends for Rx1day and Rx5day; Rx1day decreased significantly ($p <= 0.10$), while Rx5day significantly increased ($p <= 0.06$) towards a heavier-tailed distribution. This included a Sen's slope of -0.0043 to -0.01 for Rx1day and 0.022 to 0.0056 for Rx5day. In other nations, I found significant decreasing trends, becoming lighter-tailed, though this was more prevalent for Rx1day ($p <= 0.05$, Table 3).

Much like for global and land/ocean trends, the consistent significant linear increases in scale and location estimates across nations are typically showcased in the upward linear trend featured by the national 20-year and 100-year return levels (Figure 9). In Brazil, for example, Rx1day 20-year return levels at the beginning of the historical period increase by nearly 100 mm/day (from approximately 200 mm/day to nearly 300 mm/day) at about three TtC of cumulative emissions in the 1pctCO_2 case. The results also show a nearly 150 mm/day increase in 20-year return level over the same time period and scenario for India Rx1day.

Table 3. National trends for Rx1day and Rx5day precipitation for the location, scale and shape parameters under Historical + RCP 4.5 and Historical + RCP 8.5, and for 1pctCO_2. Results are given as the Sen's slope for trends in parameters, as well as the distribution tendency based on the shape parameters over the time series. *, ** and *** indicate trends that are statistically significant at or within the 10%, 5% and 1% significance levels, respectively.

United States				
Rx1day trends (Historical + RCP 4.5)				
	Trend	Sen's slope	Distribution	p-value
Location	Increasing***	0.2259	No trend	<0.01
Scale	Increasing**	0.0588		0.04
Shape	No trend	-0.0021		0.33
Rx1day trends (Historical + RCP 8.5)				
	Trend	Sen's slope	Distribution	p-value
Location	No trend	0.0781	Lighter-tail	0.11
Scale	Increasing**	0.0697		0.02
Shape	Decreasing**	-0.0038		0.05
Rx1day trends (1pctCO_2)				
	Trend	Sen's slope	Distribution	p-value
Location	Increasing***	0.6473	Lighter-tail	<0.01
Scale	Increasing***	0.3798		<0.01
Shape	Decreasing***	-0.0161		<0.01
Rx5day trends (Historical + RCP 4.5)				
	Trend	Sen's slope	Distribution	p-value
Location	Increasing***	0.3344	No trend	<0.01
Scale	No trend	0.1095		0.15
Shape	No trend	0.0005		0.80
Rx5day trends (Historical + RCP 8.5)				
	Trend	Sen's slope	Distribution	p-value
Location	Increasing***	0.3806	No trend	<0.01
Scale	Increasing**	0.1641		0.05

Shape	No trend	0.0032		0.12
Rx5day trends (1pctCO$_2$)				
	Trend	Sen's slope	Distribution	p-value
Location	Increasing***	1.2828	No trend	<0.01
Scale	Increasing***	0.4836		0.01
Shape	No trend	0.0008		0.90
Australia				
Rx1day trends (Historical + RCP 4.5)				
	Trend	Sen's slope	Distribution	p-value
Location	Increasing***	0.6755	Lighter-tail	<0.01
Scale	Increasing***	0.4171		<0.01
Shape	Decreasing*	-0.0040		0.08
Rx1day trends (Historical + RCP 8.5)				
	Trend	Sen's slope	Distribution	p-value
Location	Increasing***	0.4387	Lighter-tail	<0.01
Scale	Increasing***	0.3879		<0.01
Shape	Decreasing***	-0.0053		0.01
Rx1day trends (1pctCO$_2$)				
	Trend	Sen's slope	Distribution	p-value
Location	Increasing***	1.3903	No trend	<0.01
Scale	Increasing***	0.5118		<0.01
Shape	No trend	0.0013		0.63
Rx5day trends (Historical + RCP 4.5)				
	Trend	Sen's slope	Distribution	p-value
Location	Increasing**	0.1680	No trend	0.03
Scale	No trend	0.1027		0.11
Shape	No trend	0.0025		0.20
Rx5day trends (Historical + RCP 8.5)				
	Trend	Sen's slope	Distribution	p-value
Location	Increasing***	0.2735	No trend	0.01
Scale	Increasing*	0.1290		0.08
Shape	No trend	-0.1429		0.12
Rx5day trends (1pctCO$_2$)				
	Trend	Sen's slope	Distribution	p-value
Location	Increasing**	0.6047	No trend	0.03
Scale	Increasing***	0.5863		<0.01
Shape	No trend	-0.0019		0.63
India				
Rx1day trends (Historical + RCP 4.5)				
	Trend	Sen's slope	Distribution	p-value
Location	Increasing***	0.7067	No trend	<0.01
Scale	Increasing***	0.2075		<0.01
Shape	No trend	-0.0024		0.17
Rx1day trends (Historical + RCP 8.5)				
	Trend	Sen's slope	Distribution	p-value

Location	No trend	0.1447	Lighter-tail	0.41
Scale	Increasing**	0.1742		0.05
Shape	Decreasing**	-0.0036		0.03
Rx1day trends (1pctCO$_2$)				
	Trend	Sen's slope	Distribution	p-value
Location	Increasing***	1.5339	Heavier-tail	<0.01
Scale	Increasing***	0.6501		<0.01
Shape	Increasing*	0.0052		0.10
Rx5day trends (Historical + RCP 4.5)				
	Trend	Sen's slope	Distribution	p-value
Location	Increasing***	0.4908	No trend	<0.01
Scale	Increasing**	0.2753		0.05
Shape	No trend	0.0025		0.36
Rx5day trends (Historical + RCP 8.5)				
	Trend	Sen's slope	Distribution	p-value
Location	Increasing***	0.5600	No trend	<0.01
Scale	Increasing***	0.5129		0.01
Shape	No trend	0.0029		0.20
Rx5day trends (1pctCO$_2$)				
	Trend	Sen's slope	Distribution	p-value
Location	No trend	0.2680	No trend	0.33
Scale	Increasing***	1.5615		<0.01
Shape	No trend	0.0017		0.74
Brazil				
Rx1day trends (Historical + RCP 4.5)				
	Trend	Sen's slope	Distribution	p-value
Location	Increasing***	0.5656	Lighter-tail	<0.01
Scale	Increasing***	0.2082		<0.01
Shape	Decreasing**	-0.0043		0.03
Rx1day trends (Historical + RCP 8.5)				
	Trend	Sen's slope	Distribution	p-value
Location	No trend	0.0668	Lighter-tail	0.30
Scale	Increasing***	0.2362		<0.01
Shape	Decreasing***	-0.0091		<0.01
Rx1day trends (1pctCO$_2$)				
	Trend	Sen's slope	Distribution	p-value
Location	Increasing***	1.7119	Lighter-tail	<0.01
Scale	Increasing***	0.6501		<0.01
Shape	Decreasing*	-0.0100		0.10
Rx5day trends (Historical + RCP 4.5)				
	Trend	Sen's slope	Distribution	p-value
Location	Increasing**	0.1899	Heavier-tail	0.05
Scale	Increasing*	0.0927		0.10
Shape	Increasing*	0.0022		0.06
Rx5day trends (Historical + RCP 8.5)				

	Trend	Sen's slope	Distribution	p-value
Location	Increasing***	0.4122	Heavier-tail	<0.01
Scale	Increasing***	0.2175		0.01
Shape	Increasing***	0.0056		<0.01
Rx5day trends (1pctCO₂)				
	Trend	Sen's slope	Distribution	p-value
Location	Increasing***	1.1776	Heavier-tail	<0.01
Scale	Increasing***	1.1472		<0.01
Shape	Increasing**	0.0050		0.04
South Africa				
Rx1day trends (Historical + RCP 4.5)				
	Trend	Sen's slope	Distribution	p-value
Location	Increasing***	0.2980	Lighter-tail	<0.01
Scale	Increasing***	0.1233		<0.01
Shape	Decreasing**	-0.0036		0.04
Rx1day trends (Historical + RCP 8.5)				
	Trend	Sen's slope	Distribution	p-value
Location	Increasing***	0.2159	No trend	<0.01
Scale	Increasing***	0.2053		<0.01
Shape	No trend	0.0000		0.90
Rx1day trends (1pctCO₂)				
	Trend	Sen's slope	Distribution	p-value
Location	Increasing***	0.6023	No trend	<0.01
Scale	Increasing***	0.6501		<0.01
Shape	No trend	-0.0106		0.14
Rx5day trends (Historical + RCP 4.5)				
	Trend	Sen's slope	Distribution	p-value
Location	Increasing***	0.3722	No trend	<0.01
Scale	Increasing**	0.1280		0.03
Shape	No trend	-0.0011		0.74
Rx5day trends (Historical + RCP 8.5)				
	Trend	Sen's slope	Distribution	p-value
Location	Increasing***	0.3872	No trend	<0.01
Scale	Increasing***	0.1464		0.03
Shape	No trend	0.0013		0.56
Rx5day trends (1pctCO₂)				
	Trend	Sen's slope	Distribution	p-value
Location	Increasing***	0.8770	No trend	<0.01
Scale	Increasing***	0.3316		<0.01
Shape	No trend	0.0006		0.90

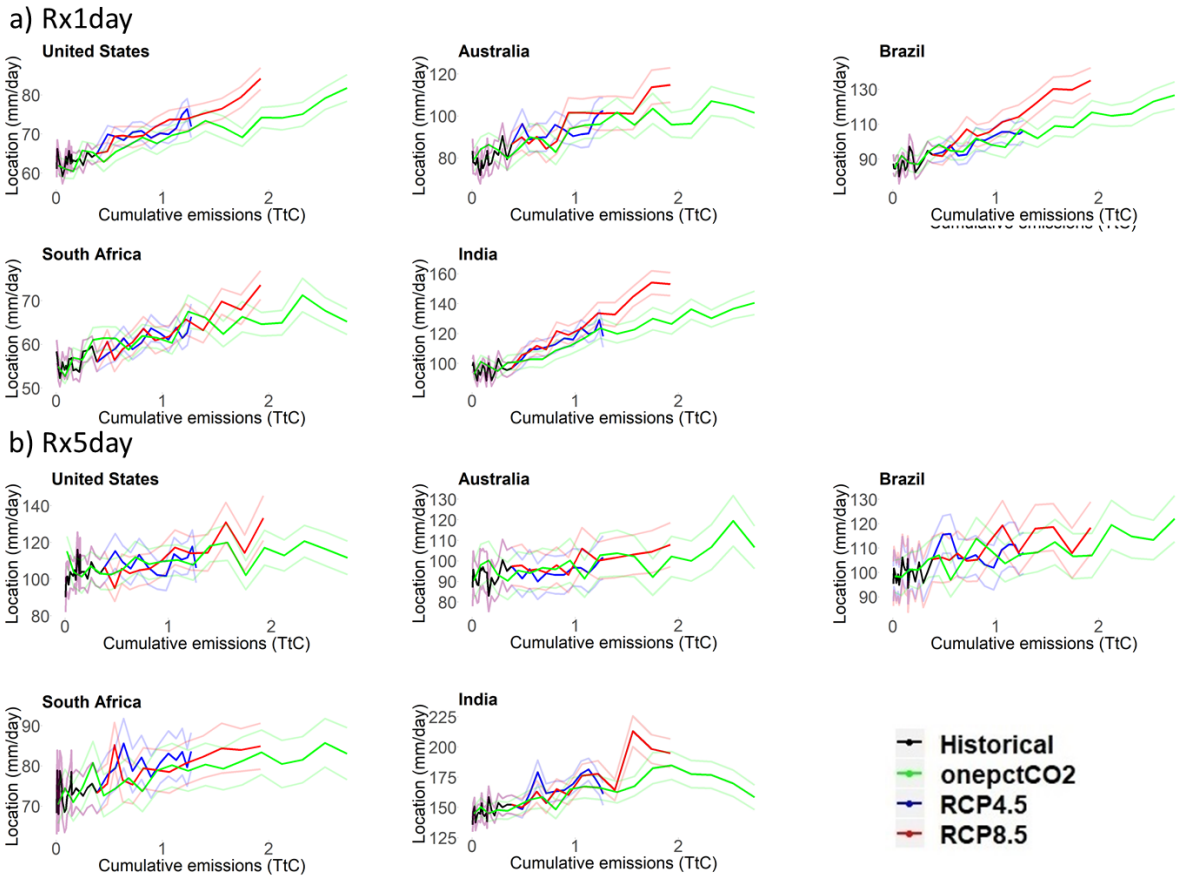

Figure 7. National trends for location parameter estimates as a function of cumulative emissions for (a) Rx1day and (b) Rx5day. The black curve represents the historical period, while the green, blue and red curves represent the 1pctCO_2, RCP 4.5 and RCP 8.5 scenarios, respectively. Transparent curves highlight the range of uncertainty that is reported based on the standard error.

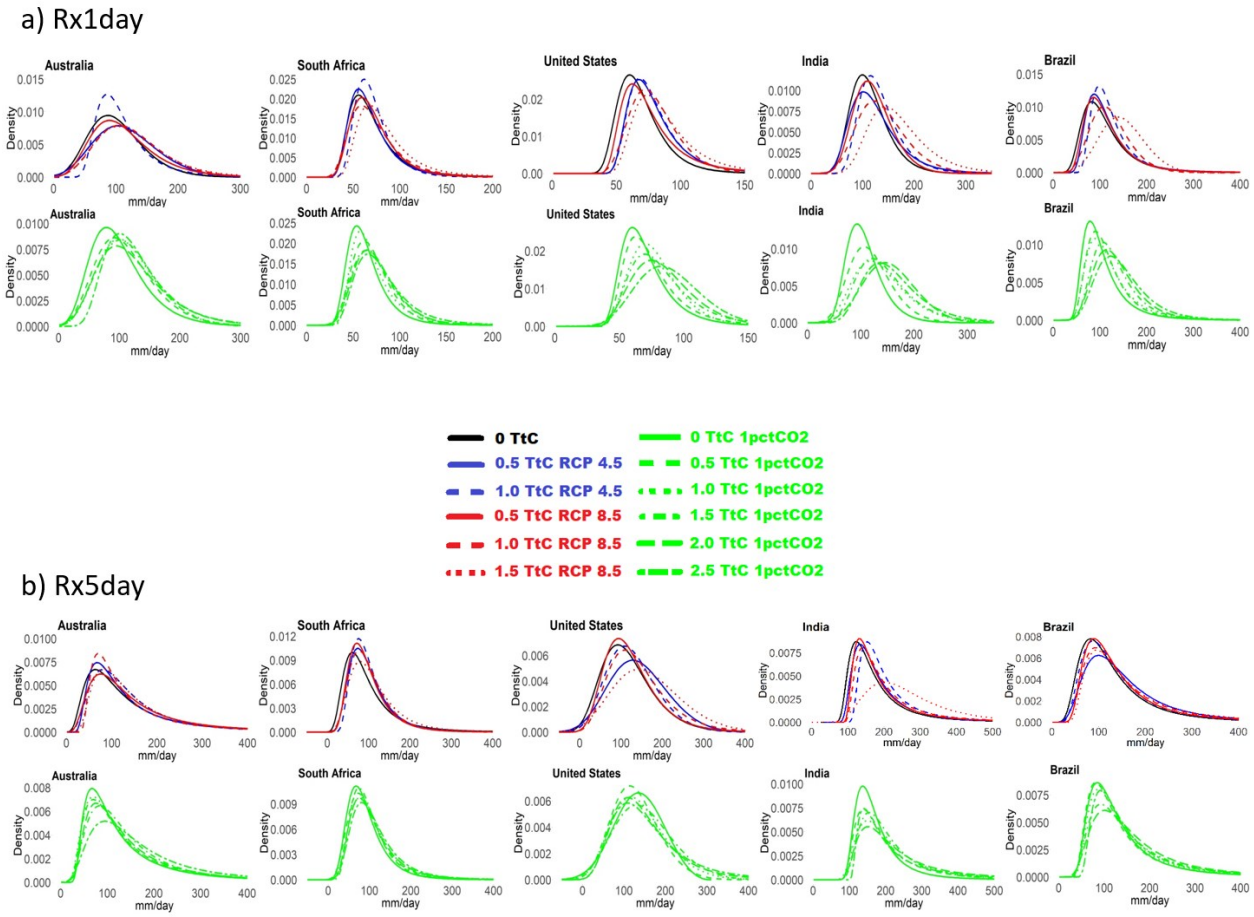

Figure 8. National probability density functions of GEV distributions displaying trends in extreme precipitation indicators. Curves represent estimates at 0 TtC, and then estimates centered on increments of 0.5 TtC thereafter. Estimates are shown for global, land and ocean for (a) Rx1day and (b) Rx5day for the historical period (black), RCP 4.5 (blue), RCP 8.5 (red), and 1pctCO_2 (green).

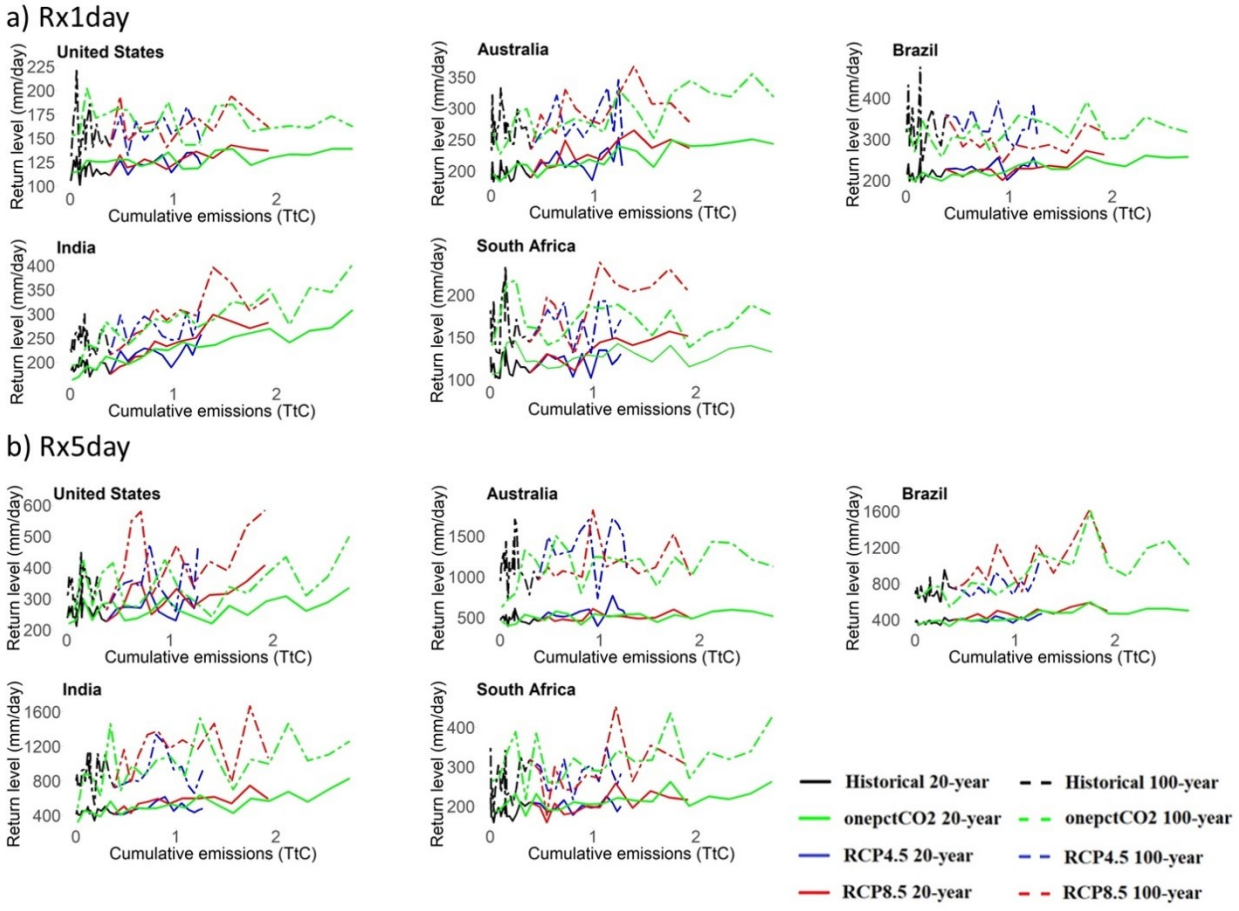

Figure 9. National 20-year and 100-year return level trends for (a) Rx1day and (b) Rx5day.

Local trends

In this section, I discuss results for the five locations used for this study. Results are summarized in Table 4, as well as in Figures 10-12.

Much like national trends, my findings show that location parameter estimates scale linearly with cumulative emissions across the five areas (Figure 10), with trends that are largely significant (p <= 0.07, Table 4). Also like globally to nationally, location parameter estimates for the selected locales trend toward higher values. As shown in Table 4, across the five areas for Rx1day and Rx5day, Sen's slope ranges from 0.10 to 0.77 mm/day (p <= 0.03). Scale parameter

trends mostly showed statistically significant increases ($p <= 0.07$) across all areas for both extreme precipitation indicators. I found a median rate of increase ranging from 0.08 to 0.84 mm/day, with the greatest increasing rate (0.84 mm/day) shown for Philippines Rx1day, under 1pctCO_2 ($p < 0.01$).

Following closely with national patterns, my results generally showed no significant trends for shape estimates at the local scale as cumulative emissions increased (Table 4). However, some notable trends exist. For Hong Kong, for instance, I found a significant decreasing trend under Historical + RCP 4.5 for Rx1day ($p = 0.02$) and 1pctCO_2 Rx5day ($p = 0.03$). For the Philippines, results showed highly significant decreases ($p < 0.01$) for Rx1day shape parameter estimates for all scenarios. Indeed, among the five areas, the results highlight the most significant decrease in shape parameter estimates with increasing cumulative emissions for Rx1day in the Philippines (Table 4). Conversely, the results showed a significant increasing trend ($p = 0.04$) for Rx5day under the 1pctCO_2 scenario, as well as for Hong Kong ($p = 0.02$), suggesting a shift towards a heavier-tailed distribution (Table 4). Finally, for Montreal, significant increases were similarly found for Historical + RCP 4.5 and Historical + RCP 8.5 ($p = 0.07$), and a significant decrease in Rx5day under the 1pctCO_2 scenario ($p = 0.04$). Across these locations, the significant trends showed a median rate of change of -0.01 to 0.01, with most transitioning from heavier-tailed to lighter-tailed behavior (Table 4). While I found no significant trends for Florida, there was a significant decrease ($p < 0.02$) for Rx1day under historical + RCP 4.5. Similar to the national, global and land/ocean scale, consistently significant increasing location and scale estimates translate in rightward shifts and stretched, flatter peaks in the GEV distribution as cumulative CO_2 emissions increase (Figure 11). While the probabilities of the highest values at 0 TtC also increase at higher emissions, as shown at other spatial scales, the

increase in probabilities is shown to be more subtle across locales as the tails of the distributions approach zero faster, similar to the overall patterns at the national scale (Figures 8 & 11). Conversely, Hong Kong showed a more gradual decline in its tails at higher CO_2 emissions (Figure 11a).

My results also show significant increases in 20-year and 100-year return levels, which like global, land, water and national trends, scale approximately linearly with cumulative emissions (Figure 12), notably in the case of Rx1day. This linearity is most distinct for St. Louis, Florida and Montreal for Rx1day, as well as for Philippines Rx5day. These increasing trends are consistent with the increases in location and scale estimates shown, which are related to progressively larger return levels in response to rising cumulative emissions.

Table 4. Local trends for Rx1day and Rx5day precipitation for the location, scale and shape parameters under Historical + RCP 4.5 and Historical + RCP 8.5, and for 1pctCO_2. Results are given as the Sen's slope for trends in parameters, as well as the distribution tendency based on the shape parameters over the time series. *, ** and *** indicate trends that are statistically significant at or within the 10%, 5% and 1% significance levels, respectively.

Hong Kong				
Rx1day trends (Historical + RCP 4.5)				
	Trend	Sen's slope	Distribution	p-value
Location	Increasing***	0.1319	No trend	0.01
Scale	Increasing**	0.0749		0.03
Shape	No trend	-0.0009		0.33
Rx1day trends (Historical + RCP 8.5)				
	Trend	Sen's slope	Distribution	p-value
Location	Increasing***	0.0953	No trend	0.01
Scale	Increasing***	0.1094		0.01
Shape	No trend	0.0000		0.98
Rx1day trends (1pctCO_2)				
	Trend	Sen's slope	Distribution	p-value
Location	No trend	0.2005	No trend	0.16
Scale	Increasing**	0.2011		0.02
Shape	No trend	0.0042		0.52
Rx5day trends (Historical + RCP 4.5)				
	Trend	Sen's slope	Distribution	p-value
Location	No trend	0.0710		0.18

Scale	Increasing***	0.1710	Heavier-tailed	0.01
Shape	Increasing**	0.0040		0.02
Rx5day trends (Historical + RCP 8.5)				
	Trend	Sen's slope	Distribution	p-value
Location	Increasing**	0.1550	No trend	0.02
Scale	Increasing***	0.1519		0.01
Shape	No trend	0.0000		0.98
Rx5day trends (1pctCO_2)				
	Trend	Sen's slope	Distribution	p-value
Location	No trend	0.1465	Heavier-tailed	0.41
Scale	Increasing**	0.4083		0.02
Shape	Increasing**	0.0066		0.03
Philippines				
Rx1day trends (Historical + RCP 4.5)				
	Trend	Sen's slope	Distribution	p-value
Location	Increasing***	0.5115	Lighter-tail	<0.01
Scale	Increasing***	0.2938		<0.01
Shape	Decreasing***	-0.0127		<0.01
Rx1day trends (Historical + RCP 8.5)				
	Trend	Sen's slope	Distribution	p-value
Location	Increasing***	0.3210	Lighter-tail	<0.01
Scale	Increasing***	0.2417		<0.01
Shape	Decreasing***	-0.0134		<0.01
Rx1day trends (1pctCO_2)				
	Trend	Sen's slope	Distribution	p-value
Location	Increasing***	0.2098	Lighter-tail	<0.01
Scale	Increasing***	0.8425		<0.01
Shape	Decreasing***	-0.0180		<0.01
Rx5day trends (Historical + RCP 4.5)				
	Trend	Sen's slope	Distribution	p-value
Location	No trend	0.0608	No trend	0.37
Scale	Increasing**	0.0926		0.03
Shape	No trend	-0.0006		0.49
Rx5day trends (Historical + RCP 8.5)				
	Trend	Sen's slope	Distribution	p-value
Location	No trend	-0.0050	No trend	0.95
Scale	Increasing***	0.1097		0.01
Shape	No trend	0.0014		0.25
Rx5day trends (1pctCO_2)				
	Trend	Sen's slope	Distribution	p-value
Location	No trend	0.0696	Heavier-tail	0.67
Scale	Increasing**	0.3835		0.04
Shape	Increasing**	0.0067		0.04
St. Louis				
Rx1day trends (Historical + RCP 4.5)				

	Trend	Sen's slope	Distribution	p-value
Location	Increasing***	0.2013	No trend	<0.01
Scale	Increasing***	0.0600		<0.01
Shape	No trend	-0.0003		0.83
Rx1day trends (Historical + RCP 8.5)				
	Trend	Sen's slope	Distribution	p-value
Location	Increasing***	0.2401	No trend	<0.01
Scale	Increasing***	0.0701		0.01
Shape	No trend	-0.0007		0.74
Rx1day trends (1pctCO_2)				
	Trend	Sen's slope	Distribution	p-value
Location	Increasing***	0.3321	No trend	<0.01
Scale	Increasing***	0.2202		<0.01
Shape	No trend	-0.0029		0.40
Rx5day trends (Historical + RCP 4.5)				
	Trend	Sen's slope	Distribution	p-value
Location	Increasing***	0.3378	No trend	<0.01
Scale	Increasing***	0.1850		<0.01
Shape	No trend	-0.0025		0.13
Rx5day trends (Historical + RCP 8.5)				
	Trend	Sen's slope	Distribution	p-value
Location	Increasing***	0.2687	No trend	0.01
Scale	Increasing***	0.1786		<0.01
Shape	No trend	0.0022		0.38
Rx5day trends (1pctCO_2)				
	Trend	Sen's slope	Distribution	p-value
Location	Increasing***	0.7695	No trend	<0.01
Scale	Increasing***	0.5139		<0.01
Shape	No trend	0.0028		0.43
Florida				
Rx1day trends (Historical + RCP 4.5)				
	Trend	Sen's slope	Distribution	p-value
Location	Increasing***	0.1666	Lighter-tail	<0.01
Scale	Increasing***	0.1200		<0.01
Shape	Decreasing**	-0.0040		0.02
Rx1day trends (Historical + RCP 8.5)				
	Trend	Sen's slope	Distribution	p-value
Location	Increasing***	0.1518	No trend	<0.01
Scale	Increasing***	0.1156		<0.01
Shape	No trend	-0.0019		0.31
Rx1day trends (1pctCO_2)				
	Trend	Sen's slope	Distribution	p-value
Location	Increasing***	0.3321	No trend	<0.01
Scale	Increasing***	0.2202		<0.01
Shape	No trend	-0.0029		0.40

Rx5day trends (Historical + RCP 4.5)				
	Trend	Sen's slope	Distribution	p-value
Location	Increasing***	0.1667	No trend	<0.01
Scale	Increasing*	0.1182		0.06
Shape	No trend	-0.0013		0.52
Rx5day trends (Historical + RCP 8.5)				
	Trend	Sen's slope	Distribution	p-value
Location	Increasing***	0.1732	No trend	0.01
Scale	Increasing*	0.1323		0.07
Shape	No trend	0.0023		0.31
Rx5day trends (1pctCO_2)				
	Trend	Sen's slope	Distribution	p-value
Location	Increasing**	0.3720	No trend	0.03
Scale	No trend	0.2861		0.14
Shape	No trend	0.0038		0.34
Montreal				
Rx1day trends (Historical + RCP 4.5)				
	Trend	Sen's slope	Distribution	p-value
Location	Increasing***	0.1032	Heavier-tail	<0.01
Scale	Increasing**	0.0250		0.02
Shape	Increasing*	0.0038		0.07
Rx1day trends (Historical + RCP 8.5)				
	Trend	Sen's slope	Distribution	p-value
Location	Increasing***	0.0643	Heavier-tail	0.01
Scale	Increasing***	0.0392		0.01
Shape	Increasing*	0.0045		0.07
Rx1day trends (1pctCO_2)				
	Trend	Sen's slope	Distribution	p-value
Location	Increasing***	0.1976	No trend	<0.01
Scale	Increasing***	0.0979		<0.01
Shape	No trend	-0.0022		0.58
Rx5day trends (Historical + RCP 4.5)				
	Trend	Sen's slope	Distribution	p-value
Location	Increasing***	0.1569	No trend	<0.01
Scale	Increasing**	0.0673		0.02
Shape	No trend	-0.0012		0.46
Rx5day trends (Historical + RCP 8.5)				
	Trend	Sen's slope	Distribution	p-value
Location	Increasing***	0.1376	No trend	<0.01
Scale	Increasing***	0.1103		<0.01
Shape	No trend	-0.0005		0.88
Rx5day trends (1pctCO_2)				
	Trend	Sen's slope	Distribution	p-value
Location	Increasing***	0.5477	Lighter-tail	<0.01
Scale	Increasing***	0.1637		<0.01

Shape	Decreasing**	-0.0100		0.04

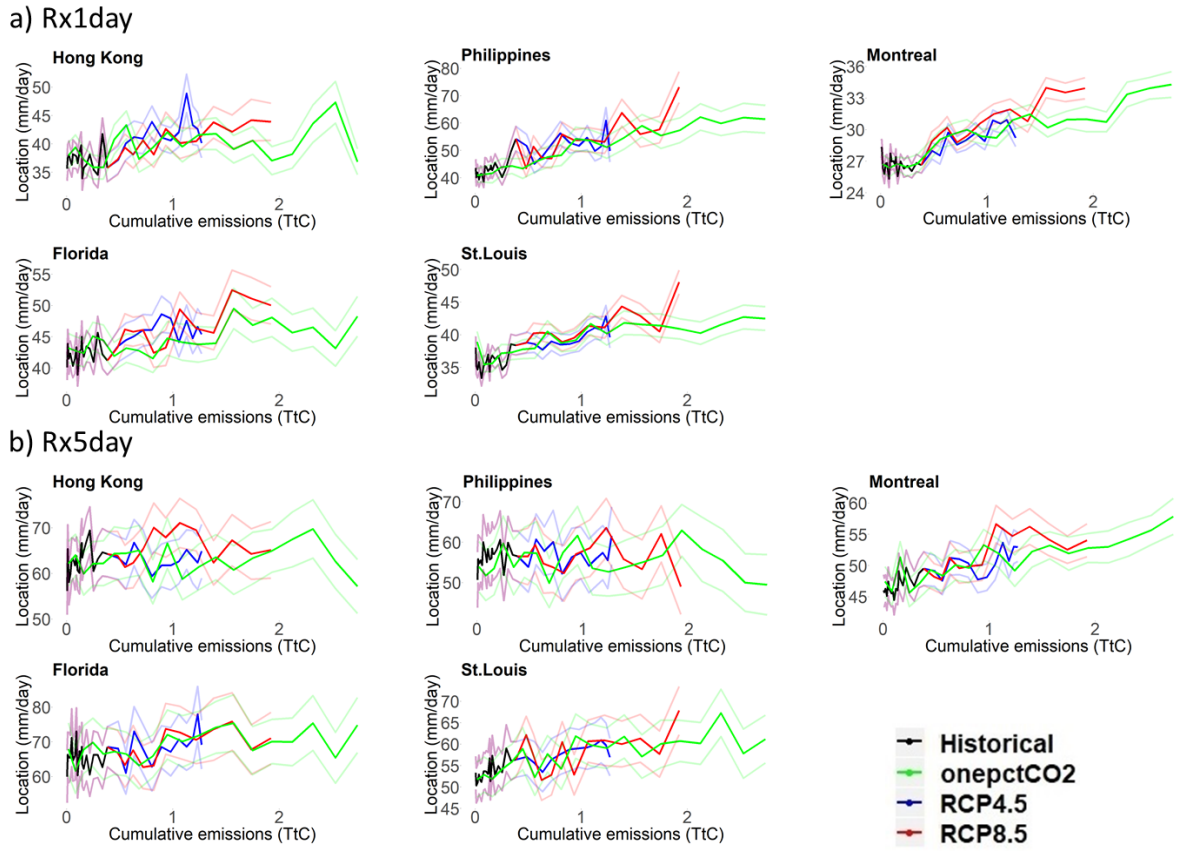

Figure 10. Local trends for location parameter estimates for (a) Rx1day and (b) Rx5day as a function of cumulative emissions. The black curve represents the historical period, while the green, blue and red curves represent the 1pctCO_2, RCP 4.5 and RCP 8.5 scenarios, respectively. Transparent curves highlight the range of uncertainty that is reported based on the standard error.

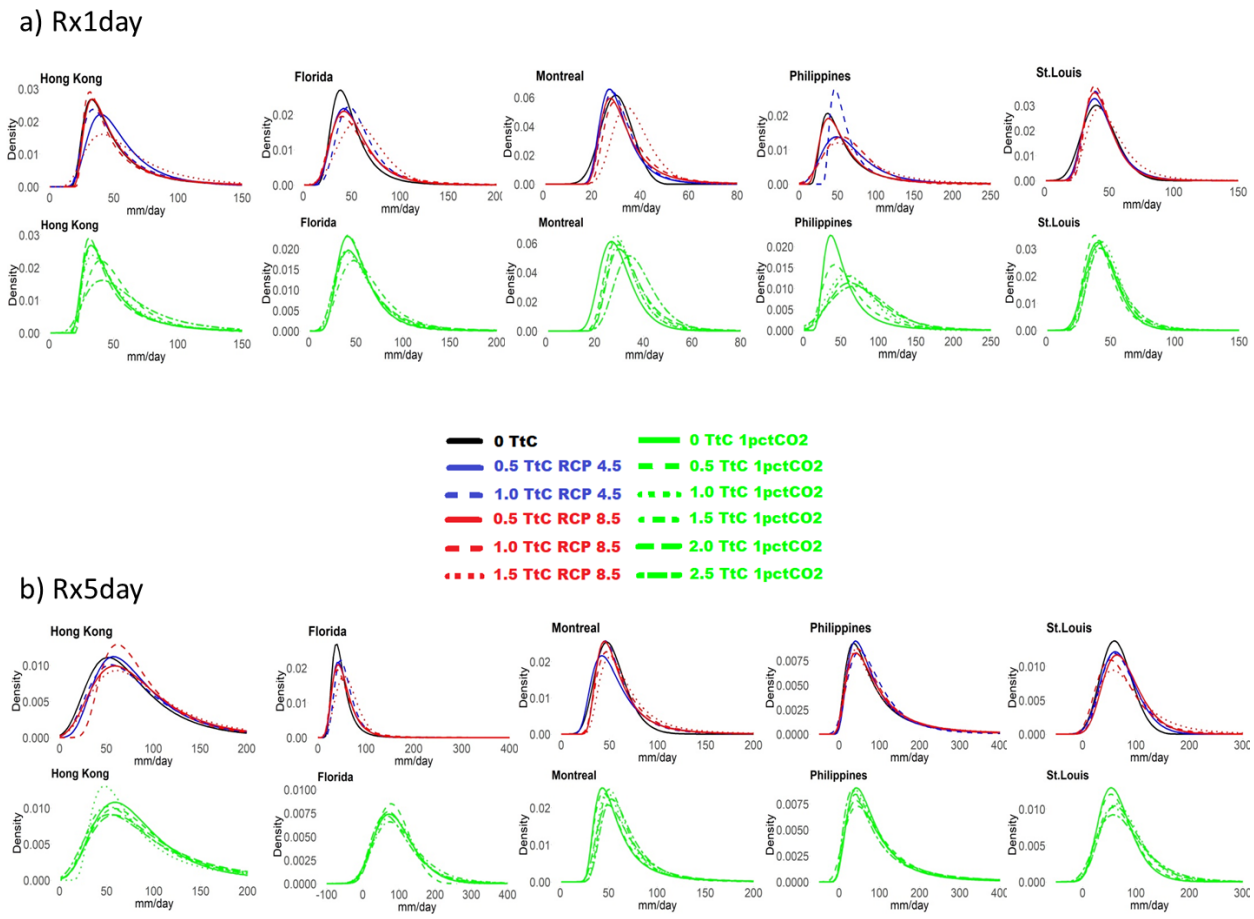

Figure 11. Local probability density functions of GEV distributions displaying trends in extreme precipitation indicators. Curves represent estimates at 0 TtC, and then estimates centered on increments of 0.5 TtC thereafter. Estimates are shown for global, land and ocean for (a) Rx1day and (b) Rx5day for the historical period (black), RCP 4.5 (blue), RCP 8.5 (red), and 1pctCO_2 (green).

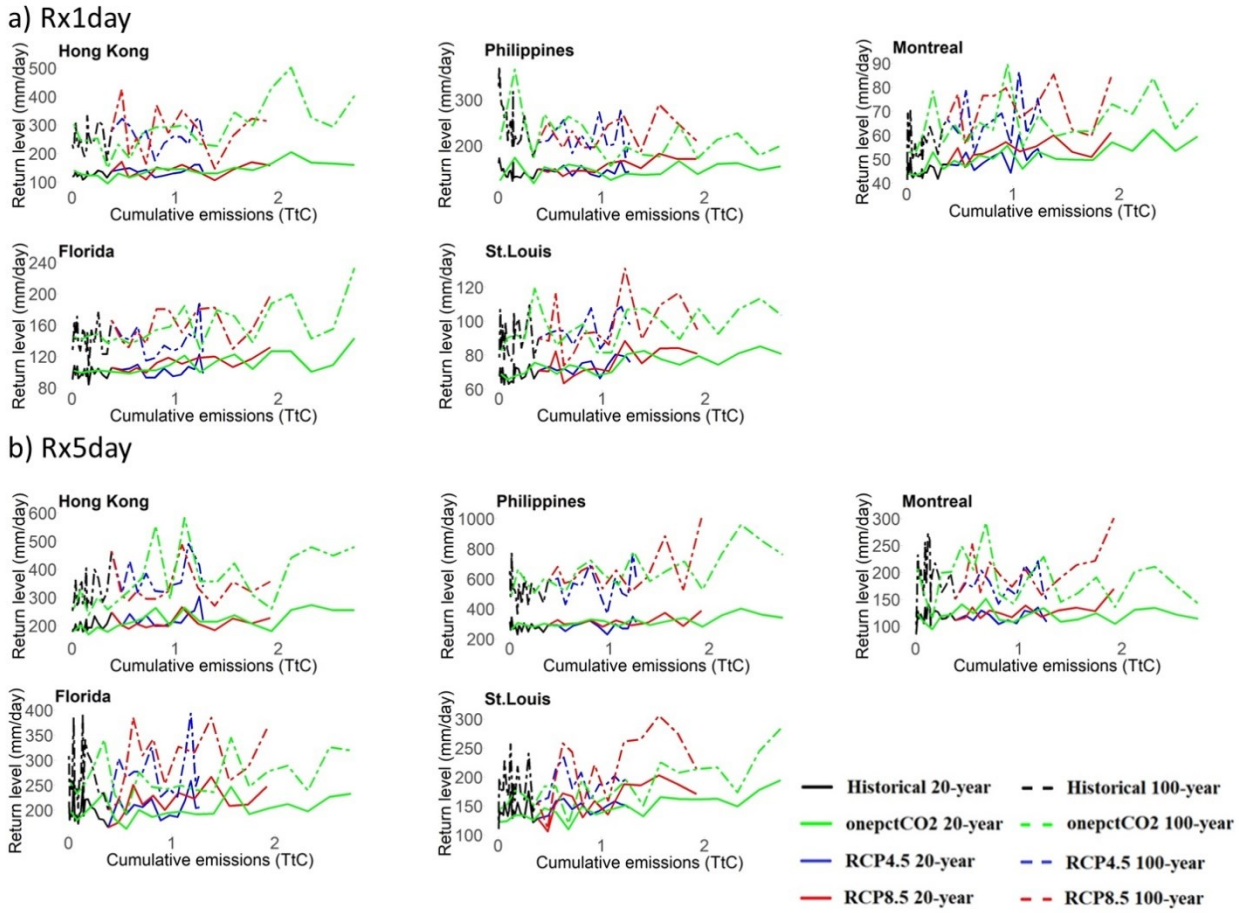

Figure 12. Local 20-year and 100-year return level trends for (a) Rx1day and for (b) Rx5day.

Discussion

My results show that a GEV analysis can be a useful statistical tool to quantify trends of global, regional and local annual precipitation maxima as a function of cumulative CO_2 emissions. Notably, I found that at all spatial scales, the location and scale parameter estimates increase most consistently and substantially for Rx1day and Rx5day as cumulative emissions increase among all scenarios, exhibiting generally the most statistically significant upward linear trends (Tables 2-4). Therefore, my findings indicate that location parameter estimates, at all spatial scales, can be approximated under the TCRE (Figures 4, 7 and 10), as well as with respect to the 20-year and 100-year return levels (Figures 6, 9 and 12). Furthermore, the robustness of

these increasing linear trends typically does not vary considerably globally to locally and would suggest that the location of the mean of annual maxima distributions increase significantly as cumulative emissions rise at all spatial scales. Indeed, the robust increases in the location and scale parameters are reflected by the progressively larger return levels characteristic of specified return periods (20-year and 100-year). For instance, a 20-year Rx1day return level of about 250 mm/day for land-only during the historical period would become an approximately 350 mm/day event at two TtC of cumulative emissions, at the end of the RCP 8.5 scenario. I also found a similar increase in 100-year return levels under the same scenario for land Rx1day.

Intuitively, these patterns would make sense, as significantly increasing trends in the location and scale parameter estimates indicate substantial rightward shifts in the means of annual maxima as cumulative emissions rise (e.g. Figures 5, 8 and 11), increasing return level intensity and annual maxima variability. Additionally, this tendency would suggest that return periods decrease at higher cumulative emissions, which would increase the frequency of specified extreme precipitation levels. For example, a 20-year return level historically would more likely be reached or exceeded much sooner at higher emissions, while newer 20-year return levels would reach higher precipitation thresholds as emissions increase. This pattern is shown for all spatial scales considered in this study and is consistent with those results presented in other works; Kirchmeier-Young & Zhang (2020), for example, showed that North American one-day and five-day annual maximum precipitation extremes intensify sharply under the influence of anthropogenic warming. These results are consistent with the strong intensification trends shown for Rx1day and Rx5day for the United States in this study, as well as more locally in the United States, in Florida and St. Louis. Furthermore, Wang et al. (2020) found significant five-day maxima increases of 4-8% for China with an additional 0.5 C of warming. Here, I also

found a similar trend for Hong Kong under Historical + RCP 4.5 and Historical + RCP 8.5, where location estimates increase significantly at higher emissions, consistent with Wang et al. (2020).

My findings also largely reveal significant decreases in the shape parameter estimates at the global scale, and when regionally constraining the analysis to land or ocean only. This implies distributions having a tendency to become less heavy-tailed at higher cumulative emissions and, thus, approaching zero probability faster for the most extreme precipitation events. Such a trend would suggest that the variance of the most extreme maxima decreases with increasing emissions, and the probability of the most extreme events, including return levels, decreases over time. However, it should be noted that return levels increase significantly in magnitude at higher emissions, even if the probability of occurrence for the most intense return levels decrease, and rightward shifts in the GEV distribution with higher emissions suggest more extreme values altogether despite lower probabilities linked to those most intense events.

Shape parameter estimates are also shown to be spatially-dependent and could be more sensitive to the type of annual maxima in question. For example, when focusing the analysis to the national and, more especially, the local scale, significant trends were largely absent in shape estimates in this study, and this was largely the case for Rx5day. One notable exception was Brazil among the selected nations. For that nation, statistically significant trends were consistently observed for annual maxima, but the actual trend in estimates varied with the extreme precipitation indicator. For instance, Brazilian Rx1day showed a decreasing trend across all scenarios (trending towards a lighter-tailed distribution), and for Rx5day, an increasing trend was conversely shown (i.e. becoming more a heavier-tailed distribution). Therefore, while extreme precipitation largely increases in frequency/intensity, some regional differences occur in

shape patterns, and also varying with the extreme precipitation index. Decreasing trends in shape estimates have previously been reported in the literature at higher emissions concentrations that were linked to more drying in the Caribbean and tropical Americas in the RCP 4.5 and RCP 8.5 scenarios in CMIP5 simulations (e.g. Costa et al., 2023). There were similar increases shown for consecutive dry days in Brazil as emissions rise (Avila-Diaz et al., 2020), consistent with the significant decreasing shape parameter trends shown for Brazil Rx1day across scenarios in this work. Drying trends were further shown for the NE Amazonian rainforest, the Mediterranean and South Africa in a multi-model ensemble in CMIP6 (Vogel et al., 2020), as well as in Ethiopia in CMIP5 RCP 4.5 and RCP 8.5 scenarios via decreases in days spent with very heavy precipitation (Teshome & Zhang, 2019), further highlighting regionally variable trends reported for extreme precipitation indices.

Nevertheless, the general lack of trend in shape parameter estimates shown here across nations and locally implies that the probabilities of occurrence and variance for the highest annual maxima quantiles do not change as emissions increase, though the highest maxima would be more intense at higher CO_2 emissions relative to those during the pre-industrial period. To that end, annual maxima would still largely intensify significantly, owing largely to (robust) increases in location and scale estimates. As such, all of the selected nations largely exhibited a significant rise in 20-year and 100-year return levels. The tendency is most noteworthy for Brazil due to shape parameter estimates for Rx5day increasing significantly, suggesting larger variance and probabilities of occurrence for intensifying values for the largest return levels (e.g. 100-year return levels). India similarly showed statistically significant increases in shape parameter estimates for one-day annual maxima under 1pctCO_2, shifting towards a heavier-tailed behavior

as cumulative emissions increased and suggesting that the newer most extreme events/return levels at higher emissions would increase in probability.

In some situations, my results also show applicability locally, such as for Hong Kong and Philippines Rx5day, and for Montreal Rx1day, where shape estimates all increase significantly (exhibiting heavier-tailed behavior) at higher cumulative emissions. The increase found here for Montreal would be consistent with those results presented in Barlow et al. (2019), where they showed heavier-tailed tendencies for the most intense North American precipitation extremes for regions affected by a large diversity of precipitation-producing systems. For the Montreal area, for example, this would suggest that the probability (and intensity) of the highest annual maxima quantiles historically, such as that of July 14th, 1987, would increase as cumulative CO_2 emissions rise. Indeed, for the Montreal area, my results show that 20-year and 100-year return levels of Rx1day increase approximately linearly with increasing cumulative emissions (Figure 12a). This is consistent with the heavier-tailed behavior of precipitation extremes documented in previous studies (e.g. Serinaldi & Kilsby, 2014; Cavanaugh et al., 2015).

The more spatially-variable shape parameter response found in this study may be explained through several factors. In particular, the greater degree of uncertainty regionally to locally may be linked to the larger sensitivities to natural variability that more readily occur at these spatial scales. This uncertainty could also be related to the coarser resolutions used to represent otherwise realistically finer-scaled weather events and, thus, represented outside of convection-permitting models. The patterns found here are, therefore, consistent with those findings presented in Innocenti et al. (2019), where negligible trends in shape parameter estimates at the grid cell level across most grid boxes over Eastern North America were shown. In general, however, there is a more consistent shift towards higher annual maxima values at

specified return periods due to consistent significant increasing trends shown for the location/scale parameter (Tables 2-4, Figures 5, 8 and 11), and a general increase in annual maxima variability, owing to the consistent significant increases in the scale parameter estimates. Therefore, the implication here is that annual maxima quantiles tend to largely become more extreme under higher cumulative emission settings, but the degree to which the probability of occurrence for the highest precipitation values change appears to be spatially-dependent.

It is also important to note that even with the lack of trend in shape parameter estimates, or in cases of statistically significant decreases in the shape parameter, the consistent increasing trends in the location and scale parameter estimates at all spatial scales still would favor heavier-tailed behavior. As such, the probability of occurrence tied to more intense extreme precipitation events would still be high at higher cumulative emissions, regardless of trends in the shape parameter.

Possible causes and implications of patterns

While several mechanisms are important for the initiation and development of extreme precipitation events, there are important base factors that should be considered. The trends towards more frequent and intense annual maximum precipitation found in this study may firstly be associated with an increased availability of atmospheric moisture that becomes more favorable at warmer temperatures in response to higher cumulative emissions. Several studies have previously documented this important temperature-moisture relationship concretely (e.g. Held & Soden, 2000; Held & Soden, 2006), where atmospheric moisture increases by approximately 7% per degree Kelvin of warming, consistent with the Clausius-Clapeyron relationship. Effectively, for every degree Kelvin of warming, a given precipitation event could

theoretically yield about 7% more precipitation (Held & Soden, 2006; Coumou & Rahmstorf, 2012). Very often, one-day maximum precipitation or sub-daily events, in particular, occur in association with (deep) convective systems, such as severe or training thunderstorms. Due to larger moisture availability under warmer background temperatures, CAPE would more frequently be enhanced on days where the potential for deep convective systems exists (Trapp et al., 2009), thereby increasing the likelihood for more intense precipitation over the course of these events if this heightened available energy could be realized through sufficient dynamical forcing. It stands to reason, then, that Rx1day and Rx5day events would favorably intensify with more atmospheric moisture available to them, and so despite the uniform decreasing shape parameter estimates at the global, ocean and land scale, the probability for observing more intensified precipitation extremes would still be high as emissions rise.

Nationally to locally, atmospheric moistening would also be important. In India, for instance, the trend towards more frequently intense one-day and five-day precipitation events suggests an enhancement in warm-season South Asian atmospheric moisture, and summer water vapor transport enhancement (e.g. Xu & Fan, 2019), that would contribute to intensified deep convective systems (i.e. thunderstorms) during the wet monsoonal period. This would be consistent with the results in this study, where robustly linear trends are shown for Rx1day 20-year and Rx1day 100-year return levels as cumulative emissions increase (Figure 9a). Moreover, the shape parameter estimates shown for Indian Rx1day and Rx5day typically reveal no significant trend though increase significantly under the 1pctCO_2 scenario (Rx1day). This finding suggests that 20- and 100-year return levels would not only substantially increase at higher cumulative emissions, but that their probability of occurrence would either increase or remain identical to historical levels.

In other instances, the increasing trend towards more intense one-day and five-day annual maxima in both Brazil and the Philippines could be the result of amplified tropical moisture available to the deep convective systems that often form in these nations. Effectively, this would increase the intensity of such events and would be consistent with the trend towards larger return levels shown for Brazil (Figure 9a-b), as well as an increase in the probability of occurrence for particularly intense Rx5day events in response to the significant increases in shape parameter estimates shown there (Table 3). Enhanced moistening may also be a significant contributor to the intensified return levels shown for the United States and Australia. The trend towards higher values of extreme precipitation could also be related to changes in the character of natural variability modes, such as ENSO period and amplitude, at higher cumulative emissions. This could amplify the frequency/intensity of annual maxima as warmer temperatures work in the same direction as natural variability (Trenberth, 2012).

It should also be noted that, as mentioned previously, the shape parameter estimate trends shown here vary considerably across spatial scale, while statistically significant increasing trends in location and scale parameters exhibit uniformity across all spatial scales. This further highlights the greater extent of uncertainty characteristic of the shape parameter. Indeed, previous studies have stressed this tendency in the evaluation of shape parameter estimates. For instance, this parameter is difficult to estimate because of the relatively short records that are inherently tied to precipitation extremes (e.g. Papalexiou & Koutsoyoannis 2013; Carney, 2016), increasing the extent of sampling bias. Correcting the sample of shape parameter estimates could, therefore, result in more conservative estimates (Carney, 2016). The more varied response of the shape parameter to cumulative emissions at the regional to local scale shown in this work is further consistent with results in other studies (e.g. Ragulina & Reitan, 2017). Papalexiou &

Koutsoyiannis (2013) and Koutsoyiannis (2004b) further showed that the response of the shape parameter ultimately may be sensitive to the geographical location based on their annual rainfall data analysis.

In general, the shift towards intensified annual maxima presents an increased likelihood for various flooding events, such as the gradual flooding that commonly develops under an accumulation of precipitation over a succession of days, or the flash-flooding variety that is commonly a by-product of intense one-day or sub-daily events. Many one-day and five-day maximum events are typically capable of producing a substantial amount of precipitation over a small period of time. The hazards induced by these events are especially important for areas characterized by low-permeable surfaces, such as urbanized areas – an important motivation for my choices for the nations and locales discussed here. The shorter return periods for Rx5day found in this study across all spatial scales does further imply a higher likelihood for longer-duration flooding that is typically manifested by such events, such as the Southern Quebec 2017 and 2019 spring flooding, the British Columbia flooding of 2021, or the September 2013 flooding event that struck Colorado (Herring et al., 2014). As shown in this study, there was a significant shift towards higher Rx5day values for the Montreal area as cumulative emissions increased. Due to the significant contributions that these precipitation events bring with them, this finding would suggest that flooding types not unlike those of spring 2017 and spring 2019 may occur more regularly as cumulative emissions increase.

Conclusion

In this study, I applied EVT by fitting a GEV to evaluate trends in global, regional and local extreme precipitation indicators by framing them in the context of global cumulative emissions. Indeed, using this method, it was possible to better understand how the location, scale

and shape of probability distributions used to model Rx1day and Rx5day behavior may change in response to higher cumulative CO_2 emissions. My results firstly show that location parameter estimates of Rx1day and Rx5day, as well as 20-year and 100-year return levels, can be approximated by the TCRE, with both showing linear responses to cumulative CO_2 emissions. My results further showed a significant increase in frequency and intensity of annual maxima at all spatial scales, as well as a corresponding reduction in return periods. This was largely due to significant and linear increases in location and scale parameter estimates across all spatial scales, favoring a trend towards larger annual maxima values, including for the highest annual maxima quantiles (e.g. 100-year return levels), with rising cumulative emissions. Although no significant trends in shape parameter estimates at smaller spatial scales, some significant increases were shown locally to nationally in this work, suggesting some increased probability and variance for more intense high-end precipitation extremes at those scales. It should be noted that even without changes in shape parameter estimate trends with higher emissions, the probability of occurrence of what would be higher-order return levels (e.g. more intense 100-year return levels) in the future would remain identical to those probabilities for those return levels during the historical period. Furthermore, these future return levels would likely represent an intensification of a given historical return level in light of increases in the location/scale parameter estimates shown here.

These results expand on studies that previously used EVT to analyze trends in extreme precipitation and other climatic extremes (e.g. Barlow et al., 2019; Innocenti et al., 2019) but also based on a variety of spatial scales using simulated precipitation data historically and across emissions scenarios. At the same time, these findings further suggest that present-day and historical precipitation extremes become a new normal in the future as cumulative emissions

increase, and so return levels of specified return periods historically become more frequent/regular and intense at higher emissions. Therefore, my results imply trends favoring precipitation extremes that would more favorably yield flooding, notably for those regions and localities already situated near or along flood plains. In urbanized settings, flash-flooding may increasingly become a hazard as one-day events (Rx1day), for example, intensify and occur more frequently. Such events may also more often lead to landslides and other related hazards, especially in tropical regions.

In light of international agreements that limit global warming to thresholds of around 1.5 Celsius relative to the preindustrial period, the findings presented in my study highlight that the character of one-day and five-day annual maxima, at all spatial scales, could respond robustly in frequency and intensity to even small amounts of warming tied to lower amounts of additional cumulative CO_2 emissions. As global temperatures rise, it becomes increasingly critical to develop a management framework that strives to better mitigate impacts associated with flooding, as well as other environmental hazards that are common with precipitation extremes. I further stress that this study focused on annual precipitation maxima directly, rather than considering a more holistic approach that would incorporate environmental conditions critical for the generation of such extremes. It could, therefore, be of interest for future works to consider factors that may play a role in the development of precipitation extremes, such as using dynamical and thermodynamical factors as possible covariates, and how these together may respond to different emissions scenarios.

Chapter 5: Estimating the remaining carbon budget for global, regional and local extreme precipitation thresholds

This chapter is also being prepared for publication.

Abstract

Precipitation extremes are among the most impactful forms of weather to human society. As cumulative CO_2 emissions rise, such extremes are expected to increase in frequency and/or intensity, with significant intensification regionally with more magnified warming observed at those finer spatial scales. There is growing interest in determining the degree to which global cumulative carbon emissions need to be reduced in order to avoid particularly significant/dangerous precipitation thresholds, with this interest being heightened at the regional to local scale. In the present chapter, I extend TRCE-based analyses of previous chapters to estimate allowable future cumulative carbon emissions (remaining carbon budgets) consistent with avoiding future extreme precipitation thresholds. Data from nine Coupled Model Intercomparison Project Phase 5 (CMIP5) model simulations were used to quantify trends in the most extreme Rx1day and Rx5day precipitation events by placing them in the context of cumulative CO_2 emissions. As an extension of the GEV analysis explored previously, I found that present-day 20-year return levels of precipitation become 10-year return levels at generally low amounts of additional cumulative CO_2 emissions. This is also true for the cumulative emissions required for the present-day 100-year return levels to become 20-year levels in the future. Collectively, these results suggest that present-day precipitation extremes will become more common in the future if global cumulative CO_2 emissions are permitted to rise in even small additional quantities. I show that more stringent carbon emissions targets than those specified in recent international agreements are needed to avert the changes in return levels of precipitation extremes considered here.

Introduction

Extreme weather events refer to events that occur at the extremes of a specified climatology. Statistically, these events are typically located within the tails of a normal distribution. Although there exists a substantial amount of research dedicated to studying extreme weather events, there also remains no widely-accepted definition of what constitutes either a weather or climate extreme (Stephenson et al., 2008). For precipitation extremes, however, as mentioned previously, the Intergovernmental Panel on Climate Change Intergovernmental Panel on Climate Change Managing the Risks of Extreme Events and Disasters to Advance Climate Change Adaptation (IPCC SREX) defines changes in heavy to extreme precipitation in relation to late-20th century 90th percentile or greater values, such as 95th to 99th percentile events (Herring et al., 2014). However, the wide range of definitions of what constitutes an extreme event partly accounts for the trends reported across the body of climate impacts literature, which fuels uncertainty as to future responses for such events (McGregor et al., 2005; Stephenson et al., 2008; Zhang et al., 2017; Pendergrass, 2018; Pendergrass et al., 2019; Moore et al., 2023).

Despite their rare nature, it is these weather events that often bring with them devastating short- and long-term effects to human society, including loss of life and significant property damages, as well as environmental stresses that can last for decades at a time. While the Paris Agreement aims to ideally maintain a mean global warming value of 1.5 C or less relative to the pre-industrial period, it remains unclear as to how the character of weather extremes, as well as their environmental conditions, will respond to such warming thresholds. This is especially relevant regionally, since observed and expected warming at those spatial scales are generally

larger than the global mean response to continued rising cumulative emissions (e.g. Dupont & Pearman, 2006).

The study of precipitation extremes is, thus, of importance because of the ability of such events to induce potentially catastrophic damage as a result of (flash-) flooding, particularly in growing urbanized settings where surface permeability is already so low. As a result of successive or compounding extremes (e.g. Sun et al., 2023), the flooding that emerges from extreme precipitation events could sometimes trigger, for example, devastating mudslides and landslides as surfaces become increasingly unstable in the wake of substantial precipitation amounts that fall over such short durations. Significant one-day maximum precipitation events can further lead to flash-flooding (e.g. the recent historical New York City flash-flooding event of September 29th, 2023, the Libyan flash-flooding of early-September 2023, or with respect to the extreme one-day rainfall event that struck the Fort Lauderdale area on April 12th, 2023). At the same time, excessive amounts of precipitation that occur over a succession of days to weeks can result in more gradual flooding as a result of quickly saturating soils and/or anomalously high water levels within watersheds.

In response to a warmer global (and regional) climate, environments may become more conducive to heavy to extreme precipitation development, increasing the likelihood of more frequent and intense events. However, there exists a large range of trends across climate model simulations of precipitation extremes. This is likely attributable to regional differences, as well as to the simulated differences of the broader atmospheric circulation features that enable these events to develop (Pendergrass et al., 2016). Despite the spread of results in the climate impacts literature, the general expectation is for global precipitation extremes to increase in both

magnitude and frequency as temperatures rise (IPCC AR6; Knutson et al., 2010; Hartmann et al., 2013; Moore et al., 2023). For instance, Myhre et al. (2019) showed that the most intense precipitation events significantly increase in occurrence for every degree Celsius of global warming. Similar results were shown for global heavy precipitation events, including enhanced South Asian precipitation fueled by an intensified warm-season monsoonal circulation into the future (Moore et al., 2015; Katzenberger et al., 2022), as well as historically over the 1901-2020 period (e.g. Falga & Wang, 2022). Precipitation extremes are generally expected to become as much as 32-55% more frequent by 2100 (Thackeray et al., 2022). Regionally, such precipitation events are similarly shown to increase in both intensity and frequency. For example, in the arid regions of China, extreme precipitation increased in intensity over the 1960-2016 period (Wang et al., 2022), as well as in future simulations under 1.5 C to 2.0 C warming in Eastern Africa across extreme precipitation indices (Ayugi et al., 2022), and in terms of extremely wet days in Brazil under RCP scenarios (Avila-Diaz et al., 2020).

Carbon budgets have been shown to have useful applications for exploring trends across a variety of climate variables, notably for avoiding specified global warming thresholds (e.g. van der Ploeg, 2018; Rogelj et al., 2019). In their broadest form, carbon budgets may be defined as the total allowable cumulative CO_2 emissions that meet or avoid a specified global warming threshold, or for some other given climate indicator that may be of interest. The concept of carbon budgeting has, thus, received considerable attention since its central appearance in the IPCC Fifth Assessment Report (AR5) and has since become a widely adopted framework for guiding climate policy (Lahn, 2020). As such, the application of carbon budgets provides a useful framework by which I can estimate thresholds of global warming in efforts of reducing global carbon emissions by some prescribed quantity.

Carbon budgets can be calculated based on the well-established linear relationship that exists between temperature and cumulative CO_2 emissions. This linearity is known as the Transient Climate Response to cumulative CO_2 Emissions (TCRE), which proportionally links anthropogenic global cumulative carbon emissions with global temperature change (Matthews et al., 2009; Gillette et al., 2013; MacDougall, 2016). Such trends may extend to the sub-global scale. Results from a more regionally-constrained analysis, for example, have shown that regional temperature similarly scales approximately linearly with cumulative CO_2 emissions, as well as over land and ocean (e.g. Leduc et al., 2016). However, while this linearity is captured well, large uncertainties surround estimates of the (regional) TCRE. This, to some extent, subsequently affects the usefulness of the carbon budget conceptually (Jones & Friedlingstein, 2020), partly due to the warming contributions originating with non-CO_2 forcings thar are not captured in the TCRE framework (Millar et al., 2016; Partanen et al., 2020). Uncertainties also stem from the choice of methodological framework, as well as the assumptions factored into calculations of the carbon budget (Matthews et al., 2020). The slope of the TCRE further varies among models in light of the differences in representation of the carbon cycle and climate feedbacks (e.g. Bruhwiler et al., 2021, MacDougall et al., 2016).

Other studies have identified linear responses to carbon emissions for climate variables outside of temperature, extending the scope of the TCRE. For example, Zickfield et al. (2012) showed approximately linear reductions in September Arctic sea ice in response to rising cumulative emissions. Regional TCRE estimates of precipitation were also shown in Partanen et al. (2017), where precipitation exhibits a linear increase with increasing cumulative emissions. Similar near-linear relationships were also shown for the response of indicators of extreme precipitation from global to sub-global scales to cumulative carbon emissions (Moore et al.,

2023). However, this linearity may be regionally-dependent. For instance, Pendergrass et al. (2019) show that tropical extreme precipitation follows non-linear tendencies as emissions rise, although this pattern was displayed only in one model among a suite of CMIP5 models used in their study.

In this Chapter, I aim to further explore the relationship between cumulative CO_2 emissions and precipitation extremes by using the carbon budget concept to estimate allowable cumulative CO_2 emissions associated with various extreme precipitation thresholds. This allows me to define remaining carbon budgets (RCBs) that are associated with extreme precipitation thresholds at global, regional and local scales using climate model output from the CMIP5 model ensemble. By framing precipitation extremes in using the concept of remaining carbon budgets, I endeavor to examine the degree to which emissions would need to be reduced to avoid particularly significant future extreme precipitation thresholds globally, regionally, as well as locally using various emissions scenarios.

Methodology

I describe here in detail the methods for this chapter, with a focus on a description of the carbon budgeting design used as an extension of the Generalized Extreme Value (GEV) analysis articulated previously in Chapter 4.

Model, emissions scenarios and precipitation data

As explored in Chapters 3 and 4, I use here the same suite of 9 CMIP5 models described previously, with the CanESM2 model serving as the host model (~2.8 x 2.8 degree grid cell system, representing 8192 grid cells, with each cell covering an approximately 300-square

kilometer area on the Earth's surface) for the interpolation procedure. I further used the same emissions scenarios as in previous chapters, including a scenario describing a 1% increase in CO_2 emissions per year until a quadrupling occurs relative to the pre-industrial period (1pctCO_2, which spans 140 years), as well as two Representative Concentration Pathway (RCP) scenarios (RCP 4.5 and RCP 8.5, each covering a 90-year period, from 2006 to 2095) which were joined with simulations of historical emissions (145 years) that begin at the pre-industrial period (defined as 1861). Emissions are represented in units of teratons of carbon (TtC). Also following the work done in the preceding chapters, I use the same extreme precipitation indicators that characterize what is known as annual one-day maxima (Rx1day) and five-day maxima (Rx5day) events (in units of millimeters per day (mm/day)) that correspond to each emission scenario for each of the CMIP5 models used herein. These extreme precipitation events capture all types of precipitation and effectively are derived from the largest annual maxima of precipitation extremes extracted for each grid cell across models for each emissions scenario. As with the analyses conducted in Chapters 3 and 4, all data manipulations and plotting were conducted in R programming software.

Global, land, ocean, national, and locational selection

I begin this analysis with an examination of global patterns of Rx1day and Rx5day to obtain estimates of RCBs globally. I then constrained the analysis to land-only by applying a mask to all land grid cells. This then made it possible to similarly estimate carbon budgets for precipitation extremes of interest across land collectively. Assessing RCBs associated with precipitation extremes over land is desirable, since this is where human populations and terrestrial lifeforms collectively reside. However, an assessment of RCBs over oceanic regions in their entirety would also carry some scientific value due to extreme precipitation events often

forming over such regions before drifting onto land. This is especially true with those extreme precipitation events linked to tropical cyclones, forming over oceanic source regions prior to drifting over land, including landfalling situations. In other cases, (severe) thunderstorms can form quickly over water before advancing onto land areas and potentially cause substantial flooding, especially in sub-tropical and tropical regions. Therefore, some examination of oceanic extreme precipitation events would be of importance and, as such, I proceeded conducting an ocean-only analysis by applying a mask over land areas, effectively serving to isolate ocean/water grid cells, as applied in Chapter 3 and 4. The global analysis considers all grid cells, capturing all land and water cells. Extending this analysis beyond the global and land/ocean scale, I selected specific land areas as a representation of my regional analysis, and much like previous chapters, this selection was used to compare those trends found globally in terms of trends of Rx1day and Rx5day.

Regions and locales selected in this chapter represent the same selection from the previous chapter (Chapter 4). Since an extension of the GEV analysis from Chapter 4 is applied here as a tool for estimating the remaining carbon budget, I focus on these regional to local selections as a representation for regions and locations globally. Furthermore, as previously highlighted in Chapter 4, this selection captures regions and locations that carry large population densities, have coastal areas that lie at or below sea level, are vulnerable to precipitation extremes altogether, and have recently experienced catastrophic flooding linked to recent extreme precipitation events.

As described in Chapters 3 and 4, regions are chosen as nations, while locales are represented at the grid cell or as a small grouping of cells. The regional selection, therefore, corresponds to the United States, Brazil, South Africa, India, and Australia, while the local

selection uses Montreal, St. Louis, Florida, the Philippines, and Hong Kong. As with Chapter 4, analyses corresponding to these selections are meant to be representative of all regions and locations and so are not meant to be an exhaustive selection.

Fitting a GEV to derive RCBs of precipitation thresholds

In Chapter 4, I previously used Extreme Value Theory (EVT) to examine trends in the most extreme Rx1day and Rx5day events at the global to local scale under the three emissions scenarios outlined above, as well as with respect to the historical period. EVT is a popular tool in statistics that is used as a means to model the behavior of extreme values through time, which are located within the tails of a given distribution. GEV distributions, a sector of EVT, are well known for their ability to model extremes across a wide range of fields. GEV distributions are widely adopted for the modelling of weather extremes, including extreme precipitation and extreme heat events (e.g. Rypkema & Tuljapurkar, 2021). In the present chapter, I extend the GEV analysis by using TCRE estimates of return level values derived from Chapter 4. These frameworks are, therefore, combined to determine the RCBs globally to locally across a set of emissions scenarios based on selected present-day return levels. The present-day return levels in this study were based on the final block or sub-period comprising the historical period (i.e. the 20^{th} block) derived from the block maxima approach detailed in Chapter 4.

Threshold selection for remaining carbon budgets

Here, I outline the procedure involved for selecting specific return levels in order to compute RCBs at various spatial scales.

In this chapter, I utilize the concept of the Remaining Carbon Budget in relation to specified extreme precipitation return levels. The RCB is defined here as the remaining

allowable global cumulative (CO_2) emissions associated with specified changes in extreme precipitation values relative to the present-day period. As mentioned in previous chapters, the historical period runs over 145 years, ending in 2005. Under the block maxima approach previously employed in Chapter 4 that made use of a Generalized Extreme Value (GEV) distribution, these 145 years were grouped into seven-year blocks, with blocks similarly allocated for the time series pertaining to all emissions scenarios (i.e. RCP 4.5, RCP 8.5, and 1pctCO_2). Since the final blocks were comprised of less than seven years in the case of the historical period and the RCP scenarios, these were removed to ensure that the number of years across each block (or sub-period) was inherently the same, as described in the previous chapter. However, as also mentioned in Chapter 4, the "present-day" period was adjusted to the first block of the RCP scenarios (which ends in 2012), as this is more representative of the present-day. Also, although the 1pctCO_2 scenario considers the response of Rx1day and Rx5day to cumulative CO_2 emissions only, this scenario is of interest for this analysis, as it can show the extent of RCBs needed to meet extreme precipitation thresholds in a hypothetical or counterfactual future world with additional CO_2 forcing only.

The selection of extreme precipitation indicators (Rx1day and Rx5day) used in this study was based on return level values derived from the GEV analysis conducted previously. The present-day GEV parameter estimates are, therefore, based on the first block of the RCP periods, and so return levels were chosen in this manner. Specifically, the baseline return levels were selected from the first block that initiates the RCP 4.5 period, representing the present-day baseline for both RCP scenarios. This return level was selected as the baseline value, as the RCP 4.5 emissions characterizing the first block are closer to the actual emissions that occurred during that period. This is used to calculate the cumulative emissions between this block and those

future blocks that carry the value at which the present-day 20-year or 100-year return level is met and/or exceeded as either 10-year or 20-year return levels in the future.

As such, using the block maxima method, I was specifically able to compute RCBs by determining first when in the future present-day 20-year return levels (95^{th} percentiles) become 10-year return levels (i.e. 90^{th} percentiles). This procedure was then similarly applied for determining when present-day 100-year return levels (99^{th} percentiles) become the 20-year return level into the future. Finding the 90^{th} percentile values at the present-day and other periods are determined by fitting a GEV distribution that is associated with the present-day block and other blocks, making it possible to calculate percentiles of interest using these probability distributions. The present-day 95^{th} (and 99^{th}) percentile values of extreme precipitation indicators are chosen for this work as baselines, as these are commonly used as a threshold selection for (extreme) precipitation indices across the body of climate impacts literature for flood risk assessment, infrastructural management and collectively climate change adaptation (e.g. Chang et al., 2022; Zhou et al., 2024). Furthermore, it is these events that represent the heaviest of precipitation (IPCC, 2021). It is further of interest, since it often signifies a significantly higher magnitude of precipitation event, which increases the likelihood for potentially catastrophic impacts in already vulnerable locations and regions. As such, these can be useful quantities for notably regional to local risk management efforts in the context of RCBs, providing further insight as to approximately when such present-day return levels can be met and/or exceeded in the future under different cumulative emissions scenarios at sub-global scales.

Block maxima that characterize the future period fall into the RCP scenarios, which are those blocks that follow the last block of the historical period to complete the time series. The RCP scenarios comprise a total of 12 blocks, following the 20 blocks characterizing the

historical period. However, as mentioned previously, the first of the 12 blocks comprising the RCP 4.5 scenario is treated as the adjusted ending block of the historical period (i.e. present-day).

I then applied a similar analysis for the 1pctCO_2 scenario. That said, in the case of 1pctCO_2, since there is no real reference point that signals the end of the historical period, I instead used the present-day emissions value of the historical period (i.e. 2012 under RCP 4.5) to determine when the present-day begins in the 1pctCO_2 scenario. This served as a meaningful present-day emissions value in the 1pctCO_2 case and was used to calculate RCBs similarly based on the point at which corresponding 20-year return level values at present-day emissions reach/exceed 10-year return levels in upcoming blocks. This was similarly applied for when present-day 100-year levels reach or exceed 20-year levels. Using this approach for the 1pctCO_2 case further intuitively makes sense, since the historical value would represent a more realistic present-day estimate in light of historical present-day emissions being linked to not only CO_2 forcing, but also non-CO_2 forcing. As a result, it was a more reasonable choice to use as the present-day value for 1pctCO_2. This was applied across all spatial scales, from globally to locally.

Calculating the remaining carbon budget

In this section, I describe the procedure involved for calculating RCBs. In accordance with the selection procedure described in the previous sub-section, I firstly calculate RCBs based on the difference between present-day cumulative CO_2 emissions and those CO_2 emissions corresponding to the point at which present-day 20-year return level values reach and/or exceed the future 10-year return levels. Similarly, RCBs were computed based on the difference in

present-day CO_2 emissions and those emissions at the point present-day 100-year return level values reach and/or exceed the present-day 20-year return level. In each case, this was applied for both extreme precipitation indicators, for Rx1day and Rx5day, and across all spatial scales, from globally to locally. It is also important to note that there are some situations where either present-day 20-year or 100-year return levels never meet and/or surpass 10-year or 20-year return levels in future block maxima. In such cases, I proceed by calculating RCBs based on the block containing the next largest value found in the future blocks making up the RCP and 1pctCO_2 scenarios. As a result, RCBs can mathematically be represented under the following formulations:

$$RCB_{Return\ level20} = E_{\text{Future 10-year level}} - E_{\text{Present 20-year level}} \quad (1)$$

$$RCB_{Return\ level100} = E_{\text{Future 20-year level}} - E_{\text{Present 100-year level}} \quad (2)$$

where $RCB_{Return\ level20}$ represents the difference between the cumulative CO_2 emissions associated with the future block maxima whose 10-year return level value matches/exceeds the present-day 20-year return level value for extreme precipitation indicators ($E_{\text{Future 10-year level}}$), and those cumulative CO_2 emissions tied to the present-day 20-year return level ($E_{\text{Present 20-year level}}$). $RCB_{Return\ level100}$ similarly corresponds to the difference between the cumulative CO_2 emissions associated with the block maxima containing the point at which 20-year return levels in the future reach and/or exceed the present-day 100-year return level ($E_{\text{Future 20-year level}}$), and those cumulative CO_2 emissions associated with the block containing the present-day 100-year return level value ($E_{\text{present 100-year level}}$).

I then computed the standard errors associated with these RCBs, as represented by the standard error bars included in the RCB figures provided below, as well as numerically in data tables. RCB standard errors were calculated across scenarios by using the carbon emissions spanning the blocks from the present-day period to the point at which the 95th and 99th return level percentile is met or exceeded.

Results

I present here results for global, land and ocean RCBs that are linked to future return levels relative to present-day values. Figures 1-2 and Table 1 provide a summary of these findings.

Global, land and ocean patterns of RCBs

Globally, my results consistently show RCB values of less than 0.80 TtC (+/- 0.06 to 0.09 TtC) across scenarios with respect to present-day 20-year return levels becoming 10-year return levels in the future for both Rx1day and Rx5day (Figure 1, Table 1). The largest RCBs are shown for the Rx1day 1pctCO_2 case (i.e. 1.67 TtC +/- 0.16 TtC), while the smallest values are shown for RCP 4.5 and RCP 8.5, and with RCP 4.5 values being consistently larger across both extreme precipitation indicators. When constraining the analysis to land and ocean only (Figure 1, Table 1), these patterns continue to be largely observed, with the smallest values displayed for the RCP scenarios (i.e. largely 0.15-0.79 TtC +/- 0.04-0.08 TtC) and highest in 1pctCO_2 (up to 2.08 TtC +/- 0.18 TtC). In the case of the RCP scenarios, the size of the RCBs is overall smaller for land Rx1day than it is for ocean, and at the global scale but is larger with respect to Rx5day. RCBs are further larger for RCP 8.5 than RCP 4.5 for land, which differs from the results given

for the global or ocean scale. Also, land and ocean budgets are shown to be consistently larger across Rx5day than for Rx1day, overall similar to those patterns at the global scale (Table 1, Figure 1). Globally and for ocean only, RCBs are mostly at their smallest for RCP 4.5, though the lowest RCB coincides with 1pctCO_2 land Rx1day (0.12 TtC +/- 0.06 TtC). As such, these findings highlight that the extent of RCBs is lower for the RCP scenarios and mostly higher in the case of 1pctCO_2 across global, land and ocean. Intuitively, this makes sense, since the RCP scenarios include non-CO_2 forcing, causing baseline/threshold values to be matched and/or exceeded sooner into the future under lower cumulative CO_2 emissions.

For present-day 100-year values becoming 20-year return levels in the future, my findings show similar RCB patterns globally, for land only, as well as for ocean (Figure 2, Table 1). However, as compared with present-day 20-year return levels (95th percentiles) becoming future 10-year levels (i.e. 90th percentiles) described previously, the RCB values shown here are generally larger across scenarios in the future across all spatial scales. As described previously, RCBs are generally largest under the 1pctCO_2 scenario, and mostly for Rx5day overall. To that end, the highest value occurs globally (2.16 TtC +/- 0.17 TtC), and then for land- and ocean-only Rx1day (2.08 TtC +/- 0.18 TtC). With respect to the ocean scale, the RCB value is also large for Rx1day (1.67 TtC +/- 0.16 TtC). By contrast, the lowest RCBs are found with the RCP scenarios, but the lowest values are dependent on the scenario in question. For example, for either extreme precipitation indicator, the lowest RCBs are found with RCP 8.5 across global, land and ocean; in the RCP 8.5 case, for instance, the RCB value is shown to be as low as 0.15 TtC (+/- 0.04 TtC) for ocean Rx1day and Rx5day, as well as for both global Rx1day and land Rx5day. For land Rx1day, however, the RCB is similar across both RCP scenarios, with 0.23-0.24 TtC (+/- 0.05 TtC) of additional emissions being required to match or exceed the present-

day 269 mm/day event in the future (Table 1). Also noteworthy is that values of RCBs, at least for the global and ocean case, are generally larger in both RCP 4.5 and RCP 8.5 for Rx1day and Rx5day, but values are consistently higher for 1pctCO_2 for Rx5day than for Rx1day across all spatial scales. This suggests that lesser additional cumulative emissions are generally required to meet or exceed thresholds in Rx1day than Rx5day, including with respect to Rx1day carrying smaller budgets under 1pctCO_2 (Table 1, Figure 1).

It is further worth noting that baseline/threshold values are larger globally than for either ocean or land (Figures 1-2). This pattern would be an artifact of the block maxima approach, in which only the largest value for each year across each model is extracted. Since the maximum value must occur over either ocean or land, the annual maxima extracted globally must also be either equal to or greater than the maxima over ocean or land each year. This effectively ensures that the global scale annual maxima will always carry values equal to or larger than ocean or land. By contrast, in Chapter 3, which involved spatially averaging across grid cells, this yielded the larger annual values at the ocean/water scale than globally, since the average comes from averaging over the largest values which are often found over the ocean.

Table 1. Global, land and ocean remaining carbon budgets (RCBs) for Rx1day and Rx5day under different emissions scenarios. RCBs are calculated based on the difference in cumulative carbon emissions between when the present-day 20-year return levels become 10-year return levels in the future, and those emissions at present-day. Similarly, RCBs were calculated based on the difference in cumulative emissions between when present-day 100-year return levels become 20-year return levels in the future, and emissions at present-day. Standard errors (SE) are provided for each RCB value. RCBs and SEs are given in units of teratons of carbon (TtC).

Global			
Rx1day 20-year becoming 10-year return level			
Scenario	Baseline (mm/day)	RCB (TtC)	SE (TtC)
RCP4.5	375	0.57	0.07
RCP8.5	375	0.15	0.04
1pctCO_2	375	0.50	0.07

Rx5day 20-year becoming 10-year return level			
Scenario	Baseline (mm/day)	RCB (TtC)	SE (TtC)
RCP4.5	929	0.79	0.08
RCP8.5	929	0.15	0.04
1pctCO_2	929	1.67	0.16
Rx1day 100-year becoming 20-year return level			
Scenario	Baseline (mm/day)	RCB (TtC)	SE (TtC)
RCP4.5	463	0.75	0.08
RCP8.5	463	0.15	0.04
1pctCO_2	463	0.80	0.11
Rx5day 100-year becoming 20-year return level			
Scenario	Baseline (mm/day)	RCB (TtC)	SE (TtC)
RCP4.5	1633	0.65	0.08
RCP8.5	1633	0.59	0.08
1pctCO_2	1633	2.16	0.17
Land			
Rx1day 20-year becoming 10-year return level			
Scenario	Threshold (mm/day)	RCB (TtC)	SE (TtC)
RCP4.5	269	0.23	0.05
RCP8.5	269	0.24	0.05
1pctCO_2	269	0.12	0.06
Rx5day 20-year becoming 10-year return level			
Scenario	Baseline (mm/day)	RCB (TtC)	SE (TtC)
RCP4.5	790	0.79	0.08
RCP8.5	790	1.44	0.14
1pctCO_2	790	2.08	0.18
Rx1day 100-year becoming 20-year return level			
Scenario	Baseline (mm/day)	RCB (TtC)	SE (TtC)
RCP4.5	291	0.23	0.05
RCP8.5	291	0.24	0.05
1pctCO_2	291	0.12	0.06
Rx5day 100-year becoming 20-year return level			
Scenario	Baseline (mm/day)	RCB (TtC)	SE (TtC)
RCP4.5	1217	0.79	0.08
RCP8.5	1217	0.15	0.04
1pctCO_2	1217	2.08	0.18
Ocean			
Rx1day 20-year becoming 10-year return level			
Scenario	Baseline (mm/day)	RCB (TtC)	SE (TtC)
RCP4.5	361	0.65	0.08
RCP8.5	361	0.15	0.04
1pctCO_2	361	0.80	0.11
Rx5day 20-year becoming 10-year return level			
Scenario	Baseline (mm/day)	RCB (TtC)	SE (TtC)
RCP4.5	810	0.75	0.08

RCP8.5	810	0.15	0.04
1pctCO_2	810	2.08	0.18
Rx1day 100-year becoming 20-year return level			
Scenario	Baseline (mm/day)	RCB (TtC)	SE (TtC)
RCP4.5	425	0.75	0.08
RCP8.5	425	0.15	0.04
1pctCO_2	425	2.08	0.18
Rx5day 100-year becoming 20-year return level			
Scenario	Baseline (mm/day)	RCB (TtC)	SE (TtC)
RCP4.5	1347	0.41	0.06
RCP8.5	1347	0.15	0.04
1pctCO_2	1347	1.67	0.16

a) Rx1day

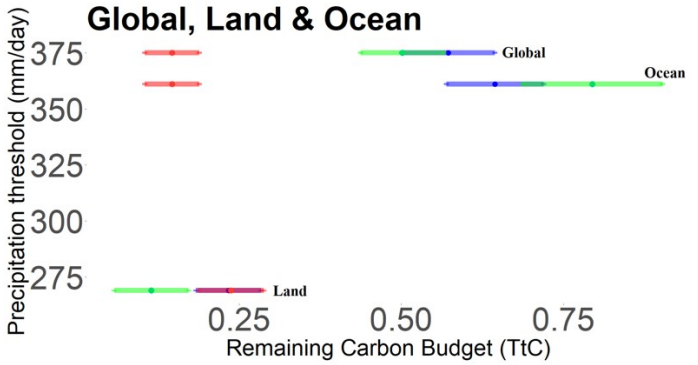

b) Rx5day

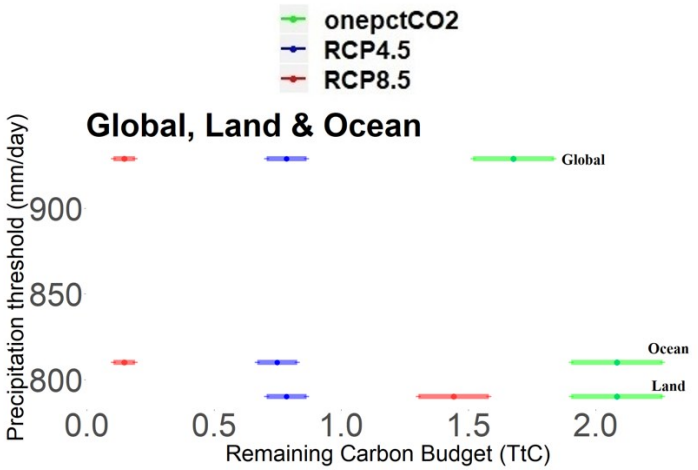

Figure 1. Global, land and ocean remaining carbon budgets (RCBs) for present-day 20-year return levels (95th percentiles) reaching 10-year return levels (90th percentiles) in the future across emissions scenarios corresponding to a) Rx1day and b) Rx5day. RCBs are calculated relative to the emissions at the present-day, with the present-day 20-year return level being

used as the baseline here. Error bars are representative of the standard errors calculated for the derived RCBs.

a) Rx1day

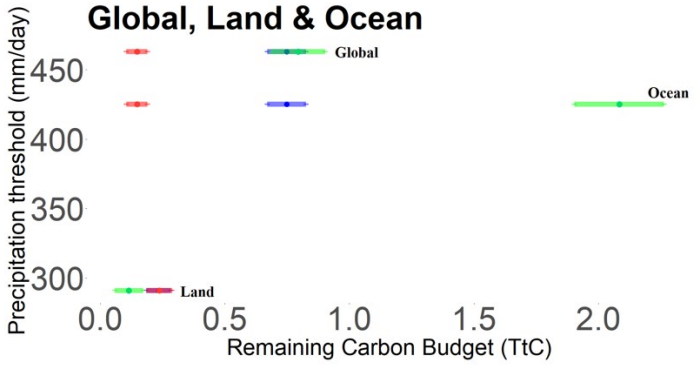

b) Rx5day

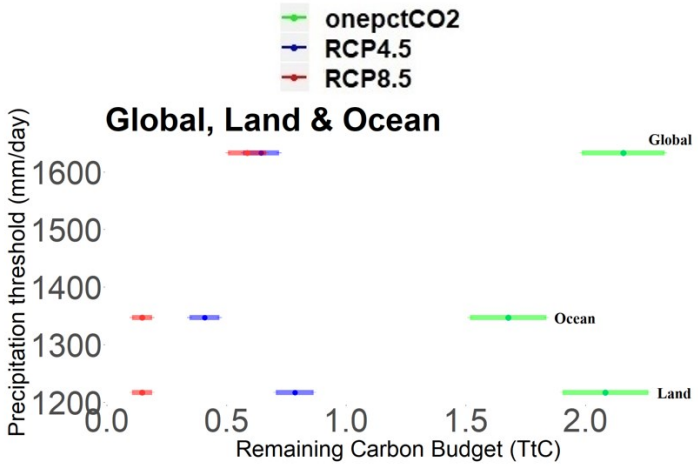

Figure 2. Global, land and ocean remaining carbon budgets (RCBs) for present-day 100-year return levels (99th percentiles) reaching 20-year return levels (95th percentiles) in the future across emissions scenarios corresponding to a) Rx1day and b) Rx5day. RCBs are calculated relative to the emissions at the present-day, with the present-day 100-year return level being used as the baseline here. Error bars are representative of the standard errors calculated for the derived RCBs.

Regional/National patterns of RCBs

In this section, I assess national/regional patterns of RCBs corresponding to meeting and/or exceeding 20-year and 100-year return levels into the future, focusing on comparisons between them and global to land- and ocean-only estimates. Results are summarized in Figures 3-4 and Table 2.

Nations/regions selected for this study show similar trends to global, land and ocean patterns of RCBs across scenarios for present-day 20-year return levels becoming 10-year return levels into the future. Similarly with global, land and ocean, the greatest values of RCBs are consistently shown for the 1pctCO_2 scenario, and the lowest under generally the RCP scenarios, notably with respect to RCP 4.5 (Table 2), for both extreme precipitation indicators. Together with somewhat more variability for the RCP scenarios than what is showcased globally to land and ocean, the results show a consistent trend towards increasing RCBs across scenarios nationally. For all nations examined, much like at the global, land and ocean scales, but with the exception of Brazil, Australia and South Africa Rx5day under RCP 8.5, and United States Rx1day under RCP 8.5, the RCB values were consistently well under 1 TtC across the RCP scenarios (a range of 0.15-0.90 TtC +/- 0.04-0.10 TtC) (Figure 3, Table 2), and largest for 1pctCO_2 (up to 2.29 TtC +/-0.19 TtC in the case of United States Rx1day and Rx5day).

There are further some notable patterns that differ from the results outlined in the previous sub-section. Indeed, RCP 8.5 shows larger RCBs than for RCP 4.5, representing a reversal from the global to land and ocean pattern. With the exception of India, nations largely show higher RCP 8.5 values than for RCP 4.5, especially under Rx1day (Figure 3, Table 2). The results also reveal less uniformity in the distribution of RCBs from one nation to the other,

suggesting higher variability when constraining the analysis to the national scale. For example, as mentioned, the United States had the smallest RCB, with only 0.15 TtC (+/- 0.04 TtC) of additional carbon emissions being required to reach its Rx5day of 268 mm/day under RCP 8.5. South Africa additionally showed a small RCB of 0.23 TtC +/- 0.05 TtC for reaching its Rx5day threshold. Conversely, the United States carried the largest value for 1pctCO_2 with respect to Rx1day, as outlined previously (i.e. 2.29 TtC +/- 0.19 TtC). Furthermore, Brazil showed consistently the largest RCB values across the RCP scenarios (0.75-1.26 TtC +/- 0.08-0.13 TtC). Australia also displayed high RCBs with respect to RCP 8.5, with values of as much as 0.90-1.26 TtC (+/- 0.10-0.13 TtC) (Table 2). For the United States Rx5day, RCBs of 0.15-0.32 TtC (+/- 0.04-0.06 TtC) were shown across the RCP scenarios, representing the smallest national RCP budgets altogether, and from globally to locally (Figure 3, Table 2). South Africa also had a small RCB for its Rx1day (0.23 TtC +/- 0.05 TtC) for RCP 4.5. An overall small spread was similarly shown for India's Rx5day, having a modest range of RCBs (0.34-0.41 TtC +/- 0.06 TtC) across the RCP 4.5 to RCP 8.5 scenarios. For 1pctCO_2, India's Rx5day and South Africa's Rx1day showed the lowest additional amounts of cumulative carbon emissions, with 0.79-0.80 TtC +/- 0.11 TtC being needed. As such, at the national scale, my results show more variability in the extent of remaining budgets under the RCP scenarios, relative to the somewhat smaller range of 0.15-2.08 TtC (+/- 0.04-0.18 TtC) found for global, land and ocean trends across scenarios.

For present-day 100-year return levels becoming 20-year values into the future, the results also generally show more variation in RCB values relative to what was displayed for global, land and ocean. Whereas the global and ocean cases consistently showed larger Rx5day RCB values in both RCP scenarios than in Rx1day, the results highlight that, at the national

scale, there is a tendency towards an opposing pattern, in which Rx1day RCBs are somewhat larger than those of Rx5day overall (Figure 4, Table 2). This also applies in terms of larger RCB values appearing in Rx1day than Rx5day for the 1pctCO_2 scenario. Further, there is more of a trend towards larger RCBs across nations than globally, and relative to land and ocean, under the RCP scenarios for both Rx1day and Rx5day. For example, the United States is shown to have the largest RCB under the 1pctCO_2 scenario for both extreme precipitation indicators, as does India and South Africa for Rx5day (2.29 TtC +/- 0.19 TtC). This RCB amount surpasses the maximum of 2.16 TtC +/- 0.17 TtC shown for global Rx5day patterns (Table 1). That said, with respect to the 1pctCO_2 case, there is a near-similar RCB maxima distribution (i.e. values often exceeding 2.00 TtC, from globally to nationally). The results also point towards RCB values often exceeding 1.00 TtC for the RCP 8.5 scenario, as compared with those values at the global, land and ocean scale which remained well below 1.00 TtC (Table 1) for that scenario. The largest RCBs, overall, appeared with South Africa Rx5day under 1pctCO_2, Australia and Brazil Rx5day, as well as India's Rx5day with respect to the 1pctCO_2 scenario, and in terms of United States Rx1day. The smallest overall values of RCBs were conversely shown for India Rx1day, and for Rx5day in the United States across scenarios.

Collectively, the results point towards more sizable RCBs at the regional/national scale than with global, land and ocean estimates of Rx1day and Rx5day metrics for thresholds, but with more varied values of RCBs under both the RCP 4.5 and RCP 8.5 scenarios. This includes a trend towards larger RCB values nationally from the global, land and ocean scales across scenarios for present-day 99th percentile events reaching future 95th percentile return levels, most especially for RCP 8.5 and 1pctCO_2, as with the overall shift from global and land/ocean towards the national scales, and with somewhat larger values for Rx1day than for Rx5day. Similarly, the

size of the RCBs generally increases in the case of 20-year events reaching future 10-year events when shifting from the global/land/ocean scale to the national one. Much like in the global to land/ocean case, larger RCBs were generally found for present-day 100-year return levels becoming 20-year return levels into the future, as compared with those RCBs linked to 20-year return levels becoming 10-year events in the future, but values are overall larger at the national level.

Table 2. National remaining carbon budgets (RCBs) for Rx1day and Rx5day under different emissions scenarios. RCBs are calculated based on the difference in cumulative carbon emissions between when the present-day 20-year return levels become 10-year return levels in the future, and those emissions at present-day. Similarly, RCBs were calculated based on the difference in cumulative emissions between when present-day 100-year return levels become 20-year return levels in the future, and emissions at present-day. Standard errors (SE) are provided for each RCB value. RCBs and SEs are given in units of teratons of carbon (TtC).

United States			
Rx1day 20-year becoming 10-year return level			
Scenario	Baseline (mm/day)	RCB (TtC)	SE (TtC)
RCP4.5	127	0.70	0.08
RCP8.5	127	1.08	0.14
1pctCO_2	127	2.29	0.19
Rx5day 20-year becoming 10-year return level			
Scenario	Baseline (mm/day)	RCB (TtC)	SE (TtC)
RCP4.5	268	0.32	0.06
RCP8.5	268	0.15	0.04
1pctCO_2	268	2.29	0.19
Rx1day 100-year becoming 20-year return level			
Scenario	Baseline (mm/day)	RCB (TtC)	SE (TtC)
RCP4.5	173	0.70	0.08
RCP8.5	173	1.08	0.12
1pctCO_2	173	2.29	0.19
Rx5day 100-year becoming 20-year return level			
Scenario	Baseline (mm/day)	RCB (TtC)	SE (TtC)
RCP4.5	323	0.32	0.06
RCP8.5	323	0.15	0.04
1pctCO_2	323	2.29	0.19
Australia			
Rx1day 20-year becoming 10-year return level			
Scenario	Baseline (mm/day)	RCB (TtC)	SE (TtC)

RCP4.5	213	0.75	0.08
RCP8.5	213	0.90	0.10
1pctCO_2	213	1.31	0.14
Rx5day 20-year becoming 10-year return level			
Scenario	Baseline (mm/day)	RCB (TtC)	SE (TtC)
RCP4.5	562	0.65	0.08
RCP8.5	562	1.26	0.13
1pctCO_2	562	1.31	0.14
Rx1day 100-year becoming 20-year return level			
Scenario	Baseline (mm/day)	RCB (TtC)	SE (TtC)
RCP4.5	260	0.75	0.08
RCP8.5	260	0.90	0.10
1pctCO_2	260	2.08	0.18
Rx5day 100-year becoming 20-year return level			
Scenario	Baseline (mm/day)	RCB (TtC)	SE (TtC)
RCP4.5	1491	0.65	0.08
RCP8.5	1491	0.45	0.07
1pctCO_2	1491	1.87	0.17
India			
Rx1day 20-year becoming 10-year return level			
Scenario	Baseline (mm/day)	RCB (TtC)	SE (TtC)
RCP4.5	223	0.79	0.08
RCP8.5	223	0.74	0.09
1pctCO_2	223	1.31	0.14
Rx5day 20-year becoming 10-year return level			
Scenario	Baseline (mm/day)	RCB (TtC)	SE (TtC)
RCP4.5	415	0.41	0.06
RCP8.5	415	0.34	0.06
1pctCO_2	415	0.79	0.11
Rx1day 100-year becoming 20-year return level			
Scenario	Baseline (mm/day)	RCB (TtC)	SE (TtC)
RCP4.5	297	0.79	0.08
RCP8.5	297	0.90	0.10
1pctCO_2	297	0.93	0.11
Rx5day 100-year becoming 20-year return level			
Scenario	Baseline (mm/day)	RCB (TtC)	SE (TtC)
RCP4.5	765	0.41	0.06
RCP8.5	765	1.26	0.13
1pctCO_2	765	2.29	0.19
Brazil			
Rx1day 20-year becoming 10-year return level			
Scenario	Baseline (mm/day)	RCB (TtC)	SE (TtC)
RCP4.5	229	0.75	0.08
RCP8.5	229	1.26	0.13
1pctCO_2	229	2.08	0.18

Rx5day 20-year becoming 10-year return level			
Scenario	Baseline (mm/day)	RCB (TtC)	SE (TtC)
RCP4.5	408	0.79	0.08
RCP8.5	408	1.26	0.13
1pctCO_2	408	1.31	0.14
Rx1day 100-year becoming 20-year return level			
Scenario	Baseline (mm/day)	RCB (TtC)	SE (TtC)
RCP4.5	353	0.75	0.08
RCP8.5	353	1.25	0.13
1pctCO_2	353	1.87	0.17
Rx5day 100-year becoming 20-year return level			
Scenario	Baseline (mm/day)	RCB (TtC)	SE (TtC)
RCP4.5	718	0.79	0.08
RCP8.5	718	1.25	0.13
1pctCO_2	718	1.31	0.14
South Africa			
Rx1day 20-year becoming 10-year return level			
Scenario	Baseline (mm/day)	RCB (TtC)	SE (TtC)
RCP4.5	119	0.65	0.08
RCP8.5	119	0.74	0.09
1pctCO_2	119	0.80	0.11
Rx5day 20-year becoming 10-year return level			
Scenario	Baseline (mm/day)	RCB (TtC)	SE (TtC)
RCP4.5	206	0.23	0.05
RCP8.5	206	1.07	0.12
1pctCO_2	206	2.08	0.18
Rx1day 100-year becoming 20-year return level			
Scenario	Baseline (mm/day)	RCB (TtC)	SE (TtC)
RCP4.5	165	0.65	0.08
RCP8.5	165	1.25	0.13
1pctCO_2	165	0.80	0.11
Rx5day 100-year becoming 20-year return level			
Scenario	Baseline (mm/day)	RCB (TtC)	SE (TtC)
RCP4.5	300	0.65	0.08
RCP8.5	300	1.07	0.12
1pctCO_2	300	2.29	0.19

a) Rx1day

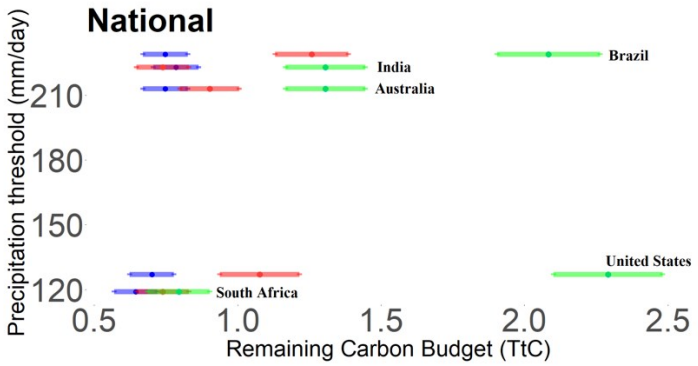

b) Rx5day

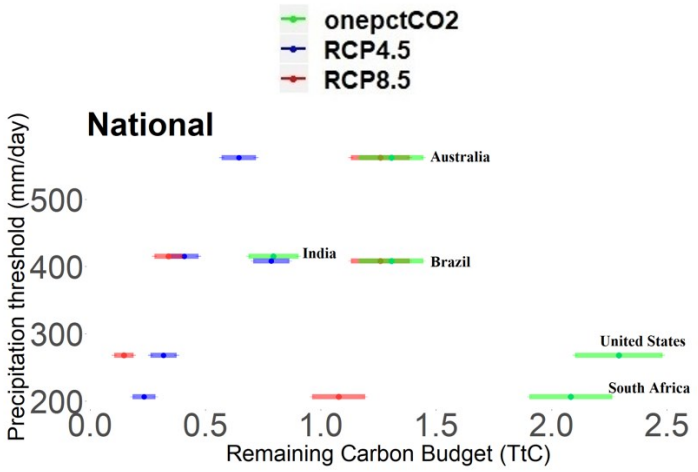

Figure 3. National remaining carbon budgets (RCBs) for present-day 20-year return levels (95th percentiles) reaching 10-year return levels (90th percentiles) in the future across emissions scenarios corresponding to a) Rx1day and b) Rx5day. RCBs are calculated relative to the emissions at the present-day, with the present-day 20-year return level being used as the baseline here. Error bars are representative of the standard errors calculated for the derived RCBs.

a) Rx1day

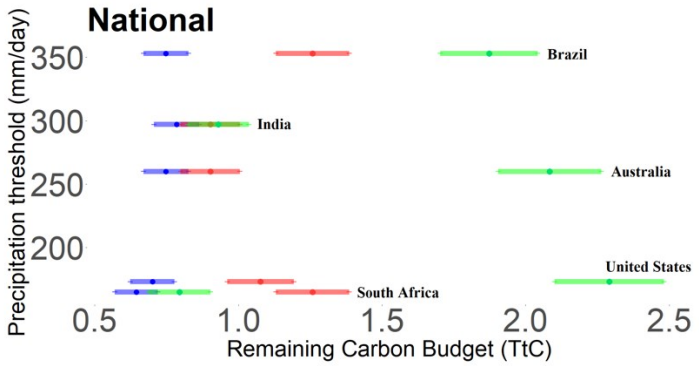

b) Rx5day

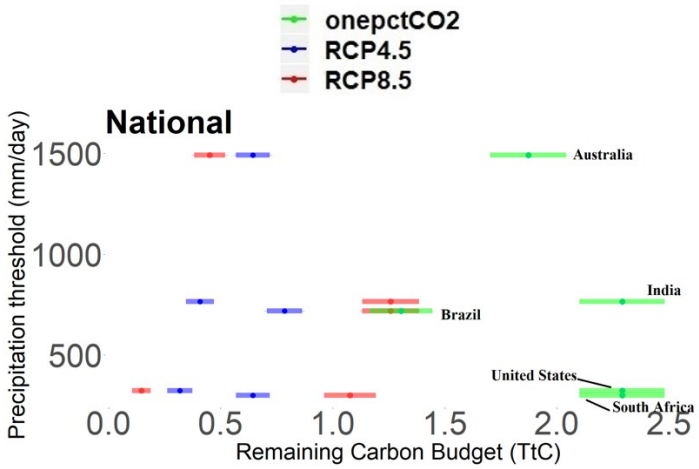

Figure 4. National remaining carbon budgets (RCBs) for present-day 100-year return levels (99th percentiles) reaching 20-year return levels (95th percentiles) in the future across emissions scenarios corresponding to a) Rx1day and b) Rx5day. RCBs are calculated relative to the emissions at the present-day, with the present-day 100-year return level being used as the baseline here. Error bars are representative of the standard errors calculated for the derived RCBs.

Local patterns of RCBs

In this sub-section, I discuss findings for local RCB patterns. Results are presented in Figures 5-6 and Table 3.

RCB estimates locally/at the grid cell across scenarios capture the broader national/regional trends discussed in the previous sub-section, and generally at the global to land and ocean scale. Indeed, the findings largely show that present-day 20-year return levels require consistently small additional amounts of cumulative CO_2 emissions in order to become future 10-year return levels across all scenarios, as compared with present-day 100-year return levels reaching future 20-year values (Figures 5-6, Table 3). For the five locales examined, the results similarly reveal that the largest values of RCBs occur with the 1pctCO_2 scenario, and smaller values across the RCP 4.5 and RCP 8.5 scenarios, with the exception of Montreal Rx5day having a smaller remaining budget for 1pctCO_2 than with either RCP 4.5 or RCP 8.5. However, the results are somewhat more varied in the local analysis than those patterns shown for globally to nationally. That said, much like at the national scale, RCBs are shown here to have a tendency of being larger for RCP 8.5 than for RCP 4.5, similarly representing a reversal in the pattern from the global scale, and in terms of land- and ocean-only. However, the generally larger values across RCP scenarios at the local scale shown signify a more significant distinction from the national scale, with values more often appearing as about 1.50 TtC or greater for 1pctCO_2 (Figure 5-6, Table 3), leading to a larger spread of RCBs across scenarios. This is similar to the global scale Rx5day under 1pctCO_2, though RCBs are shown here to be slightly more often greater than 1.00 TtC for RCP 8.5 than nationally (Tables 2 and 3). Much like at the global to land and ocean scale, RCBs are overall larger for Rx5day than they are for Rx1day, though with increased variability at the local scale (Table 3). That being mentioned, for both St. Louis and Florida, an opposing pattern was observed, with both locales consistently having RCBs larger for Rx1day than for Rx5day (Table 3). The overall largest RCBs were found in the Philippines across extreme precipitation indicators and scenarios (0.70-1.87 TtC +/- 0.08-0.17 TtC), while

St. Louis showcased the smallest values among the studied locales for its Rx5day events (0.08-1.13 +/- 0.04-0.13 TtC), followed by Montreal Rx5day (0.45-0.57 TtC +/- 0.07 TtC) (Figure 5, Table 3). St. Louis itself carried the absolute smallest RCB under RCP 4.5 for Rx5day (0.08 TtC), as well as the smallest 1pctCO_2 budget (1.13 TtC).

With respect to the present-day 100-year return levels becoming future 20-year levels, the results also display a similar pattern to what was shown for globally to nationally for RCBs. As described previously, the RCBs corresponding to the RCP scenarios trend towards smaller values than the consistently larger values shown in the 1pctCO_2 scenario (Figure 6, Table 3). Much like at the national scale, the largest RCBs tied to the 1pctCO_2 scenario locally are often higher than what was captured globally, as well as with respect to land and ocean. However, for 1pctCO_2, RCBs are generally slightly lower than at the national scale, though the RCBs corresponding to the RCP scenarios are slightly higher than at the national scale overall. The highest values of RCBs are found in St. Louis and Florida under 1pctCO_2, where 2.08 TtC and 2.29 TtC (+/- 0.18-0.19 TtC) of cumulative emissions occur, respectively, for Rx1day. For Hong Kong and Philippines Rx5day, as well as for Montreal's Rx1day, RCB values for 1pctCO_2 was also large (1.87 TtC +/- 0.17 TtC). Conversely, the lowest RCBs are found for St. Louis Rx5day (0.15 TtC +/- 0.04 TtC) across the local RCP scenarios, similar to the present-day 20-year return level for St. Louis becoming the 10-year value into the future. In Florida, RCBs are shown to be 0.70 TtC and 0.90 TtC (+/- 0.08-0.10 TtC) for RCP 4.5 and RCP 8.5, respectively. At the national scale, this is consistent with the lower RCB values found for the United States' Rx5day (0.15-0.32 +/- 0.04-0.06 TtC), and with respect to RCBs being smaller in Rx5day than in Rx1day. Indeed, Rx5day for the United States similarly displayed the lowest RCBs across selected nations.

Table 3. Local remaining carbon budgets (RCBs) for Rx1day and Rx5day under different emissions scenarios. RCBs are calculated based on the difference in cumulative carbon emissions between when the present-day 20-year return levels become 10-year return levels in the future, and those emissions at present-day. Similarly, RCBs were calculated based on the difference in cumulative emissions between when present-day 100-year return levels become 20-year return levels in the future, and emissions at present-day. Standard errors (SE) are provided for each RCB value. RCBs and SEs are given in units of teratons of carbon (TtC).

Hong Kong area			
Rx1day 20-year becoming 10-year return level			
Scenario	Baseline (mm/day)	RCB (TtC)	SE (TtC)
RCP4.5	145	0.70	0.08
RCP8.5	145	1.26	0.13
1pctCO_2	145	1.49	0.15
Rx5day 20-year becoming 10-year return level			
Scenario	Baseline (mm/day)	RCB (TtC)	SE (TtC)
RCP4.5	199	0.75	0.08
RCP8.5	199	0.59	0.08
1pctCO_2	199	1.87	0.17
Rx1day 100-year becoming 20-year return level			
Scenario	Baseline (mm/day)	RCB (TtC)	SE (TtC)
RCP4.5	322	0.75	0.08
RCP8.5	322	1.26	0.13
1pctCO_2	322	1.68	0.16
Rx5day 100-year becoming 20-year return level			
Scenario	Baseline (mm/day)	RCB (TtC)	SE (TtC)
RCP4.5	316	0.75	0.08
RCP8.5	316	0.59	0.08
1pctCO_2	316	1.87	0.17
Philippines			
Rx1day 20-year becoming 10-year return level			
Scenario	Baseline (mm/day)	RCB (TtC)	SE (TtC)
RCP4.5	145	0.70	0.08
RCP8.5	145	1.44	0.14
1pctCO_2	145	1.67	0.16
Rx5day 20-year becoming 10-year return level			
Scenario	Baseline (mm/day)	RCB (TtC)	SE (TtC)
RCP4.5	291	0.75	0.08
RCP8.5	291	1.44	0.14
1pctCO_2	291	1.87	0.17
Rx1day 100-year becoming 20-year return level			
Scenario	Baseline (mm/day)	RCB (TtC)	SD (TtC)
RCP4.5	211	0.70	0.08
RCP8.5	211	1.08	0.12
1pctCO_2	211	1.31	0.14

Rx5day 100-year becoming 20-year return level			
Scenario	Baseline (mm/day)	RCB (TtC)	SD (TtC)
RCP4.5	603	0.75	0.08
RCP8.5	603	1.44	0.14
1pctCO_2	603	1.87	0.17
St. Louis area			
Rx1day 20-year becoming 10-year return level			
Scenario	Baseline (mm/day)	RCB (TtC)	SE (TtC)
RCP4.5	73	0.65	0.08
RCP8.5	73	0.74	0.09
1pctCO_2	73	2.08	0.18
Rx5day 20-year becoming 10-year return level			
Scenario	Baseline (mm/day)	RCB (TtC)	SE (TtC)
RCP4.5	133	0.08	0.04
RCP8.5	133	0.15	0.04
1pctCO_2	133	1.13	0.13
Rx1day 100-year becoming 20-year return level			
Scenario	Baseline (mm/day)	RCB (TtC)	SE (TtC)
RCP4.5	93	0.65	0.08
RCP8.5	93	0.74	0.09
1pctCO_2	93	2.08	0.18
Rx5day 100-year becoming 20-year return level			
Scenario	Baseline (mm/day)	RCB (TtC)	SE (TtC)
RCP4.5	164	0.15	0.04
RCP8.5	164	0.15	0.04
1pctCO_2	164	1.13	0.13
Florida			
Rx1day 20-year becoming 10-year return level			
Scenario	Baseline (mm/day)	RCB (TtC)	SE (TtC)
RCP4.5	103	0.75	0.08
RCP8.5	103	1.44	0.14
1pctCO_2	103	1.49	0.15
Rx5day 20-year becoming 10-year return level			
Scenario	Baseline (mm/day)	RCB (TtC)	SE (TtC)
RCP4.5	222	0.70	0.08
RCP8.5	222	0.90	0.10
1pctCO_2	222	1.13	0.13
Rx1day 100-year becoming 20-year return level			
Scenario	Baseline (mm/day)	RCB (TtC)	SE (TtC)
RCP4.5	145	0.75	0.08
RCP8.5	145	1.44	0.14
1pctCO_2	145	2.29	0.19
Rx5day 100-year becoming 20-year return level			
Scenario	Threshold (mm/day)	RCB (TtC)	SE (TtC)
RCP4.5	303	0.70	0.08

RCP8.5	303	0.90	0.10
1pctCO_2	303	1.13	0.13
Montreal area			
Rx1day 20-year becoming 10-year return level			
Scenario	Baseline (mm/day)	RCB (TtC)	SE (TtC)
RCP4.5	48	0.57	0.07
RCP8.5	48	0.45	0.07
1pctCO_2	48	1.49	0.15
Rx5day 20-year becoming 10-year return level			
Scenario	Baseline (mm/day)	RCB (TtC)	SE (TtC)
RCP4.5	120	0.70	0.08
RCP8.5	120	1.44	0.14
1pctCO_2	120	0.24	0.07
Rx1day 100-year becoming 20-year return level			
Scenario	Baseline (mm/day)	RCB (TtC)	SE (TtC)
RCP4.5	61	0.57	0.08
RCP8.5	61	1.44	0.14
1pctCO_2	61	1.87	0.17
Rx5day 100-year becoming 20-year return level			
Scenario	Baseline (mm/day)	RCB (TtC)	SE (TtC)
RCP4.5	181	0.70	0.08
RCP8.5	181	1.44	0.14
1pctCO_2	181	0.24	0.07

a) Rx1day

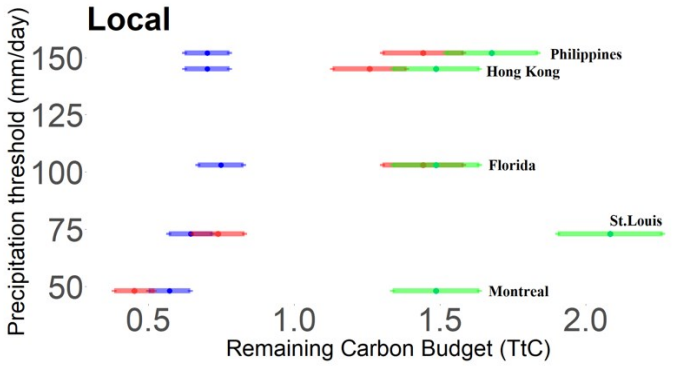

b) Rx5day

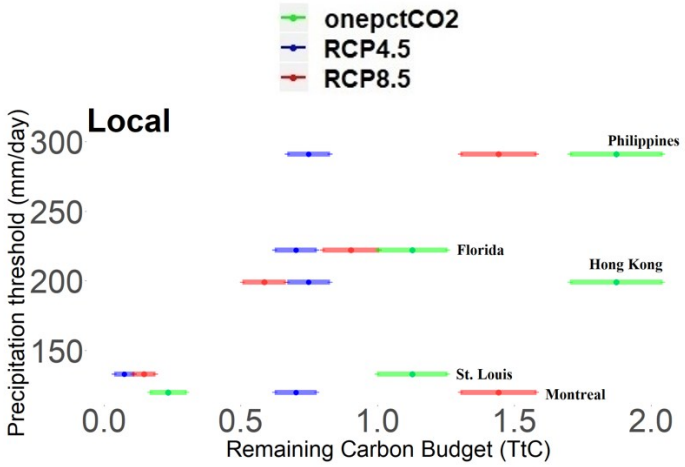

Figure 5. Local remaining carbon budgets (RCBs) for present-day 20-year return levels (95th percentiles) reaching 10-year return levels (90th percentiles) in the future across emissions scenarios corresponding to a) Rx1day and b) Rx5day. RCBs are calculated relative to the emissions at the present-day, with the present-day 20-year return level being used as the baseline here. Error bars are representative of the standard errors calculated for the derived RCBs.

a) Rx1day

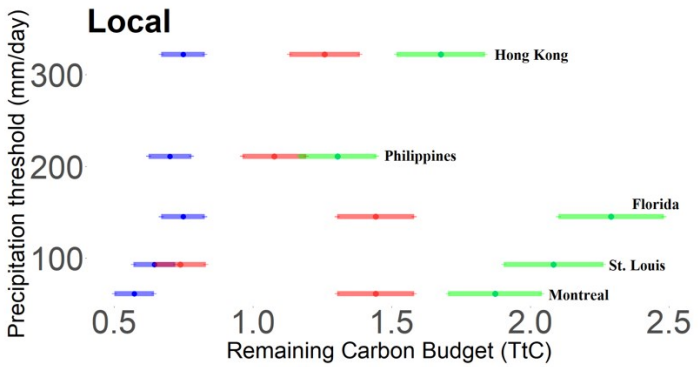

b) Rx5day

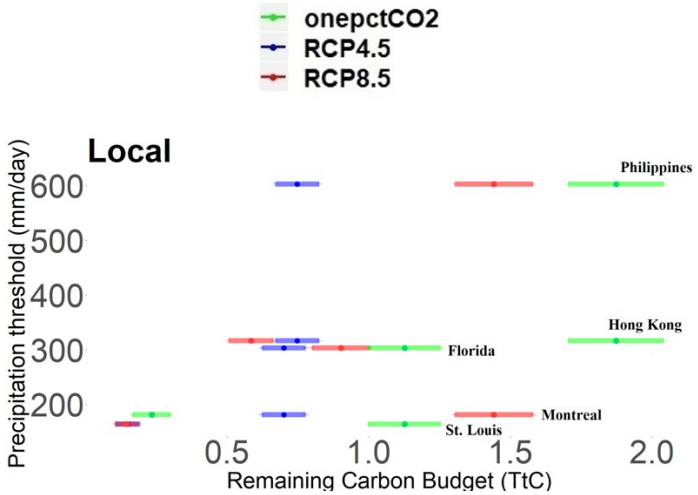

Figure 6. Local remaining carbon budgets (RCBs) for present-day 100-year return levels (99th percentiles) reaching 20-year return levels (95th percentiles) in the future across emissions scenarios corresponding to a) Rx1day and b) Rx5day. RCBs are calculated relative to the emissions at the present-day, with the present-day 100-year return level being used as the baseline here. Error bars are representative of the standard errors calculated for the derived RCBs.

Discussion

Extending the TCRE-based analysis from Chapters 3 and 4, I was able to estimate here the cumulative carbon emissions needed to meet or exceed various extreme precipitation return level thresholds pertaining to Rx1day and Rx5day. It was, therefore, possible to derive RCBs to determine the point at which present-day 20-year and 100-year return levels (90th and 99th

percentiles) become 10-year or 20-year return levels (90^{th} and 95^{th} percentiles) in the future across emissions scenarios from the global to local scale. My findings generally show that from globally to locally, RCB values are lowest across the RCP scenarios (i.e. RCP 4.5 and RCP 8.5) and highest under the 1pctCO_2 scenario. However, whether RCBs are lower or higher across scenarios, notably in the RCPs, is spatially-dependent, as well as varying with the return level threshold choice. Indeed, there is more variability in RCB values when shifting the analysis from the global scale to the local one. Most commonly for RCBs required for 20-year (95^{th} percentile) return levels to reach 10-year (90^{th} percentile) return levels, the lowest values of RCBs coincide with RCP 4.5 than with RCP 8.5 consistently nationally to locally, but the reverse holds true at the global scale, as well as for ocean.

100-year to 20-year return level trends

Similarly, in terms of the present-day 100-year return level becoming 20-year return levels into the future, RCBs corresponding to RCP 4.5 are generally smaller than for RCP 8.5 across all spatial scales, with again the exception of globally and ocean only. In both situations, the point at which these return levels are reached and/or exceeded frequently coincides at earlier future blocks in the RCP scenarios. In the case of thresholds being reached by the first block of the RCP scenarios, this represents the minimum RCB of approximately 0.08 TtC (+/-0.04 TtC) of additional cumulative emissions from the present-day block (i.e. the first block comprising the RCP 4.5 scenario); at the national to even local scale, the RCB value is as low as 0.08 TtC (+/- 0.04 TtC) in the case of St. Louis Rx5day for the RCP 4.5 scenario, and 0.12 TtC (+/- 0.04 TtC) under 1pctCO_2 (i.e. land Rx1day for meeting both thresholds).

For the 100-year trends, RCBs are generally larger across the cumulative emissions scenarios (Figures 2, 4 and 6, Tables 1-3). This is due to the 100-year return level value more regularly being reached deeper into the future (i.e. such values are found in latter block maxima). As a result, 100-year return levels represent RCBs requiring larger emissions sizes in order to be matched and/or exceeded. Nevertheless, although RCBs are generally larger with respect to 100-year return levels becoming future 20-year levels, the same tendency is observed; that is, budgets are similarly smaller in the RCP scenarios than in 1pctCO_2. This pattern is further maintained as RCBs overall increase across scenarios with decreasing spatial scale.

Emissions scenario differences

Intuitively, the consistently low RCBs found here would make sense in the RCP cases, since it is the RCP scenarios that encompass a combination of non-CO_2 and CO_2 forcings. This compares with the 1pctCO_2 scenario, which is driven by CO_2 only, as opposed to the collective response originating with CO_2 and non-CO_2 forcings included in the RCP scenarios that would otherwise match the realistic climate response more closely. Such differences are reflected in my results, where smaller values of RCBs consistently occur with the RCP scenarios than for 1pctCO_2, from globally to locally, for reaching and/or exceeding both present-day return levels considered. Effectively, such emissions trajectories described for the RCP scenarios reduce the extent of allowable additional CO_2 emissions needed to reach the precipitation thresholds in question. Therefore, it stands to reason that thresholds of extreme precipitation, or potentially other climate/weather extremes, could be achieved sooner into the future if either of the RCP scenarios examined here are followed in light of the collective contributions from both CO_2 and non-CO_2 forcings. However, the extent to which this occurs varies with the extreme precipitation

indicator, spatial scale and threshold selection, with RCBs being consistently at their lowest overall globally, for land, and for ocean with respect to the RCP scenarios for reaching present-day 100-year return level values. RCBs are also generally lower when focusing the analysis to reaching present-day 20-year return level thresholds, as compared with reaching and/or exceeding 100-year return levels, and they are shown to be overall lower for Rx1day than for Rx5day.

Altogether, these findings suggest that specified extreme precipitation thresholds can more quickly be reached at the global scale, as well as in terms of land and ocean. Conversely, more CO_2 emissions are largely required across scenarios when constraining the analysis to the national to local scale, notably for matching or exceeding 100-year return levels. In terms of reaching 20-year return levels, RCBs also similarly increase from globally to locally, though RCBs linked with 1pctCO_2 decrease slightly overall from nationally to locally (Tables 2 and 3). Nevertheless, at smaller spatial scales (i.e. nationally to locally), similar patterns are observed across scenarios for Rx1day and Rx5day, in which RCBs are at their lowest for the RCP scenarios (lowest values dependent on the threshold choice, spatial scale and extreme precipitation indicator) and consistently largest for 1pctCO_2.

As described previously, values of RCBs are shown to be mostly higher for RCP 8.5 than for RCP 4.5 for reaching and/or exceeding extreme precipitation thresholds (Figures 1-6, Tables 1-3). Since cumulative CO_2 emissions are prescribed to increase more aggressively in RCP 8.5, especially over the course of the latter half of that scenario, this would further explain why RCBs are very often larger than in RCP 4.5. Correspondingly, the higher emissions characteristic of RCP 8.5 result in higher specified return level values being reached sooner into the future, as

compared with similar values occurring later in the RCP 4.5 situation (mostly in the case for reaching/surpassing the present-day 100-year return level).

Conversely, I showed that the 1pctCO_2 scenario consistently drives the largest RCBs, from globally to locally. As mentioned, this pattern is likely to be an artifact of this scenario being comprised of CO_2 emissions only, effectively increasing the RCB amounts needed for the same thresholds to be reached/exceeded. Therefore, under a CO_2-only scenario, it would imply that more CO_2 emissions would be necessary to reach a given present-day return level. For example, in the United States, the 20-year return level of 127 mm/day for Rx1day (Table 2) is shown here to be linked to an RCB of 0.70 TtC (+/- 0.08 TtC) under RCP 4.5 and 1.08 TtC (+/- 0.14 TtC) for RCP 8.5 in terms of matching/exceeding this value into the future, but this same baseline value (127 mm/day) is also shown to have a 2.29 TtC (+/- 0.19 TtC) RCB under 1pctCO_2 (Table 2).

In a counterfactual world, then, where cumulative CO_2 emissions are the sole greenhouse gas, this provides some indication of how much cumulative CO_2 emissions would be required to reach some extreme precipitation threshold. It should be noted, however, that in some cases, RCBs appear in low amounts under even 1pctCO_2 for reaching/exceeding present-day 20-year thresholds into the future, as well as in terms of reaching/exceeding present-day 100-year return levels (e.g. global Rx5day), stressing that relatively small additional cumulative CO_2 emissions alone can be sufficient for reaching thresholds of precipitation extremes sooner than later. This includes, in some instances, at the national scale, as well as at the local scale (Tables 2-3), suggesting that relatively small additional increases in CO_2 by itself similarly would be enough to meet specified present-day return level thresholds. Particularly significant is the result shown

for land-only Rx1day, where the RCB is lowest (0.12 TtC) for 1pctCO_2 for both thresholds (Table 2). At the same time, the lower RCB values mostly shown for RCP 4.5 indicate that the more stringent efforts to limit global emissions by ideally stabilizing these emissions by 2040 may not be ambitious enough to avoid specified thresholds of precipitation extremes. This implies that particularly dangerous levels of Rx1day and Rx5day are, as mentioned, often reached rather quickly into the future with only minimal amounts of additional cumulative CO_2 emissions at all spatial scales in question, whether for reaching more intense 10- to 20-year return levels into the future, or for reaching present-day 100-year thresholds in future as 20-year return levels.

Similarities between national and local patterns

Some connections could further be made between national and local trends, as outlined previously. In the United States, for example, higher values of RCBs are shown for Rx1day in that nation for the RCP scenarios for reaching/exceeding thresholds, including being larger than for Rx5day. This diverges from the overall trend of RCBs being characteristically larger for Rx5day than Rx1day, including consistently across both extreme precipitation threshold categories (Tables 1-3). Subsequently, Florida displays a similar tendency, with Rx5day values being much smaller than for Rx1day across RCP scenarios, tracing well the overall pattern shown for the United States/national scale (Table 3) to a locale in that nation. In the case of St. Louis, the results similarly point to lower RCBs for Rx5day than for Rx1day for reaching present-day 20-year and 100-year return levels (Table 3). For both Florida and St. Louis, 1pctCO_2 RCBs are further among the lowest under Rx5day, similar to what is shown at the national scale (United States) for that scenario. Ultimately, the United States generally shows

small RCBs in principally the RCP scenarios to reach specified selected present-day return level thresholds, with similar or increasing sizes of RCBs when advancing to the local scale in that nation (i.e. Florida and St. Louis) for reaching/exceeding both threshold selections into the future.

Overall patterns

In cases of larger RCBs at the national to local level for either RCP 4.5 or RCP 8.5, as described above, higher amounts occur as a result of their present-day return levels being matched and/or surpassed later into the future, as opposed to earlier in it in, or close to the first block maxima. However, in most cases, my findings indicate that RCBs are still often well under 1 TtC of cumulative CO_2 emissions for reaching thresholds across all spatial scales for either Rx1day or Rx5day. This is consistently the case for RCP 4.5. As such, similar RCBs occurring across scenarios in a few cases suggest that more intense precipitation extremes into the future can be achieved simultaneously, regardless of the emissions pathway. The allowable cumulative emissions, thus, required to meet a given extreme precipitation threshold value in the future would arguably be quite small across scenarios in light of recent global carbon emission rates alone, especially in terms of the total annual emissions featured in the year 2022. Indeed, as shown for some nations and locations, present-day 100-year return levels can become 20-year return levels with additional allowable cumulative emissions that are well under 1 TtC, such as the United States and correspondingly Florida and St. Louis for Rx5day more locally, as outlined previously. This may further be representative of patterns in other nations, as well as locations within those nations, that are not examined in this work.

The smaller amounts of RCBs needed to meet or reach extreme precipitation thresholds into the future also reflect the climate sensitivity to even comparatively small global cumulative emission rises. This suggests that precipitation extremes, including the most intense among these, can strengthen quickly and become more frequent when global CO_2 emission concentrations only increase by (relatively) low amounts. This implies that, for instance, present-day 20-year return levels become more regular into the future, along with newer, intensified versions of these present-day return levels. This is suggested by these values becoming 10-year return levels, or through present-day 100-year levels becoming 20-year events with sometimes very limited additional cumulative CO_2 emissions.

To that end, corresponding rises in global to regional temperature would likely foster environmental settings that would be conducive to more intense precipitation extremes as emissions increase. Indeed, the results indirectly show here the importance of the magnified regional warming that realistically drives the rising global mean temperature pattern (e.g. Sun & Ao, 2013). This warming is especially significant at mid- to high-latitudes, which would likely act to increase the regional climate sensitivity at those latitudes to such warming as global emissions rise. The findings presented here would, therefore, broadly support those results presented in Sun et al., (2023), showing that (extreme) precipitation increases most significantly at low- and mid-latitudes. This is consistent with the overall smaller RCB values that are observed when constraining the analysis globally, highlighting the notion that future global, land and ocean values of Rx1day and Rx5day can occur sooner than for nationally to locally with respect to reaching specified thresholds. This would be especially true in the case of RCP 8.5, where cumulative CO_2 emissions are as low as 0.15 TtC +/- 0.04 TtC, regardless of the present-day return level in question (Table 1). The patterns shown for oceanic areas further suggest

important implications for land, since intensified precipitation extremes that originate over oceans can drift over land areas, causing potentially significant damages from hazards like flash-flooding and storm surge. This would further indicate intensified precipitation extremes in source regions that are critical for the development of tropical cyclones, for example, which is notably concerning for those cyclones that potentially make landfall and induce exacerbated coastal storm surge (e.g. Gori et al., 2021). Such patterns over the oceans, thus, imply that tropical cyclones may inherit intensified precipitation rates at relatively small increases of cumulative CO_2 emissions in the future. Indeed, the results show here that ocean precipitation extremes reach specified return level thresholds quickly into the future (Table 1).

Although RCBs are generally largest at especially the local scale for reaching and/or exceeding present-day return levels, the results presented in this work also do show that some locales (and nations) can, indeed, achieve more intense precipitation extremes in the near-future at small additional CO_2 emissions. This would be in light of likely faster intensification rates regionally, possibly attributable to the more magnified warming rates that realistically occur at finer spatial scales than what is captured globally.

At the same time, it should be noted that the RCP scenarios are treated (slightly) differently between CMIP5 and the Coupled Model Intercomparison Project Phase 6 (CMIP6). For instance, RCP 8.5 in CMIP5 carries CO_2 concentrations that are approximately 20% less than in CMIP6's Shared Socio-economical Pathways (SSP) 5-8.5 (Bourdeau-Goulet & Hassanzadeh, 2021). Despite these differences in the representation of this particular scenario, the results presented for RCP 8.5 in this work still could reflect meaningful RCBs relative to the present-day. Indeed, the present-day, centered on 2012, precedes years that showed largely aggressive

increases in globally-measured cumulative emissions. This further suggests less time for 20-year or 100-year levels to reach the designated thresholds considered herein. Furthermore, most recent years' emissions have been particularly high; in 2022 and 2023 alone, record levels of global CO_2 emissions were observed, with levels in 2023 surpassing the record emissions achieved just a year prior. As such, CMIP5's definition of RCP 8.5's emissions throughout the 21st century may, thus, be a closer representation or approximation of reality.

Possible causes for trends

In particular, as temperatures rise, this increases the atmosphere's ability to hold more water vapor content, which is a central component in the development of more intense precipitation extremes, as well as for many other weather/climate extremes collectively. This is consistent with the Clausius-Clapeyron relationship, which describes an increase in atmospheric water vapor content of approximately 7% per degree Kelvin/Celsius of warming (e.g. Donat et al., 2013). This enhanced humidification would, thus, fuel precipitation development within the synoptic to mesoscale systems that often produce these events, mostly through enhanced atmospheric instability (i.e. higher CAPE) that favor increased updraft speeds in deep convective systems. It is, therefore, likely that such intensification in the Rx1day and Rx5day extremes examined here are at least partly the result of more intensified thunderstorms, such as enhancements in the environments required for the development of particularly strong to severe thunderstorms (e.g. Trapp et al., 2007; Moore et al., 2015; Edwards et al., 2018), as well as other modes of deep convection. With decreasing latitudinal thermal gradients, this may also include a shift towards slower propagation speeds of mid-latitude cyclones. In turn, this weakened gradient further could translate into weaker jet streams and 500-millibar/mid-tropospheric flow that may

slow the movement of mesoscale convective systems that typically organize within the synoptic-scale environments. Such environments would favor slower-moving thunderstorms, which have been linked to extreme one-day rainfall events (e.g. Hu et al., 2021). Furthermore, precipitation enhancements, notably in one-day amounts into the future may be associated with substantial intensification rates in rainfall in tropical cyclones (e.g. Tan et al., 2022). To another end, the intensified 20-year return levels shown here (Chapter 4) for Rx5day at all spatial scales from their approximate present-day values also suggests potentially more atmospheric blocking at higher emission concentrations. Such blocking could create atmospheric/jet stream configurations more suitable for significant five-day precipitation (Rx5day) events through, for instance, active atmospheric rivers, where plumes of moisture are more frequently allowed to fuel mid-latitude cyclone families over the same regions repeatedly for extended periods.

Enhancements in important global climate modulators of natural variabilities, such as the El Nino Southern Oscillation (ENSO), may further play a role in directing precipitation events towards more intensified thresholds (e.g. Moore et al., 2015), especially as this natural variability works in the same direction as climate change during particularly (strong) El Nino years. At the same time, the South Asian wet monsoonal circulation may be enhanced at higher cumulative emissions (e.g. Supharatid et al., 2022), which may be linked to the intensified 20-year and 100-year return levels and location parameter estimates shown in Chapter 4 for India, as well as correspondingly the lower RCBs needed to reach India's present-day return levels for Rx1day in particular (Table 2).

Such factors could largely explain why more intense precipitation thresholds may not necessarily require significantly more global CO_2 emission concentrations relative to present-day

values in order to meet the selected thresholds; in some cases, as mentioned previously, the same remaining carbon budgets can sometimes overlap with similar precipitation thresholds across scenarios. Therefore, the implication here is that extreme precipitation thresholds can be reached under a small range of RCBs across cumulative emissions scenarios.

Conclusion

In this chapter, I extended TCRE-based analyses conducted in previous chapters to derive RCBs pertaining to specified thresholds of return levels of precipitation extremes across different spatial scales. It was, therefore, possible to estimate RCBs corresponding to the point at which present-day 20-year and 100-year return levels of Rx1day and Rx5day become 10-year and 20-year levels into the future globally to locally, which was the focus of this chapter. My results specifically show that for present-day 20-year return levels becoming 10-year return levels in the future, and the point at which present-day 100-year return levels become future 20-year return levels, RCBs are shown to appear in mostly limited amounts across emissions scenarios used in this study. To that end, the RCP scenarios have consistently the least amount of additional allowable emissions (notably for RCP 4.5), and with 1pctCO_2 conversely having the largest globally to locally for Rx1day and Rx5day, regardless of return level selection. Although RCB values trended higher when focusing my analysis to the national to local scales (notably in the 100-year return level analysis), some lower amounts of RCBs sometimes still emerged for the nations/regions to locales considered herein. That said, at all spatial scales, there was generally more overlap across the RCP scenarios, but nationally to locally, there were further some cases where the RCBs tied to the 1pctCO_2 scenario more closely approached those RCBs associated

with RCP 4.5 and RCP 8.5 (such as for land-only, India, Brazil, South Africa, Hong Kong, the Philippines, Florida, and Montreal).

My results, therefore, offer a different lens through which precipitation extreme indicators can be viewed in relation to global cumulative emissions by deriving estimates of remaining carbon budgets that are linked to particularly dangerous extreme precipitation levels. This is especially important at regional to local scales, where larger gaps in the body of climate impacts literature occur. These findings could further potentially be of value in the climate adaptation and policy sectors by way of better contextualizing emissions targets that are linked with various extreme precipitation thresholds of interest. Notably, I showed that RCBs at all spatial scales are generally small in terms of meeting specified emissions targets tied to the selected extreme precipitation thresholds examined herein. The extent of RCBs shown suggest that even small amounts of additional global CO_2 emissions can have a profound impact on extreme precipitation events at all spatial scales. Regional magnifications of global warming, especially at higher latitudes, thus, raise concern as to regional (extreme) precipitation responses in the future. To that end, I showed that, globally to locally, progressively more significant extreme precipitation levels can be reached quickly in the future, requiring only very small RCBs to meet such thresholds going forward. As such, despite efforts to satisfy emissions targets specified in the Paris Climate Agreement that are compatible with thresholds of 1.5 C to 2.0 C of global warming relative to the pre-industrial period, I stress that much more stringent targets are instead necessary in the hope of avoiding the potential catastrophic impacts that surround more intensified precipitation extremes into the future. This is especially important for areas and regions that are already below sea level, and where (flash-) flooding is or has become a growing concern. More extreme and frequent precipitation thresholds can be notably impactful in

urbanized centers, as well as along the flood plain where coastal flooding can be particularly significant. I acknowledge, however, that my study employs a broad approach for examining precipitation extremes, which realistically appear at the sub-synoptic spatial scales that are not meaningfully captured in the coarser model resolutions used for the simulations of extreme precipitation events studied in this work. Therefore, upcoming studies could perhaps use a similar methodological approach to explore these or similar events at finer scales, or more meaningfully the complex environmental conditions that are important to the development of precipitation extremes altogether, which could improve the predictability of such events. However, an improvement in model resolution would not necessarily be sufficient to correspondingly improve precipitation projections; rather, a fundamental approach would be to more directly improve the model physics of precipitation and precipitation extremes collectively.

Chapter 6: Overall Conclusions

In this dissertation, I analyzed trends in precipitation extremes at a variety of spatial scales by framing them in the context of cumulative (CO_2) emissions, primarily determining whether precipitation extremes, including the most intense extremes, can be approximated by the TCRE, similar to the extent to which global to regional temperatures are framed in previous works. As part of this research, I also endeavored to address uncertainties in trends of the most extreme precipitation events in response to rising concentrations of cumulative emissions by using GEV analyses, as well as placing extremes in the context of the remaining carbon budget. I specifically employed simulated precipitation data from a consistent set of nine GCMs participating in the CMIP5 to examine trends of global, regional and local precipitation extremes by using the extreme precipitation indicators commonly studied in the body of climate impacts literature (Rx1day and Rx5day). This data was used to address three important overlapping research objectives in this work, which were further investigated in the three principal chapters that are centered on the TCRE framework. First, I endeavored to frame spatially averaged Rx1day and Rx5day precipitation extreme indicators as a function of cumulative (CO_2) emissions and determine whether linear trends exist at various spatial scales. In my next chapter, I applied EVT for the selected extreme precipitation indicators by using specifically the GEV analysis to model extreme precipitation behavior. I then proceeded to use GEV analyses to frame location parameter estimates and specified return levels as a function of cumulative emissions, determining similarly whether these trends can similarly be approximated by the TCRE at the global to local scale. In an attempt to further apply TCRE estimates of precipitation extreme indictors to derive RCBs linked to thresholds of the most extreme

precipitation, in Chapter 5 of this work, I outline two primary objectives: Firstly, I estimate RCBs that are linked to present-day 20-year return levels becoming 10-year return level values in the future by applying GEV analyses previously derived in Chapter 4, and secondly: determine the RCB pertaining to the point at which present-day 100-year return levels become the 20-year return level across scenarios, globally to locally. This introduces a meaningful approach to quantify precipitation extremes and provide some insight as to remaining cumulative CO_2 emissions required to reach selected precipitation thresholds that may be deemed as dangerous to disastrous. This work also offers a new dimension for understanding trends in extreme precipitation events at the regional to local scale and, as such, attempts to address some of the uncertainty associated with such events in the climate impacts literature.

I firstly found that trends for selected extreme precipitation indicators largely scale linearly with increasing global cumulative emissions, showing that these indicators can be well approximated by the TCRE framework. Assessing the TCRE at the regional scale also reveals that linear trends in precipitation extremes occur at sub-global scales, as multiple nations studied here exhibit the (strong) linear tendencies that are captured globally to land and ocean. My results, therefore, show that the TCRE can be applied and extended to extreme precipitation, from especially globally to regionally. At the local scale, I conversely found no robust trends for Rx1day and Rx5day, though linearity may still exist and could simply be masked by background noise caused by the natural variability that would more readily be expected at such finer spatial scales. In the next stage of this work, I showed that chosen thresholds of precipitation extremes become more intense and frequent with increasing cumulative emissions, with consistently increasing linear trends in location and

scale parameter estimates for both Rx1day and Rx5day at all spatial scales. Shape parameter estimates showed generally no significant trends at regional to local scales, but there were more consistently statistically significant decreasing trends displayed globally, for ocean, and for land only. The implication, therefore, is that the probabilities of occurrence for (the most) intense Rx1day and Rx5day events would decrease over time. For nationally to locally, the lack of significant trends in the shape parameter estimates suggest that the probabilities of the most intense events in the future remain approximately the same as the present-day and historically altogether. However, this also suggests that these extreme precipitation events would still become more intense under the same or lesser probabilities historically, as location parameter estimates can similarly be approximated by the TCRE. The patterns of the TCRE are further reflective in the more intense and frequent return levels selected for this study, from globally to locally, as emissions rise. It should also be noted that increases in the location and scale parameter estimates, nevertheless, favor a trend towards heavier-tailed behavior, despite trends in the shape parameter. That said, increasing trends in the shape parameter combined with increases in location and shape are particularly concerning, which was shown be the case in this work for some nations and locales.

Expanding on these findings, I further show that selected thresholds of Rx1day and Rx5day return levels do not generally require a significant amount of additional global (CO_2) emissions in order to be reached. For example, present-day 20-year return levels can become a 10-year return level into the future relatively quickly across emissions scenarios; this is especially the case in both the RCP 4.5 and RCP 8.5 scenarios, with the latter representing a substantial amount of annual cumulative emissions that are prescribed to

occur throughout the 21st century. However, even in a counterfactual world comprised of only CO_2 emissions (as in the 1pctCO_2 case), the budgets are still shown in this study to be relatively limited for land-only, and for some of the studied nations and locations as emissions rise. These findings suggest that the most intense precipitation extremes, therefore, strengthen very rapidly with even relatively small amounts of additional annual cumulative emissions from present-day amounts. This stresses the need to establish more ambitious (CO_2) emissions targets in order to avoid particularly dangerous extreme precipitation events at all spatial scales. Such intensification in precipitation extremes could include more substantial precipitation rates observed over the duration of tropical cyclones, as well as during strong to severe thunderstorms, which act to exacerbate the impacts of (flash-) flooding that are linked to deep convection collectively. Currently-deemed weak convective systems may, for example, also respond robustly to small increases in global emissions, as even these systems would favorably produce more significant precipitation rates as atmospheric moistening is expected to increase with warmer global temperatures. Indeed, all forms of precipitation extremes rely on some extent of atmospheric moisture (humidification) as part of their development, making moistening central to better understand the evolution in (extreme) precipitation characteristics over time, and the systems that produce them. Indeed, in light of the expectation for increased humidification in a warmer global to local climate, precipitation extremes are likely to increase in both frequency and intensity, including at rates that exceed the Clausius-Clapeyron relation. The linear increase in extreme precipitation shown here would be consistent with the wealth of studies that have previously documented the (robust) increases expected with atmospheric humidification as cumulative emissions rise

into the future. Part of this increase would come from enhanced atmospheric instability, as moistening is crucial for the deep convective systems (such as, again, (severe) thunderstorms and tropical cyclones)) that account for the majority of precipitation extremes to begin with, including the most extreme precipitation events. The combination of warmer temperatures and higher concentrations of atmospheric moisture would, thus, contribute to enhanced CAPE that favors more robust deep convection. The extent of enhanced moistening would also be instrumental in the more persistent wetter patterns that occur over a succession of days (i.e. enhanced Rx5day events), such as through large-scale patterns that are associated with atmospheric rivers.

It should also be noted that I analyzed precipitation extremes broadly in this dissertation, as such events are realistically occurring at much finer spatial scales as compared with the much coarser resolutions considered herein. To that end, future research could potentially endeavor to examine precipitation extremes using finer-scale analyses, as well as, more importantly, the environmental conditions that are often necessary for the development of such events. Collectively, however, these findings stress that currently established global warming targets associated with specified cumulative emissions thresholds are insufficient to avert particularly significant precipitation extreme events into the (near-) future. To that end, present-day and recent precipitation extremes are and have been a growing concern to human society, especially with respect to (flash-) flooding events and their short- to even long-term effects. The extent to which these events intensify and increase in frequency in response to even small increases in global cumulative emissions is shown here to be substantial. Thus, unless climate policy efforts can push global greenhouse gas emissions targets to considerably lower thresholds relative

to currently stipulated international agreements, it is likely that precipitation extremes, including the most intense precipitation extremes, will favorably increase in both frequency and intensity as cumulative emissions continue to rise. That said, meeting currently established and/or agreed-upon global emissions/warming targets would more likely mitigate the impacts associated with particularly disastrous precipitation events, but the findings here, nevertheless, indicate that precipitation extremes would become much more intense at such emissions targets, or even at lower amounts globally and at sub-global scales. As also shown, the RCBs consider only CO_2 emissions, and so the collective global to regional climate response to global greenhouse forcing would realistically be quicker with smaller CO_2 emissions, as is indicated in the RCP scenarios. As such, it is with more necessity to develop policy frameworks that strive to aggressively adapt to a world that may feature (much) more significant extremes if emissions are allowed to rise at rates that are compatible with the 1.5 C to 2 C global warming thresholds, or, as shown in this work, well under this desired range.

References

Aditya, F., Gusmayanti, E., & Sudrajat, J. (2021, November). Rainfall trend analysis using Mann-Kendall and Sen's slope estimator test in West Kalimantan. In *IOP conference series: earth and environmental science* (Vol. 893, No. 1, p. 012006). IOP Publishing.

Aleshina, M. A., Semenov, V. A., & Chernokulsky, A. V. (2021). A link between surface air temperature and extreme precipitation over Russia from station and reanalysis data. *Environmental Research Letters*, *16*(10), 105004.

Alexander, L. V., & Arblaster, J. M. (2017). Historical and projected trends in temperature and precipitation extremes in australia in observations and CMIP5. *Weather and Climate Extremes, 15*, 34-56.

Allan, R. P., Willett, K. M., John, V. O., & Trent, T. (2022). Global changes in water vapor 1979–2020. *Journal of Geophysical Research: Atmospheres*, *127*(12), e2022JD036728.

Allen, J. T. (2018). Climate change and severe thunderstorms. In *Oxford research encyclopedia of climate science*.

Assis, L. C., Calijuri, M. L., Silva, D. D., Rocha, E. O., Fernandes, A. L. T., & Silva, F. F.A model-based site selection approach associated with regional frequency analysis for modeling extreme rainfall depths in minas gerais state, southeast brazil. *Stochastic Environmental Research and Risk Assessment, 32*(2), 469-484. doi:10.1007/s00477-017-1481-1

Avila-Diaz, A., Benezoli, V., Justino, F., Torres, R., & Wilson, A. (2020). Assessing current and future trends of climate extremes across Brazil based on reanalyses and earth system model projections. *Climate Dynamics*, *55*(5-6), 1403-1426.

Ayugi, B., Jiang, Z., Iyakaremye, V., Ngoma, H., Babaousmail, H., Onyutha, C., ... & Ongoma, V. (2022). East African population exposure to precipitation extremes under 1.5° C and 2.0° C warming levels based on CMIP6 models. *Environmental Research Letters*, *17*(4), 044051.

Baker, H. S., Millar, R. J., Karoly, D. J., Beyerle, U., Guillod, B. P., Mitchell, D., ... & Allen, M. R. (2018). Higher CO2 concentrations increase extreme event risk in a 1.5 C world. *Nature Climate Change*, *8*(7), 604-608.

Ban, N., Leutwyler, D., Lüthi, D., & Schär, C. (2017). Scaling and intensification of extreme precipitation in high-resolution climate change simulations. Paper presented at the *EGU General Assembly Conference Abstracts,19,* 13419.

Bao, J., Sherwood, S. C., Alexander, L. V., & Evans, J. P. (2017). Future increases in extreme precipitation exceed observed scaling rates. *Nature Climate Change, 7*(2), 128-+. doi:10.1038/NCLIMATE3201

Barlow, M., Gutowski, W. J., Gyakum, J. R., Katz, R. W., Lim, Y., Schumacher, R. S., . . . Collow, A. (2019). North american extreme precipitation events and related large-scale meteorological patterns: A review of statistical methods, dynamics, modeling, and trends. *Climate Dynamics, 53*(11), 6835-6875.

Bas, M., & Paunov, C. Productivity in the Aftermath of a Natural Disaster: Evidence from the El Niño Floods in Ecuador. *Available at SSRN 4471721*.

Batista, M. L., Coelho, G., de Mello, C. R., & de Oliveira, M. S. (2019). Spatialization of the annual maximum daily rainfall in southeastern brazil. *Engenharia Agricola, 39*(1), 97-109. doi:10.1590/1809-4430-Eng.Agric.v39n1p97-109/2019

Bauer, N., Keller, D. P., Garbe, J., Karstens, K., Piontek, F., von Bloh, W., ... & Winkelmann, R. (2023). Exploring risks and benefits of overshooting a 1.5° C carbon budget over space and time. *Environmental Research Letters*, *18*(5), 054015.

Bayazit, M., & Önöz, B. J. H. S. J. (2007). To prewhiten or not to prewhiten in trend analysis?. *Hydrological Sciences Journal*, *52*(4), 611-624.

Bergquist, M., Nilsson, A., & Schultz, P. (2019). Experiencing a severe weather event increases concern about climate change. *Frontiers in psychology*, *10*, 220.

Bevacqua, E., Suarez-Gutierrez, L., Jézéquel, A., Lehner, F., Vrac, M., Yiou, P., & Zscheischler, J. (2023). Advancing research on compound weather and climate events via large ensemble model simulations. *Nature Communications*, *14*(1), 2145.

Bhatia, K., Vecchi, G., Murakami, H., Underwood, S., & Kossin, J. (2018). Projected response of tropical cyclone intensity and intensification in a global climate model. *Journal of Climate*, *31*(20), 8281-8303.

Birch, C. E., Jackson, L. S., Finney, D. L., Marsham, J. M., Stratton, R. A., Tucker, S., ... & Kendon, E. J. (2022). Future changes in African heatwaves and their drivers at the convective scale. *Journal of Climate*, *35*(18), 5981-6006.

Bjarke, N., Barsugli, J., Hoerling, M., Quan, X. W., & Livneh, B. (2023). When record breaking heat waves should not surprise: skewness, heavy tails and implications for risk assessment. *Authorea Preprints*.

Blanchet, J., Ceresetti, D., Molinié, G., & Creutin, J. -.A regional GEV scale-invariant framework for Intensityâ€“Durationâ€“Frequency anal. *Journal of Hydrology, 540*, 82-95. doi:10.1016/j.jhydrol.2016.06.007

Bonate, P. L. (2021). The application of extreme value theory to pharmacometrics. *Journal of Pharmacokinetics and Pharmacodynamics*, *48*(1), 83-97.

Bourdeau-Goulet, S. C., & Hassanzadeh, E. (2021). Comparisons between CMIP5 and CMIP6 models: Simulations of climate indices influencing food security, infrastructure resilience, and human health in Canada. *Earth's Future*, *9*(5), e2021EF001995.

Brooks, H. E. (2013). Severe thunderstorms and climate change. *Atmospheric research*, *123*, 129-138.

Brooks, H. E. (2016, June). Estimating the distribution of severe thunderstorms and their environments around the world. In *International Conference on Storms, The National Oceanic and Atmospheric Administration. http://www. nssl. noaa. gov/users/brooks/public_html/papers/brisbane. pdf. Accessed* (Vol. 24).

Brown, S. J.The drivers of variability in UK extreme rainfall. *International Journal of Climatology, 38*, e119. doi:10.1002/joc.5356

Bruhwiler, L., Basu, S., Butler, J. H., Chatterjee, A., Dlugokencky, E., Kenney, M. A., ... & Stanitski, D. (2021). Observations of greenhouse gases as climate indicators. *Climatic change*, *165*(1-2), 12.

Bush, E. and Lemmen D.S., editors (2019): Canada's Changing Climate Report; Government of Canada, Ottawa, ON. 444 p.

Byrne, M. P., & Schneider, T. (2016). Narrowing of the ITCZ in a warming climate: Physical mechanisms. *Geophysical Research Letters*, *43*(21), 11-350.

Butsch, C., Beckers, L. M., Nilson, E., Frassl, M., Brennholt, N., Kwiatkowski, R., & Söder, M. (2023). Health impacts of extreme weather events–Cascading risks in a changing climate.

Cai, W., Ng, B., Geng, T., Jia, F., Wu, L., Wang, G., ... & McPhaden, M. J. (2023). Anthropogenic impacts on twentieth-century ENSO variability changes. *Nature Reviews Earth & Environment*, 1-12.

Canadell, J.G., P.M.S. Monteiro, M.H. Costa, L. Cotrim da Cunha, P.M. Cox, A.V. Eliseev, S. Henson, M. Ishii, S. Jaccard, C. Koven, A. Lohila, P.K. Patra, S. Piao, J. Rogelj, S. Syampungani, S. Zaehle, and K. Zickfeld, 2021: Global Carbon and other Biogeochemical Cycles and Feedbacks. In Climate Change 2021: The Physical Science Basis. Contribution of Working Group I to the Sixth Assessment Report of the Intergovernmental Panel on Climate Change [Masson-Delmotte, V., P. Zhai, A. Pirani, S.L. Connors, C. Péan, S. Berger, N. Caud, Y. Chen, L. Goldfarb, M.I. Gomis, M. Huang, K. Leitzell, E. Lonnoy, J.B.R. Matthews, T.K. Maycock, T. Waterfield, O. Yelekçi, R. Yu, and B. Zhou (eds.)]. Cambridge University Press. In Press.

Carney, M. C. (2016). Bias correction to gev shape parameters used to predict precipitation extremes. *Journal of Hydrologic Engineering*, *21*(10), 04016035.

Chang, M., Liu, B., Wang, B., Martinez-Villalobos, C., Ren, G., & Zhou, T. (2022). Understanding future increases in precipitation extremes in global land monsoon regions. *Journal of Climate*, *35*(6), 1839-1851.

Chavaillaz, Y., Roy, P., Partanen, A. I., Da Silva, L., Bresson, É., Mengis, N., ... & Matthews, H. D. (2019). Exposure to excessive heat and impacts on labour productivity linked to cumulative CO2 emissions. *Scientific reports*, *9*(1), 13711.

Clarke, B., Otto, F., Stuart-Smith, R., & Harrington, L. (2022). Extreme weather impacts of climate change: an attribution perspective. *Environmental Research: Climate*, *1*(1), 012001.

Clarke, H., Cirulis, B., Borchers-Arriagada, N., Bradstock, R., Price, O., & Penman, T. (2023). Health costs of wildfire smoke to rise under climate change. *npj Climate and Atmospheric Science*, *6*(1), 102.

Coles, S. (2001). *An introduction to statistical modeling of extreme values*. London; New York: Springer.

Collow, A., Bosilovich, M., & Koster, R. (2017). Synoptic scale influences on increasing summertime extreme precipitation events in the northeastern united states.

Coumou, D., & Rahmstorf, S. (2012). A decade of weather extremes. *Nature climate change*, *2*(7), 491-496.

Costa, A. A., Guimarães, S. O., Sales, D. C., das Chagas Vasconcelos Junior, F., Marinho, M. W. S., Pereira, J. M. R., ... & da Silva, E. M. (2023). Precipitation extremes over the tropical Americas under RCP4. 5 and RCP8. 5 climate change scenarios: Results from dynamical downscaling simulations. *International Journal of Climatology*, *43*(2), 787-803.

Curriero, F., Patz, J., Rose, J., & Lele, S. (2001). The association between extreme precipitation and waterborne disease outbreaks in the united states, 1948-1994. *American Journal of Public Health, 91*(8), 1194-1199. doi:10.2105/AJPH.91.8.1194

de Mora, L., Swaminathan, R., Allan, R. P., Blackford, J., Kelley, D. I., Harris, P., ... & Yool, A. (2023). Choice of Forecast Scenario Impacts the Carbon Allocation at the Same Global Warming Levels. *EGUsphere*, 1-22.

Damon Matthews, H., Tokarska, K., Rogelj, J., Forster, P., Haustein, K., Smith, C., ... & Knutti, R. (2020, May). A new framework for understanding and quantifying uncertainties in the remaining carbon budget. In *EGU General Assembly Conference Abstracts* (p. 11278).

data.gouv.fr (2019). Arrondissements. Accessed on November 8th, 2019 at: https://catalog.data.gov/dataset/tiger-line-shapefile-2016-state-florida-current-county-subdivision-state-based

DATA. GOV (2019). TIGER/Line Shapefile, 2016, state, Florida, Current County Subdivision State-based. Accessed on November 8th, 2019 at: https://catalog.data.gov/dataset/tiger-line-shapefile-2016-state-florida-current-county-subdivision-state-based

Donat, M. G., Lowry, A. L., Alexander, L. V., O'Gorman, P. A., & Maher, N. (2017). More extreme precipitation in the world's dry and wet regions (vol 6, pg 508, 2016). *Nature Climate Change, 7*(2), 154-158. doi:10.1038/NCLIMATE3160

Davolio, S., Vercellino, M., Miglietta, M. M., Pitura, L. D., Laviola, S., & Levizzani, V. (2023). The influence of an atmospheric river on a heavy precipitation event over the western Alps. *Weather and Climate Extremes*, *39*, 100542.

Do, H. X., Mei, Y., & Gronewold, A. D. (2020). To what extent are changes in flood magnitude related to changes in precipitation extremes?. *Geophysical Research Letters*, *47*(18), e2020GL088684.

Donat, M. G., Alexander, L. V., Yang, H., Durre, I., Vose, R., Dunn, R. J., ... & Kitching, S. (2013). Updated analyses of temperature and precipitation extreme indices since the beginning of the twentieth century: The HadEX2 dataset. *Journal of Geophysical Research: Atmospheres*, *118*(5), 2098-2118.

Dupont, A., & Pearman, G. (2006). Heating up the planet: climate change and security.

Edwards, R., J. T. Allen, and G. W. Carbin, 2018: Reliability and climatological impacts of convective wind estimations. *J. Appl. Meteor. Climatol.*, **57**, 1825-1845, https://doi.org/10.1175/JAMC-D-17-0306.1.

EPA, 2017. Climate Change Indicators: Heavy Precipitation. Accessed on May 6th, 2019, from: https://www.epa.gov/climate-indicators/climate-change-indicators-heavy-precipitation

Estrada, F., Kim, D., & Perron, P. (2021). Spatial variations in the warming trend and the transition to more severe weather in midlatitudes. *Scientific reports*, *11*(1), 1-9.

Falga, R., & Wang, C. (2022). The rise of Indian summer monsoon precipitation extremes and its correlation with long-term changes of climate and anthropogenic factors. *Scientific reports*, *12*(1), 11985.

Fallah, B., Russo, E., Menz, C., Hoffmann, P., Didovets, I., & Hattermann, F. F. (2023). Anthropogenic influence on extreme temperature and precipitation in Central Asia. *Scientific Reports*, *13*(1), 6854.

Feng, S.; Nadarajah, S.; Hu, Q. Modeling Annual Extreme Precipitation in China Using the Generalized Extreme Value Distribution. *J. Meteorol. Soc. Jpn. Ser. II* **2007**, *85*, 599–613

Ferreira, M. (2011). On the penultimate tail behavior of Weibull-type models. *arXiv preprint arXiv:1109.3139*.

Fix, M. J., Cooley, D., Sain, S. R., & Tebaldi, C.A comparison of U.S. precipitation extremes under RCP8.5 and RCP4.5 with an application of pattern scaling. *Climatic Change, 146*(3/4), 335-347. doi:10.1007/s10584-016-1656-7

Franks, K., & Moore, T. (2021). Climate Change Vulnerability, Water, and Extreme Weather: Perspectives from Graduate Environment Students. *Journal of Sustainability Education*, *25*.

Franzke, C. L., & Torelló i Sentelles, H. (2020). Risk of extreme high fatalities due to weather and climate hazards and its connection to large-scale climate variability. *Climatic Change*, *162*(2), 507-525.

Friedlingstein, P., Andrew, R. M., Rogelj, J., Peters, G., Canadell, J. G., Knutti, R., . . . Van Vuuren, D. P. (2014). Persistent growth of CO2 emissions and implications for reaching climate targets. *Nature Geoscience, 7*(10), 709.

Frölicher, T. L., & Paynter, D. J. (2015). Extending the relationship between global warming and cumulative carbon emissions to multi-millennial timescales. *Environmental Research Letters*, *10*(7), 075002.

Fullhart, A., Goodrich, D. C., Meles, M. B., Oliveira, P. T. S., das Neves Almeida, C., de Araújo, J. C., & Burns, S. (2023). Atlas of precipitation extremes for South America and Africa based on depth-duration-frequency relationships in a stochastic weather generator dataset. *International Soil and Water Conservation Research*.

Gentilucci, M., Rossi, A., Pelagagge, N., Aringoli, D., Barbieri, M., & Pambianchi, G. (2023). GEV Analysis of Extreme Rainfall: Comparing Different Time Intervals to Analyse Model Response in Terms of Return Levels in the Study Area of Central Italy. *Sustainability*, *15*(15), 11656.

Gillett, N. P., Arora, V. K., Matthews, D., & Allen, M. R. (2013). Constraining the ratio of global warming to cumulative CO2 emissions using CMIP5 simulations. *Journal of Climate, 26*(18), 6844-6858.

Gimeno-Sotelo, L., & Gimeno, L. (2023). Where does the link between atmospheric moisture transport and extreme precipitation matter?. *Weather and Climate Extremes*, *39*, 100536.

Girard, S. Estimation methods for weibull tail-distributions.

Goldstein, J., Mirza, M., Etkin, D., & Milton, J. (2003). J2. 6 hydrologic assessment: Application of extreme value theory for climate extremes scenarios construction. In *14th Symposium on Global Change and Climate Variations, American Meteorological Society 83rd Annual Meeting*.

Gori, A., Lin, N., Xi, D., & Emanuel, K. (2022). Tropical cyclone climatology change greatly exacerbates US extreme rainfall–surge hazard. *Nature Climate Change*, *12*(2), 171-178.

Grothe, P. R., Cobb, K. M., Liguori, G., Di Lorenzo, E., Capotondi, A., Lu, Y., ... & Deocampo, D. M. (2019). Enhanced El Niño-Southern Oscillation variability in recent decades. *Geophysical Research Letters*.

Hall, T. M., & Kossin, J. P. (2019). Hurricane stalling along the North American coast and implications for rainfall. *Npj Climate and Atmospheric Science*, *2*(1), 17.

Hartmann, D.L., Klein Tank, A.M.G., Rusticucci, M., Alexander, L.V., Brönnimann, S., Charabi, Y., Dentener, F.J., Dlugokencky, E.J., Easterling, D.R., Kaplan, A., Soden, B.J., Thorne, P.W., Wild, M. and Zhai, P.M. (2013) Observations: atmosphere and surface. In: T.F. Stocker, D. Qin, G.-K. Plattner, M. Tignor, S.K. Allen, J. Boschung, A. Nauels, Y. Xia, V. Bex and P.M. Midgley (Eds.) *Climate Change 2013: The Physical Science Basis. Contribution of Working Group I to the Fifth Assessment Report of the Intergovernmental Panel on Climate Change*. Cambridge and New York, NY: Cambridge University Press.

Held, I. M., & Soden, B. J. (2000). Water vapor feedback and global warming. *Annual review of energy and the environment*, *25*(1), 441-475.

Held, I. M., & Soden, B. J. (2006). Robust responses of the hydrological cycle to global warming. *Journal of Climate, 19*(21), 5686-5699.

Henny, L., Thorncroft, C. D., & Bosart, L. F. (2023). Changes in seasonal large-scale extreme precipitation in the mid-Atlantic and Northeast United States, 1979–2019. *Journal of Climate*, *36*(4), 1017-1042.

Herring, S. C., Hoerling, M. P., Peterson, T. C., & Stott, P. A. (2014). Explaining extreme events of 2013 from a climate perspective. *Bulletin of the American Meteorological Society, 95*(9), S1-S104.

Herrington, T., & Zickfeld, K. (2014). Path independence of climate and carbon cycle response over a broad range of cumulative carbon emissions. *Earth System Dynamics, 5*(2), 409.

Hossain, I., Khastagir, A., Aktar, M. N., Imteaz, M. A., Huda, D., & Rasel, H. M. (2021). Comparison of estimation techniques for generalised extreme value (GEV) distribution parameters: a case study with Tasmanian rainfall. *International Journal of Environmental Science and Technology*, 1-14.

Howard, B. S., Hamilton, N. E., Diesendorf, M., & Wiedmann, T. (2018). Modeling the carbon budget of the Australian electricity sector's transition to renewable energy. *Renewable Energy*, *125*, 712-728.

Hu, H., Feng, Z., & Leung, L. Y. R. (2021). Linking flood frequency with mesoscale convective systems in the US. *Geophysical Research Letters*, *48*(9), e2021GL092546.

Innocenti, S., Mailhot, A., Leduc, M., Cannon, A. J., & Frigon, A. (2019). Projected changes in the probability distributions, seasonality, and spatiotemporal scaling of daily and subdaily extreme precipitation simulated by a 50-member ensemble over northeastern north america. *Journal of Geophysical Research-Atmospheres,* doi:10.1029/2019JD031210

IPCC, 2021: *Climate Change 2021: The Physical Science Basis. Contribution of Working Group I to the Sixth Assessment Report of the Intergovernmental Panel on Climate Change*[Masson-Delmotte, V., P. Zhai, A. Pirani, S.L. Connors, C. Péan, S. Berger, N. Caud, Y. Chen, L. Goldfarb, M.I. Gomis, M. Huang, K. Leitzell, E. Lonnoy, J.B.R. Matthews, T.K. Maycock, T. Waterfield, O. Yelekçi, R. Yu, and B. Zhou (eds.)]. Cambridge University Press, Cambridge, United Kingdom and New York, NY, USA, In press, doi:10.1017/9781009157896.

Igun, E., Xu, X., Hu, Y., & Jia, G. (2022). Strong heatwaves with widespread urban-related hotspots over Africa in 2019. *Atmospheric and Oceanic Science Letters*, *15*(5), 100195. *Letters*, *43*(13), 7250-7258.

Jacob, M., Neves, C., Vukadinović Greetham, D. (2020). Extreme Value Theory. In: Forecasting and Assessing Risk of Individual Electricity Peaks. Mathematics of Planet Earth(). Springer, Cham. https://doi.org/10.1007/978-3-030-28669-9_3

Janssen, E., Sriver, R., Wuebbles, D., & Kunkel, K. (2016). Seasonal and regional variations in extreme precipitation event frequency using CMIP5. *Geophysical Research Letters, 43*(10), 5385-5393.

Johnson, K.; Smithers, J. Review: Methods for the Estimation of Extreme Rainfall Events. *Water SA* **2019**, *45*, 501–512.

Jones, C. D., & Friedlingstein, P. (2020). Quantifying process-level uncertainty contributions to TCRE and carbon budgets for meeting Paris Agreement climate targets. *Environmental Research Letters*, *15*(7), 074019.

Katzenberger, A., Levermann, A., Schewe, J., & Pongratz, J. (2022). Intensification of very wet monsoon seasons in India under global warming. *Geophysical Research Letters*, *49*(15), e2022GL098856.

Kennedy, D., Parker, T., Woollings, T., Harvey, B., & Shaffrey, L. (2016). The response of high-impact blocking weather systems to climate change. *Geophysical Research*

Khandekar, M. L. (2013). Are extreme weather events on the rise?. *Energy & environment*, *24*(3-4), 537-549.

Kharin, V. V., Zwiers, F., Zhang, X., & Wehner, M. (2013). Changes in temperature and precipitation extremes in the CMIP5 ensemble. *Climatic Change, 119*(2), 345-357.

Kharin, V. V., Flato, G. M., Zhang, X., Gillett, N. P., Zwiers, F., & Anderson, K. J. (2018). Risks from climate extremes change differently from 1.5 C to 2.0 C depending on rarity. *Earth's Future*, *6*(5), 704-715.

Kirchmeier-Young, M. C., & Zhang, X. (2020). Human influence has intensified extreme precipitation in North America. *Proceedings of the National Academy of Sciences*.

Kitoh, A., & Endo, H. (2019). Future changes in precipitation extremes associated with tropical cyclones projected by large-ensemble simulations. *Journal of the Meteorological Society of Japan. Ser. II*, *97*(1), 141-152.

Kirchmeier-Young, M. C., & Zhang, X. (2020). Human influence has intensified extreme precipitation in North America. *Proceedings of the National Academy of Sciences*, *117*(24), 13308-13313.

Knapp, A. K., Beier, C., Briske, D. D., Classen, A. T., Luo, Y., Reichstein, M., . . . Weng, E. (2008). Consequences of more extreme precipitation regimes for terrestrial ecosystems. *Bioscience, 58*(9), 811-821. doi:10.1641/B580908

Knutson, T. R., McBride, J. L., Chan, J., Emanuel, K., Holland, G., Landsea, C., ... & Sugi, M. (2010). Tropical cyclones and climate change. *Nature geoscience*, *3*(3), 157-163.

Koutsoyiannis, D.Statistics of extremes and estimation of extreme rainfall: I. theoretical investigation. *Hydrological Sciences Journal-Journal Des Sciences Hydrologiques, 49*(4), 575-590.

Krasting, J., Dunne, J., Shevliakova, E., & Stouffer, R. (2014). Trajectory sensitivity of the transient climate response to cumulative carbon emissions. *Geophysical Research Letters, 41*(7), 2520-2527.

Kronnäs, V., Lucander, K., Zanchi, G., Stadlinger, N., Belyazid, S., & Akselsson, C. (2023). Effect of droughts and climate change on future soil weathering rates in Sweden. *Biogeosciences*, *20*(10), 1879-1899.

Kunkel, K. (2003). North american trends in extreme precipitation. *Natural Hazards, 29*(2), 291-305. doi:10.1023/A:1023694115864

Lahn, B. (2020). A history of the global carbon budget. *Wiley Interdisciplinary Reviews: Climate Change*, *11*(3), e636.

Le Quéré, Corinne, Robbie M. Andrew, Pierre Friedlingstein, Stephen Sitch, Julia Pongratz, Andrew C. Manning, Jan Ivar Korsbakken et al. "Global carbon budget 2017." *Earth System Science Data* 10, no. 1 (2018): 405-448.

Leduc, M., Matthews, H. D., & de Elía, R. (2016). Regional estimates of the transient climate response to cumulative CO2 emissions. *Nature Climate Change*, *6*(5), 474-478.

Lee, D., Min, S. K., Fischer, E., Shiogama, H., Bethke, I., Lierhammer, L., & Scinocca, J. F. (2018). Impacts of half a degree additional warming on the Asian summer monsoon rainfall characteristics. *Environmental Research Letters*, *13*(4), 044033.

Lhamo, T., Chen, G., Dorji, S., Tamang, T. B., Wang, X., & Zhang, P. (2023). Trends in Extreme Precipitation Indices over Bhutan. *Atmosphere*, *14*(7), 1154.

Li, L., & Chakraborty, P. (2020). Slower decay of landfalling hurricanes in a warming world. *Nature*, *587*(7833), 230-234.

Li, C., Zwiers, F., Zhang, X., Chen, G., Lu, J., Li, G., . . . Liu, M. (2019). Larger increases in more extreme local precipitation events as climate warms. *Geophysical Research Letters, 46*(12), 6885-6891. doi:10.1029/2019GL082908

Lieber, R., King, A., Brown, J., Ashcroft, L., Freund, M., & McMichael, C. (2022). ENSO teleconnections more uncertain in regions of lower socioeconomic development. *Geophysical Research Letters*, *49*(21), e2022GL100553.

Liu, S. C., Fu, C., Shiu, C. J., Chen, J. P., & Wu, F. (2009). Temperature dependence of global precipitation extremes. *Geophysical Research Letters*, *36*(17).

Lui, Y. S., Tam, C. Y., & Lau, N. C. (2019). Future changes in Asian summer monsoon precipitation extremes as inferred from 20-km AGCM simulations. *Climate Dynamics*, *52*(3-4), 1443-1459.

Luo, M., & Lau, N. C. (2020). Summer heat extremes in northern continents linked to developing ENSO events. *Environmental Research Letters*, *15*(7), 074042.

Lyons, A. L., Gaines, W. L., Lewis, J. C., Maletzke, B. T., Werntz, D., Thornton, D. H., ... & Fitkin, S. (2023). Climate change, wildfire, and past forest management challenge conservation of Canada lynx in Washington, USA. *The Journal of Wildlife Management*, *87*(5), e22410.

MacDougall, A. H., & Friedlingstein, P. (2015). The origin and limits of the near proportionality between climate warming and cumulative CO2 emissions. *Journal of Climate*, *28*(10), 4217-4230.

MacDougall, A. H. (2016). The transient response to cumulative CO 2 emissions: a review. *Current Climate Change Reports*, *2*, 39-47.

Maddox, R. A., Hoxit, L. R., Chappell, C. F., & Caracena, F. (1978). Comparison of meteorological aspects of the Big Thompson and Rapid City flash floods. *Monthly Weather Review*, *106*(3), 375-389.

Mahajan, S., Passarella, L. S., Tang, Q., Keen, N. D., Caldwell, P. M., van Roekel, L. P., & Golaz, J. C. (2023). ENSO diversity and the simulation of its teleconnections to winter precipitation extremes over the US in high resolution Earth System Models. *Geophysical Research Letters*, *50*(11), e2022GL102657.

Mallakpour, I., Sadegh, M., & AghaKouchak, A. (2018). A new normal for streamflow in California in a warming climate: Wetter wet seasons and drier dry seasons. *Journal of Hydrology*, *567*, 203-211.

Matthews, H. D., Gillett, N. P., Stott, P. A., & Zickfeld, K. (2009). The proportionality of global warming to cumulative carbon emissions. *Nature, 459*(7248), 829.

Matthews, H. D., Tokarska, K. B., Nicholls, Z. R., Rogelj, J., Canadell, J. G., Friedlingstein, P., ... & Zickfeld, K. (2020). Opportunities and challenges in using remaining carbon budgets to guide climate policy. *Nature Geoscience*, *13*(12), 769-779.

Matthews, H. D., Tokarska, K. B., Rogelj, J., Smith, C. J., MacDougall, A. H., Haustein, K., ... & Knutti, R. (2021). An integrated approach to quantifying uncertainties in the remaining carbon budget. *Communications Earth & Environment*, *2*(1), 1-11.

Matthews, H. D., Zickfeld, K., Koch, A., & Luers, A. (2023). Accounting for the climate benefit of temporary carbon storage in nature. *Nature Communications*, *14*(1), 5485.

Maxwell, J. T., Bregy, J. C., Robeson, S. M., Knapp, P. A., Soulé, P. T., & Trouet, V. (2021). Recent increases in tropical cyclone precipitation extremes over the US east coast. *Proceedings of the National Academy of Sciences*, *118*(41), e2105636118.

McGregor, G. R., Ferro, C. A., & Stephenson, D. B. (2005). Projected changes in extreme weather and climate events in Europe. *Extreme weather events and public health responses*, 13-23.

Mengis, N., & Matthews, H. D. (2020). Non-CO2 forcing changes will likely decrease the remaining carbon budget for 1.5 C. *NPJ Climate and Atmospheric Science*, *3*(1), 19.

Millar, R., Fuglestvedt, J. S., Grubb, M., Rogelj, J., Skeie, R. B., Friedlingstein, P., ... & Allen, M. R. (2016, December). Future emissions pathways consistent with limiting warming to 1.5° C. In *AGU Fall Meeting Abstracts* (Vol. 2016, pp. GC24D-04).

Mishra, V., Wallace, J. M., & Lettenmaier, D. P. (2012). Relationship between hourly extreme precipitation and local air temperature in the United States. *Geophysical Research Letters*, *39*(16).

Moore, T. R., Matthews, H. D., Simmons, C., & Leduc, M. (2015). Quantifying changes in extreme weather events in response to warmer global temperature. *Atmosphere-ocean*, *53*(4), 412-425.

Moore, T. R., Damon Matthews, H., & Chavaillaz, Y. (2023). Linking Historical and Projected Trends in Extreme Precipitation with Cumulative Carbon Dioxide Emissions. *Atmosphere-Ocean*, 1-18.

Mondal, A., & Mujumdar, P. P. (2015). On the detection of human influence in extreme precipitation over India. *Journal of Hydrology*, *529*, 1161-1172.

Mondal, A., & Mujumdar, P. P. (2017). Hydrologic extremes under climate change: non-stationarity and uncertainty. *Sustainable water resources planning and management under climate change*, 39-60.

Monteleone, B., Borzí, I., Bonaccorso, B., & Martina, M. (2023). Quantifying crop vulnerability to weather-related extreme events and climate change through vulnerability curves. *Natural Hazards*, *116*(3), 2761-2796.

Mukherjee, S., Aadhar, S., Stone, D., & Mishra, V. (2018). Increase in extreme precipitation events under anthropogenic warming in India. *Weather and climate extremes*, *20*, 45-53.

Myhre, G., Alterskjær, K., Stjern, C. W., Hodnebrog, Ø., Marelle, L., Samset, B. H., ... & Stohl, A. (2019). Frequency of extreme precipitation increases extensively with event rareness under global warming. *Scientific reports*, *9*(1), 16063.

Natural Earth (2019). Urban Areas. Accessed on November 8th, 2019 at: https://www.naturalearthdata.com/downloads/10m-cultural-vectors/10m-urban-area/

Neelin, J. D., Martinez-Villalobos, C., Stechmann, S. N., Ahmed, F., Chen, G., Norris, J. M., ... & Lenderink, G. (2022). Precipitation Extremes and Water Vapor: Relationships in Current Climate and Implications for Climate Change. *Current Climate Change Reports*, *8*(1), 17-33.

Newell, R. E., Newell, N. E., Zhu, Y., & Scott, C. (1992). Tropospheric rivers?–A pilot study. *Geophysical research letters*, *19*(24), 2401-2404.

NYC Planning (2019). Political and Administrative Districts – Download & Metadata. Accessed on November 8th, 2019 at: https://www1.nyc.gov/site/planning/data-maps/open-data/districts-download-metadata.page

Oduoye, M. O., Karim, K. A., Kareem, M. O., Shehu, A., Oyeleke, U. A., Zafar, H., ... & Adegoke, A. A. (2024). Flooding in Libya amid an economic crisis: What went wrong?. *IJS Global Health*, *7*(1), e0401.

Papalexiou, S.M. and Koutsoyiannis, D., 2013. Battle of extreme value distributions: A global survey on extreme daily rainfall. *Water Resources Research*, 49, 187–201. doi:10.1029/2012WR012557

Partanen, A. I., Leduc, M., & Matthews, H. D. (2017). Seasonal climate change patterns due to cumulative CO2 emissions. *Environmental Research Letters*, *12*(7), 075002.

Partanen, A. I., Liu, J., Smith, C. J., & Korhonen, H. (2020, May). Revisiting carbon budgets of IPCC 1.5-degree report by taking into account correlation with non-CO2 warming and TCRE. In *EGU General Assembly Conference Abstracts* (p. 19723).

Pall, P., Allen, M. R., & Stone, D. A. (2007). Testing the Clausius–Clapeyron constraint on changes in extreme precipitation under CO 2 warming. *Climate Dynamics*, *28*(4), 351-363.

Pathirana, G., Oh, J. H., Cai, W., An, S. I., Min, S. K., Jo, S. Y., ... & Kug, J. S. (2023). Increase in convective extreme El Niño events in a CO2 removal scenario. *Science Advances*, *9*(25), eadh2412.

Pendergrass, A. G. (2018). What precipitation is extreme?. *Science*, *360*(6393), 1072-1073.

Pendergrass, A. G., Coleman, D. B., Deser, C., Lehner, F., Rosenbloom, N., & Simpson, I. R. (2019). Nonlinear response of extreme precipitation to warming in CESM1. *Geophysical research letters*, *46*(17-18), 10551-10560.

Pendergrass, A. G., & Hartmann, D. L. (2014). Two modes of change of the distribution of rain. *Journal of Climate*, *27*(22), 8357-8371

Pendergrass, A. G., Reed, K. A., & Medeiros, B. (2016). The link between extreme precipitation and convective organization in a warming climate: Global radiative-convective equilibrium simulations. *Geophysical Research Letters*, *43*(21), 11-445.

Pfahl, S., O'Gorman, P., & Fischer, E. (2017). Understanding the regional pattern of projected future changes in extreme precipitation. *Nature Climate Change, 7*(6), 423-427.

Potter, E. R., Fyffe, C. L., Orr, A., Quincey, D. J., Ross, A. N., Rangecroft, S., ... & Pellicciotti, F. (2023). A future of extreme precipitation and droughts in the Peruvian Andes. *npj Climate and Atmospheric Science*, *6*(1), 96.

Priore, Y. D., Habert, G., & Jusselme, T. (2023). Exploring the gap between carbon-budget-compatible buildings and existing solutions–A Swiss case study. *Energy and Buildings*, *278*, 112598.

Rackley, S. A. (2017). *Carbon capture and storage*. Butterworth-Heinemann.

Raupach, T. H., Martius, O., Allen, J. T., Kunz, M., Lasher-Trapp, S., Mohr, S., ... & Zhang, Q. (2021). The effects of climate change on hailstorms. *Nature reviews earth & environment*, *2*(3), 213-226.

Ray, K., Giri, R. K., Ray, S. S., Dimri, A. P., & Rajeevan, M. (2021). An assessment of long-term changes in mortalities due to extreme weather events in India: A study of 50 years' data, 1970–2019. *Weather and Climate Extremes*, *32*, 100315.

Raynal-Villasenor, J. A. (2012). Maximum likelihood parameter estimators for the two populations GEV distribution. *Ijrras*, *11*(3), 350-357.

Reddy, N. M., & Saravanan, S. (2023). Extreme precipitation indices over India using CMIP6: a special emphasis on the SSP585 scenario. *Environmental Science and Pollution Research*, *30*(16), 47119-47143.

Revolutionary GIS (2019). Hong Kong Shapefile Data. Accessed in November 8th, 2019 at: https://revolutionarygis.wordpress.com/2015/09/08/hong-kong-shapefile-data/

Rex, D. F. (1950). Blocking action in the middle troposphere and its effect upon regional climate. *Tellus*, *2*(4), 275-301.

Riboldi, J. (2023). *On the connection between Rossby waves and spatially compounding weather extremes* (No. EGU23-8587). Copernicus Meetings.

Rodrigues, A., Sardinha, R. A., Pita, G., Rodrigues, A., Sardinha, R. A., & Pita, G. (2021). Fundamentals of global carbon budgets and climate change. *Fundamental Principles of Environmental Physics*, 267-308.

Rogelj, J., Forster, P. M., Kriegler, E., Smith, C. J., & Séférian, R. (2019). Estimating and tracking the remaining carbon budget for stringent climate targets. *Nature*, *571*(7765), 335-342.

Rogelj, J., D. Shindell, K. Jiang, S. Fifita, P. Forster, V. Ginzburg, C. Handa, H. Kheshgi, S. Kobayashi, E. Kriegler, L. Mundaca, R. Séférian, and M.V. Vilariño, 2018: Mitigation Pathways Compatible with 1.5°C in the Context of Sustainable Development. In: *Global Warming of 1.5°C. An IPCC Special Report on the impacts of global warming of 1.5°C above pre-industrial levels and related global greenhouse gas emission pathways, in the context of strengthening the global response to the threat of climate change, sustainable development, and efforts to eradicate poverty* [Masson-Delmotte, V., P. Zhai, H.-O. Pörtner, D. Roberts, J. Skea, P.R. Shukla, A. Pirani, W. Moufouma-Okia, C. Péan, R. Pidcock, S. Connors, J.B.R. Matthews, Y. Chen, X. Zhou, M.I. Gomis, E. Lonnoy, T. Maycock, M. Tignor, and T. Waterfield (eds.)]. In Press.

Rypkema, D., & Tuljapurkar, S. (2021). Modeling extreme climatic events using the generalized extreme value (GEV) distribution. In *Handbook of Statistics* (Vol. 44, pp. 39-71). Elsevier.

Santos, E. B., Lucio, P. S., & Santos e Silva, C. M.Seasonal analysis of return periods for maximum daily precipitation in the brazilian amazon. *Journal of Hydrometeorology, 16*(3), 973-984. doi:10.1175/JHM-D-14-0201.1

Schmidt, D. F., & Grise, K. M. (2017). The response of local precipitation and sea level pressure to Hadley cell expansion. *Geophysical Research Letters*, *44*(20), 10-573.

Seneviratne, S.I., N. Nicholls, D. Easterling, C.M. Goodess, S. Kanae, J. Kossin, Y. Luo, J. Marengo, K. McInnes, M. Rahimi, M. Reichstein, A. Sorteberg, C. Vera, and X. Zhang, 2012: Changes in climate extremes and their impacts on the natural physical environment. In: Managing the Risks of Extreme Events and Disasters to Advance Climate Change Adaptation [Field, C.B., V. Barros, T.F. Stocker, D. Qin, D.J. Dokken, K.L. Ebi, M.D. Mastrandrea, K.J. Mach, G.-K. Plattner, S.K. Allen, M. Tignor, and P.M. Midgley (eds.)]. A Special Report of Working Groups I and II of the Intergovernmental Panel on Climate Change (IPCC). Cambridge University Press, Cambridge, UK, and New York, NY, USA, pp. 109-230.

Simmons, C., & Matthews, H. (2016). Assessing the implications of human land-use change for the transient climate response to cumulative carbon emissions. *Environmental Research Letters, 11*(3), 035001.

Seneviratne, S.I., N. Nicholls, D. Easterling, C.M. Goodess, S. Kanae, J. Kossin, Y. Luo, J. Marengo, K. McInnes, M. Rahimi, M. Reichstein, A. Sorteberg, C. Vera, and X. Zhang, 2012: Changes in climate extremes and their impacts on the natural physical environment. In: Managing the Risks of Extreme Events and Disasters to Advance Climate Change Adaptation [Field, C.B., V. Barros, T.F. Stocker, D. Qin, D.J. Dokken, K.L. Ebi, M.D. Mastrandrea, K.J. Mach, G.-K. Plattner, S.K. Allen, M. Tignor, and P.M. Midgley (eds.)]. A Special Report of Working Groups I and II of the Intergovernmental Panel on Climate Change (IPCC). Cambridge University Press, Cambridge, UK, and New York, NY, USA, pp. 109-230.

Seneviratne, S. I., Donat, M. G., Pitman, A. J., Knutti, R., & Wilby, R. L. (2016). Allowable CO2 emissions based on regional and impact-related climate targets. *Nature, 529*(7587), 477-483. doi:10.1038/nature16542

Seneviratne, S.I., X. Zhang, M. Adnan, W. Badi, C. Dereczynski, A. Di Luca, S. Ghosh, I. Iskandar, J. Kossin, S. Lewis, F. Otto, I. Pinto, M. Satoh, S.M. Vicente-Serrano, M. Wehner, and B. Zhou, 2021: Weather and Climate Extreme Events in a Changing Climate. In Climate Change 2021: The Physical Science Basis. Contribution of Working Group I to the Sixth Assessment Report of the Intergovernmental Panel on Climate Change [Masson-Delmotte, V., P. Zhai, A. Pirani, S.L. Connors, C. Péan, S. Berger, N. Caud, Y. Chen, L. Goldfarb, M.I. Gomis, M. Huang, K. Leitzell, E. Lonnoy, J.B.R. Matthews, T.K. Maycock, T. Waterfield, O. Yelekçi, R. Yu, and B. Zhou (eds.)]. Cambridge University Press, Cambridge, United Kingdom and New York, NY, USA, pp. 1513–1766, doi:10.1017/9781009157896.013.

Singh, S., Goyal, M. K., & Jha, S. (2023). Role of large-scale climate oscillations in precipitation extremes associated with atmospheric rivers: nonstationary framework. *Hydrological Sciences Journal*, *68*(3), 395-411.

Sobel, A. H., Camargo, S. J., Hall, T. M., Lee, C. Y., Tippett, M. K., & Wing, A. A. (2016). Human influence on tropical cyclone intensity. *Science*, *353*(6296), 242-246.

Soden, B. J., & Held, I. M. (2006). An assessment of climate feedbacks in coupled ocean–atmosphere models. *Journal of climate*, *19*(14), 3354-3360.

Sridhar, V., Modi, P., Billah, M. M., Valayamkunnath, P., & Goodall, J. L. (2019). Precipitation extremes and flood frequency in a changing climate in southeastern virginia. *Journal of the American Water Resources Association, 55*(4), 780-799. doi:10.1111/1752-1688.12752

St.Louis-MO.GOV. (2019). Ward and Neighborhood Boundaries Dataset. Accessed on November 8th, 2019 at: https://www.stlouis-mo.gov/data/datasets/dataset.cfm?id=85

Stansfield, A. M., & Reed, K. A. (2023). Global tropical cyclone precipitation scaling with sea surface temperature. *npj Climate and Atmospheric Science*, *6*(1), 60.

Stephenson, D. B., Diaz, H. F., & Murnane, R. J. (2008). Definition, diagnosis, and origin of extreme weather and climate events. *Climate extremes and society*, *340*, 11-23.

Steinfeld, D., Sprenger, M., Beyerle, U., & Pfahl, S. (2022). Response of moist and dry processes in atmospheric blocking to climate change. *Environmental Research Letters*, *17*(8), 084020.

Stillman, J. H. (2019). Heat waves, the new normal: summertime temperature extremes will impact animals, ecosystems, and human communities. *Physiology*, *34*(2), 86-100.

Stott, P. A., Christidis, N., Otto, F. E. L., Sun, Y., Vanderlinden, J., van Oldenborgh, G. J., . . . Zwiers, F. W. (2016). Attribution of extreme weather and climate-related events. *Wiley Interdisciplinary Reviews-Climate Change, 7*(1), 23-41. doi:10.1002/wcc.380

Sugi, M., Murakami, H., & Yoshimura, J. (2012). On the mechanism of tropical cyclone frequency changes due to global warming. *気象集誌. 第 2 輯*, *90*(0), 397-408.

Sun, J., & Ao, J. (2013). Changes in precipitation and extreme precipitation in a warming environment in China. *Chinese Science Bulletin*, *58*, 1395-1401.

Sun, P., Zou, Y., Yao, R., Ma, Z., Bian, Y., Ge, C., & Lv, Y. (2023). Compound and successive events of extreme precipitation and extreme runoff under heatwaves based on CMIP6 models. *Science of The Total Environment*, *878*, 162980.

Supharatid, S., Nafung, J., & Aribarg, T. (2022). Projected changes in temperature and precipitation over mainland Southeast Asia by CMIP6 models. *Journal of Water and Climate Change*, *13*(1), 337-356.

Tachiiri, K., Hajima, T., & Kawamiya, M. (2019). Increase of the transient climate response to cumulative carbon emissions with decreasing CO2 concentration scenarios. *Environmental Research Letters*, *14*(12), 124067.

Tan, X., Liu, Y., Wu, X., Liu, B., & Chen, X. (2022). Examinations on global changes in the total and spatial extent of tropical cyclone precipitation relating to rapid intensification. *Science of The Total Environment*, *853*, 158555.

Tangang, F., Juneng, L., & Aldrian, E. (2017). Observed changes in extreme temperature and precipitation over indonesia. *International Journal of Climatology, 37*(4), 1979-1997.

Taszarek, M., Allen, J., Púčik, T., Groenemeijer, P., Czernecki, B., Kolendowicz, L., ... & Schulz, W. (2019). A climatology of thunderstorms across Europe from a synthesis of multiple data sources. *Journal of Climate*, *32*(6), 1813-1837.

Taszarek, M., Allen, J. T., Brooks, H. E., Pilguj, N., & Czernecki, B. (2021). Differing trends in United States and European severe thunderstorm environments in a warming climate. *Bulletin of the American Meteorological society*, *102*(2), E296-E322.

Tebaldi, C., & Knutti, R. (2018). Evaluating the accuracy of climate change pattern emulation for low warming targets. *Environmental Research Letters*, *13*(5), 055006.

Teshome, A., & Zhang, J. (2019). Increase of extreme drought over Ethiopia under climate warming. *Advances in Meteorology*, *2019*, 1-18.

Thackeray, C. W., Hall, A., Norris, J., & Chen, D. (2022). Constraining the increased frequency of global precipitation extremes under warming. *Nature Climate Change*, *12*(5), 441-448.

Tippett, M. K., Lepore, C., & Cohen, J. E. (2016). More tornadoes in the most extreme US tornado outbreaks. *Science*, *354*(6318), 1419-1423.

Tokarska, K. B., Zickfeld, K., & Rogelj, J. (2019). Path independence of carbon budgets when meeting a stringent global mean temperature target after an overshoot. *Earth's Future*, *7*(12), 1283-1295.

Tokarska, K. B., Arora, V. K., Gillett, N. P., Lehner, F., Rogelj, J., Schleussner, C. F., ... & Knutti, R. (2020). Uncertainty in carbon budget estimates due to internal climate variability. *Environmental Research Letters*, *15*(10), 104064.

Thompson, V., Kennedy-Asser, A. T., Vosper, E., Lo, Y. E., Huntingford, C., Andrews, O., ... & Mitchell, D. (2022). The 2021 western North America heat wave among the most extreme events ever recorded globally. *Science advances*, *8*(18), eabm6860.

Trapp, R. J., Diffenbaugh, N. S., Brooks, H. E., Baldwin, M. E., Robinson, E. D., & Pal, J. S. (2007). Changes in severe thunderstorm environment frequency during the 21st century caused by anthropogenically enhanced global radiative forcing. *Proceedings of the National Academy of Sciences*, *104*(50), 19719-19723.

Trapp, R. J., Diffenbaugh, N. S., & Gluhovsky, A. (2009). Transient response of severe thunderstorm forcing to elevated greenhouse gas concentrations. *Geophysical Research Letters*, *36*(1).

Trenberth, K. E. (2012). Framing the way to relate climate extremes to climate change. *Climatic Change, 115*(2), 283-290.

Tripathy, K. P., Mukherjee, S., Mishra, A. K., Mann, M. E., & Williams, A. P. (2023). Climate change will accelerate the high-end risk of compound drought and heatwave events. *Proceedings of the National Academy of Sciences*, *120*(28), e2219825120.

Triphonia, J.N.; Joachim, R.; Edwin, R.; Shaban, N.; Michel, D.S.M. Modeling of Extreme Maximum Rainfall using Extreme Value Theory for Tanzania. *Int. J. Sci. Innov. Math. Res. IJSIMR* **2016**, *4*, 34–45.

Ullah, S., You, Q., Ullah, W., Sachindra, D. A., Ali, A., Bhatti, A. S., & Ali, G. (2023). Climate change will exacerbate population exposure to future heat waves in the China-Pakistan economic corridor. *Weather and Climate Extremes*, *40*, 100570.

Utsumi, N., Seto, S., Kanae, S., Maeda, E. E., & Oki, T. (2011). Does higher surface temperature intensify extreme precipitation?. *Geophysical research letters*, *38*(16).

Utsumi, N., & Kim, H. (2022). Observed influence of anthropogenic climate change on tropical cyclone heavy rainfall. *Nature Climate Change*, *12*(5), 436-440.

van der Ploeg, F. (2018). The safe carbon budget. *Climatic change*, *147*(1-2), 47-59.

van Westen, R. M., Dijkstra, H. A., & Bloemendaal, N. (2023). Mechanisms of tropical cyclone response under climate change in the community earth system model. *Climate Dynamics*, 1-16.

Valverde, M. C., & Marengo, J. A. (2014). Extreme rainfall indices in the hydrographic basins of Brazil. *Open Journal of Modern Hydrology*, *2014*.

Van den Besselaar, E. J. M., A. M. G. Klein Tank, and T. A. Buishand. "Trends in European precipitation extremes over 1951–2010." *International Journal of Climatology* 33.12 (2013): 2682-2689.

Ville de Montreal. (2019). Portails Donnees Ouvertes. Accessed November 8th, 2019 at: http://donnees.ville.montreal.qc.ca/dataset/polygones-arrondissements/resource/62f7ce10-36ce-4bbd-b419-8f0a10d3b280

Vincent, L., & Mekis, E. (2006). Changes in daily and extreme temperature and precipitation indices for canada over the twentieth century. *Atmosphere-Ocean, 44*(2), 177-193. doi:10.3137/ao.440205

Vogel, M. M., Hauser, M., & Seneviratne, S. I. (2020). Projected changes in hot, dry and wet extreme events' clusters in CMIP6 multi-model ensemble. *Environmental Research Letters*, *15*(9), 094021.

Walsh, K. J. E., McBride, J. L., Klotzbach, P. J., Balachandran, S., Camargo, S. J., Holland, G., . . . Sugi, M. (2016). Tropical cyclones and climate change. *Wiley Interdisciplinary Reviews-Climate Change, 7*(1), 65-89. doi:10.1002/wcc.371

Walsh, K. J., Camargo, S. J., Knutson, T. R., Kossin, J., Lee, T. C., Murakami, H., & Patricola, C. (2019). Tropical cyclones and climate change. *Tropical Cyclone Research and Review*, *8*(4), 240-250.

Wang, F., Shao, W., Yu, H., Kan, G., He, X., Zhang, D., ... & Wang, G. (2020). Re-evaluation of the power of the Mann-Kendall test for detecting monotonic trends in hydrometeorological time series. *Frontiers in Earth Science*, *8*, 14.

Wang, G., Zhang, Q., Yu, H., Shen, Z., & Sun, P. (2020). Double increase in precipitation extremes across China in a 1.5° C/2.0° C warmer climate. *Science of The Total Environment*, *746*, 140807.

Wang, X., Li, Y., Yan, M., & Gong, X. (2022). Changes in temperature and precipitation extremes in the arid regions of China during 1960–2016. *Frontiers in Ecology and Evolution*, *10*, 902813.

Wartenburger, R., Hirschi, M., Donat, M. G., Greve, P., Pitman, A. J., & Seneviratne, S. I. (2017). Changes in regional climate extremes as a function of global mean temperature: an interactive plotting framework. *Geoscientific Model Development*, *10*(9), 3609-3634.

Whan, K., & Zwiers, F.The impact of ENSO and the NAO on extreme winter precipitation in north america in observations and regional climate models. *Climate Dynamics, 48*(5/6), 1401-1411. doi:10.1007/s00382-016-3148-x

Woollings, T., Barriopedro, D., Methven, J., Son, S. W., Martius, O., Harvey, B., ... & Seneviratne, S. (2018). Blocking and its response to climate change. *Current climate change reports*, *4*, 287-300.

World Meteorological Organization. (2022). Floods. Retrieved at: https://public.wmo.int/en/resources/world-meteorological-day/previous-world-meteorological-days/climate-and-water/floods#:~:text=Flash%20floods%20account%20for%20approximately,than%205%2C000%20lives%20lost%20annually.

World Meteorological Organization. (2022). Climate change undermines nearly all sustainable development goals. Retrieved at: https://public.wmo.int/en/media/press-release/climate-change-undermines-nearly-all-sustainable-development-goals#:~:text=Between%201970%20and%202021%2C%20there,developing%20economies%2C%20undermining%20sustainable%20development.

Wu, L., Zhao, H., Wang, C., Cao, J., & Liang, J. (2022). Understanding of the effect of climate change on tropical cyclone intensity: a review. *Advances in Atmospheric Sciences*, *39*(2), 205-221.

Xi, D., Lin, N., & Gori, A. (2023). Increasing sequential tropical cyclone hazards along the US East and Gulf coasts. *Nature Climate Change*, *13*(3), 258-265.

XU, Z., & FAN, K. (2019). Projected changes in summer water vapor transport over east asia under the 1.5° C and 2.0° C global warming targets. *Atmospheric and Oceanic Science Letters, 12*(2), 124-130.

Yuan, X., Wang, Y., Ji, P., Wu, P., Sheffield, J., & Otkin, J. A. (2023). A global transition to flash droughts under climate change. *Science*, *380*(6641), 187-191.

Zhai, P., Yu, R., Guo, Y., Li, Q., Ren, X., Wang, Y., ... & Ding, Y. (2016). The strong El Niño of 2015/16 and its dominant impacts on global and China's climate. *Journal of Meteorological Research*, *30*(3), 283-297.

Zhang, X., Wan, H., Zwiers, F. W., Hegerl, G. C., & Min, S. K. (2013). Attributing intensification of precipitation extremes to human influence. *Geophysical Research Letters*, *40*(19), 5252-5257.

Zhang, H., Wang, Y., Park, T. W., & Deng, Y. (2017). Quantifying the relationship between extreme air pollution events and extreme weather events. *Atmospheric Research*, *188*, 64-79.

Zhang, W., & Zhou, T. (2020). Increasing impacts from extreme precipitation on population over China with global warming. *Science Bulletin*, *65*(3), 243-252.

Zhou, X., Cheng, Y., Liu, L., Huang, Y., & Sun, H. (2023). Significant Increases in Water Vapor Pressure Concurs with Climate Warming Globally. *Water*, *15*(18), 3219.

Zhou, Z., Kim, Y. T., Im, E. S., & Kwon, H. H. (2024). Impact of Anthropogenic Warming on Future Unprecedented Droughts in California: Insights From Multiple Indices and Multi-Model Projections. *Earth's Future*, *12*(1), e2023EF003856.

Zickfeld, K., Arora, V., & Gillett, N. (2012). Is the climate response to CO2 emissions path dependent? *Geophysical Research Letters, 39*(5)

Zilli, M. T., Carvalho, L. M., Liebmann, B., & Silva Dias, M. A. (2017). A comprehensive analysis of trends in extreme precipitation over southeastern coast of Brazil. *International Journal of Climatology*, *37*(5), 2269-2279.